

POLYTECHNIQUE MONTRÉAL

affiliée à l'Université de Montréal

**Stochastic Modelling of Infrastructures Deterioration and Interventions based
on Network-Scale Visual Inspections**

ZACHARY HAMIDA

Département de génie civil, géologique et des mines

Thèse présentée en vue de l'obtention du diplôme de *Philosophiæ Doctor*
génie civil

Octobre 2020

POLYTECHNIQUE MONTRÉAL

affiliée à l'Université de Montréal

Cette thèse intitulée :

**Stochastic Modelling of Infrastructures Deterioration and Interventions based
on Network-Scale Visual Inspections**

présentée par **Zachary HAMIDA**

en vue de l'obtention du diplôme de *Philosophiæ Doctor*
a été dûment acceptée par le jury d'examen constitué de :

Bruno MASSICOTTE, président

James-A. GOULET, membre et directeur de recherche

Matteo POZZI, membre externe

Luc CHOUINARD, membre externe

DEDICATION

To my family, Fatema, Abdul-hadi, Tamara, Brothers & Sisters.

To my friends and colleagues... .

I send your way love & admiration.

ACKNOWLEDGEMENTS

I would like to express my sincere appreciation to my academic advisor Prof. James-A. Goulet, for his continuous support and guidance throughout this thesis.

I would also like to thank and acknowledge the Transportation Ministry of Quebec Province (MTQ), Canada, for their support and fund to this project, as well as Mr. René Gagnon for facilitating the access to the inspections and interventions database employed in this thesis.

RÉSUMÉ

Les infrastructures de transport sont précieuses parce qu'elles touchent une multitude d'aspects allant de la société et l'économie, à l'environnement. La gestion et l'entretien des infrastructures de transport à l'échelle du réseau sont directement associés à la capacité de surveiller et de prévoir la détérioration de ces infrastructures. L'inspection visuelle est une approche courante pour la surveillance des infrastructures à l'échelle du réseau, car elle fournit une évaluation directe et à grande échelle de l'état de détérioration des structures. L'une des principales limites des inspections visuelles est que l'évaluation est subjective, et donc l'incertitude des observations varie selon les inspecteurs. De plus, les incertitudes des observations peuvent dépendre de l'état de l'élément structurel. Ces facteurs présentent des défis dans l'interprétation des données d'inspection, ce qui limite la capacité à modéliser la détérioration ainsi que de quantifier l'amélioration de l'état de santé au éléments suite aux activités de maintenance. L'objectif de ce travail est d'améliorer l'utilité globale des données d'inspection visuelle à l'échelle du réseau, pour mieux comprendre le comportement de dégradation des infrastructures au fil du temps. Ceci est réalisé en développant des méthodes basées sur les données qui permettent: a) d'estimer l'état de détérioration et la vitesse de détérioration des infrastructures, b) de quantifier l'incertitude des observations en fonction de l'état de détérioration de l'élément structurel et de l'inspecteur responsable de l'évaluation, c) d'exploiter la structure commune attributs des infrastructures pour améliorer la performance du modèle de dégradation, d) quantification de l'effet des interventions, et e) l'estimation des états de détérioration globaux pour les ponts et pour le réseau. Les méthodes proposées dans cette thèse sont vérifiées à l'aide de données synthétiques et validées à partir de données d'inspection réelles du réseau de ponts au Québec. L'application de ces méthodes a montré une quantification efficace des incertitudes des inspecteurs ainsi qu'une estimation robuste de l'état de détérioration et de la vitesse sur la base d'un nombre limité d'observations par élément structurel. Par ailleurs, les méthodes développées ont également démontré une bonne performance dans la quantification de l'effet des interventions localement pour chaque élément structurel, et à l'échelle du réseau. Dans l'ensemble, les méthodes proposées améliorent la capacité d'interprétation des inspections visuelles, qui fournissent des bases solides pour la prise de décision à l'échelle du réseau et la planification de la maintenance.

ABSTRACT

Transportation infrastructures are valuable assets that affect a multitude of aspects, such as the society, the economy and the environment. Managing and maintaining transportation infrastructure on a network-scale is directly associated with the capacity to monitor and forecast the deterioration of these infrastructures. Visual inspection is a common approach for the network-scale monitoring of infrastructures, as it provides direct and broad evaluation for the deterioration state of the structure. One of the main limitations of visual inspections is the evaluations being subjective, and thus the uncertainty of observations vary among different inspectors. In addition, observation uncertainties are dependent on the structural element condition. Those factors present challenges in interpreting the inspection data, which limits the capacity of modelling the deterioration as well as quantifying the improvement in the health state following maintenance activities. The purpose of this work is to improve the overall utility of network-scale visual inspection data, to better understand the deterioration behaviour of infrastructures over time. This is achieved by developing data-driven methods that allow: a) estimating the deterioration condition and speed of infrastructures, b) quantifying observations uncertainty based on the deterioration state of the structural element and the inspector responsible for the evaluation, c) exploiting the common structural attributes of infrastructures to improve the deterioration model performance, d) quantifying the effect of interventions, and e) estimating the overall deterioration state for bridges and the entire network. The methods proposed in this thesis are verified using synthetic data and validated using real inspection data from the network of bridges in Quebec. The application of these methods have shown effective quantification of the inspector uncertainty along with robust estimation for the deterioration condition and speed based on limited number of observations per structural element. Furthermore, the developed methods have also demonstrated a good performance in quantifying the effect of interventions locally for each structural element, and on a network-scale. Altogether, the proposed methods improve the capacity of interpreting visual inspections, which provide solid foundations for network-scale decision making and maintenance planning.

TABLE OF CONTENTS

DEDICATION	iii
ACKNOWLEDGEMENTS	iv
RÉSUMÉ	v
ABSTRACT	vi
TABLE OF CONTENTS	vii
LIST OF TABLES	x
LIST OF FIGURES	xii
LIST OF SYMBOLS AND ACRONYMS	xix
LIST OF APPENDICES	xxiv
 CHAPTER 1 Introduction	 1
1.1 Motivation	1
1.2 Network-Scale Monitoring of Bridges	2
1.3 Research Objectives	4
1.4 Thesis Outline	4
1.5 Co-Authored Papers	4
 CHAPTER 2 Literature Review	 6
2.1 Bridge Management System (BMS)	6
2.2 Network-Scale Monitoring Using Visual Inspections	6
2.3 Modelling Deterioration & Time Series Data	7
2.3.1 Discrete Markov Model (DMM)	8
2.3.2 Regression Methods	10
2.3.3 State-Space Models	12
2.4 Effect of Interventions	15
2.5 Bridge Deterioration State & Network-Scale Analyses	16
2.6 Conclusions from the Literature Review	17

CHAPTER 3 Modelling Deterioration Using State-Space Models	18
3.1 Introduction	18
3.2 Visual Inspections Characteristics	18
3.2.1 Inspectors Uncertainty	18
3.2.2 State-Dependant Uncertainty	19
3.2.3 Monotonicity and State Constraints	21
3.3 Modelling Deterioration Using State-Space Models	22
3.4 Model Parameter Estimation	24
3.5 Case Studies	26
3.5.1 Visual Inspections and Synthetic Data	26
3.5.2 SSM Model Verification & Analyses with Synthetic Data	28
3.5.3 SSM Model Validation & Analyses with Real Data	33
3.6 Conclusion	37
CHAPTER 4 Integrating Structural Attributes in Deterioration Analysis	39
4.1 Introduction	39
4.2 Kernel Regression (KR)	39
4.3 Integrating Structural Attributes in Deterioration Analysis	41
4.3.1 Model Parameters & Estimation Framework	41
4.3.2 Recursive Estimation for the Deterioration Speed	43
4.4 Deterioration Analyses with SSM-KR	44
4.4.1 Model Verification Using Synthetic Data	44
4.4.2 Model Validation Using Real Data	49
4.5 Conclusion	53
CHAPTER 5 Quantifying the Effects of Interventions on Structural Elements	55
5.1 Introduction	55
5.2 Interventions Database	55
5.2.1 Interventions in the Real Case Study	56
5.2.2 Simulating Interventions and Synthetic Data	56
5.3 Quantifying the Effects of Interventions on Structural Elements	57
5.3.1 Integrating Interventions within SSM-KR	57
5.3.2 State Estimation and Model Parameters	59
5.4 Case Studies	60
5.4.1 Model Verification Using Synthetic Data	60
5.4.2 Model Validation Using Real Data	64
5.5 Conclusion	68

CHAPTER 6 Network-Scale Deterioration Analyses	69
6.1 Introduction	69
6.2 Network-Scale Data	69
6.2.1 Structural Element Groups	69
6.2.2 Bridge-level Data	71
6.3 Network-Scale Deterioration Analyses	71
6.3.1 Estimating the Deterioration State of a Bridge	72
6.3.2 Estimating the Deterioration State of the Network	73
6.3.3 Deterioration States Aggregation Method	74
6.3.4 Missing Data and Outliers	74
6.4 Case Studies	78
6.4.1 Deterioration Analyses for a Bridge Without Interventions	78
6.4.2 Deterioration Analyses of Bridge With Interventions	82
6.4.3 Deterioration State of the Network	85
6.4.4 Network-Scale Effect of Interventions and Investments	89
6.5 Conclusion	91
CHAPTER 7 Conclusion	92
7.1 Thesis Conclusions	92
7.2 Limitations	93
7.2.1 State Constraints	94
7.2.2 Kernel Regression & Structural Attributes	94
7.2.3 Deterioration Speed Estimate Following an Intervention	94
7.2.4 Observations Error Estimate for the Inspectors	95
7.3 Future Work	95
7.3.1 Supporting the Model with Additional Deterioration Information . .	95
7.3.2 Handling Abnormal Observations in Real Time	96
7.3.3 Planning Network-Scale Interventions	96
REFERENCES	98
APPENDICES	106

LIST OF TABLES

Table 3.1	Estimated model parameters from synthetic inspection data.	29
Table 3.2	Estimated model parameters from real inspection data.	34
Table 4.1	Estimation results of model parameters for synthetic data.	47
Table 4.2	Estimation results of SSM-KR parameters for real data.	51
Table 4.3	Comparison between SSM-KR and SSM based on the log-likelihood in the training, validation and testing sets	53
Table 5.1	Types of synthetic interventions with their corresponding expected improvement represented by an expected value and a standard deviation.	56
Table 5.2	Estimated model parameters for synthetic interventions.	60
Table 5.3	The error in the state estimate following an intervention represented by the expected error \pm standard deviation and skewness γ for a sample of 414 synthetic structural elements.	63
Table 5.4	Estimated model parameters for interventions on the front wall structural elements.	64
Table 5.5	Estimated model parameters for interventions on the beam structural elements.	66
Table 6.1	Structural element groups sorted using descending order based on the number of elements in each category.	70
Table 6.2	Structural element categories sorted using descending order based on the number of elements in bridge b_{990}	78
Table 6.3	Structural element categories sorted using descending order based on the number of elements in bridge b_{3348}	82
Table 6.4	Aggregated expected improvement in the condition for the primary structural elements \mathcal{G}_1 and the secondary structural elements \mathcal{G}_2	89
Table D.1	Table of synthetic interventions h_r applied for a given health condition and a priority index.	109
Table F.1	Categories of inspected structural elements in the network.	112
Table F.2	Categories of structural elements that are visually inspected in bridge b_{990}	113
Table F.3	Categories of structural elements that are visually inspected in bridge b_{3348}	113
Table G.1	Effect of interventions on the primary categories of structural elements.	114
Table G.2	Effect of interventions on the secondary categories of structural elements.	115

Table H.1	Number of structures B and elements E with visual inspection data, in addition to the total number of elements with reported interventions E_r , elements with missing data E_Φ , and the total number of outlier observations N_ϕ , for each primary structural category \mathcal{S}_1	116
Table H.2	Number of structures B and elements E with visual inspection data, in addition to the total number of elements with reported interventions E_r , elements with missing data E_Φ , and the total number of outlier observations N_ϕ , for each secondary structural category \mathcal{S}_2	117
Table H.3	Model type and parameters representing the process error and the initial state for the deterioration condition, speed and acceleration, in each primary structural category \mathcal{S}_1	118
Table H.4	Model type and parameters representing the process error and the initial state for the deterioration condition, speed and acceleration, in each secondary structural category \mathcal{S}_2	119

LIST OF FIGURES

Figure 1.1	Information hierarchy for network-scale database	3
Figure 2.1	Examples for corrosion of reinforcement in structural elements taken from the Manual of Inspection [7].	7
Figure 2.2	Discrete Markov model states with the arrows representing all the possible transitions in a deterioration model.	9
Figure 2.3	Example of applying the PDF truncation method for a state vector with a single constraint $\dot{\mu}_{t t} < 0$	15
Figure 3.1	Transformation function $g(\cdot)$ with different n values.	20
Figure 3.2	Examples of state transformation with the proposed transformation function.	21
Figure 3.3	Structural degradation model for predicting and forecasting the deterioration state of structural element e_p^j from time t to time T	23
Figure 3.4	Sample of synthetic inspections $y_{t,1}^{623}$ taken from a true deterioration condition of synthetic structural element e_1^{623} using synthetic inspectors I_i	28
Figure 3.5	Scatter plot of inspectors true $\sigma_V(I_i)$ vs. estimated $\sigma_V(I_i)$ with a dashed line representing the initial value at the start of the optimization. . .	29
Figure 3.6	Condition deterioration analysis based on the observations $\tilde{y}_{t,1}^{837} \in [25, 100]$ of the synthetic structural element e_1^{837} , with error bars representing the inspectors true (wide whiskers) & estimated (narrow whiskers) uncertainties, and the shaded area representing the forecast period. . .	30
Figure 3.7	Deterioration speed estimate for synthetic structural elements, with the shaded area representing the forecast period. . . .	30
Figure 3.8	Condition deterioration analysis based on the observations $\tilde{y}_{t,1}^{792} \in [25, 100]$ of the synthetic structural element e_1^{792} with error bars representing the Inspectors true (wide whiskers) & estimated (narrow whiskers) uncertainties, and the shaded area representing the forecast period. . .	31
Figure 3.9	Absolute average error in forecast time for the expected condition, speed and acceleration based on the true condition, speed and acceleration respectively, with the 95% confidence interval ($\pm 2\sigma$) for each error. . . .	32
Figure 3.10	Scatter plot for the model estimate of the condition $\tilde{\mu}_{t T,p}^j$ vs. the true condition $\tilde{x}_{t,p}^j$ at forecast years 1, 5 and 10. . . .	32

Figure 3.11	The probability of the true condition being within the 95% confidence interval of the model predicted state for the model with the true parameters (dashed) and the estimated parameters.	33
Figure 3.12	Histogram for the estimated $\sigma_V(I_i)$ values in the transformed space for real inspectors (total: 194 inspectors) with a dashed line representing the initial value at the start of the optimization.	34
Figure 3.13	Condition deterioration analysis based on observations $\tilde{y}_{t,1}^{14} \in [25, 100]$ of the real structural element e_1^{14} with error bars representing the inspectors estimated uncertainties, and the shaded area representing the forecast period.	35
Figure 3.14	Deterioration speed estimate for real structural elements, with the shaded area representing the forecast period.	35
Figure 3.15	Condition deterioration analysis based on observations $\tilde{y}_{t,1}^{8233} \in [25, 100]$ of the real structural element e_1^{8233} with error bars representing the inspectors estimated uncertainties, and the shaded area representing the forecast period.	36
Figure 3.16	Deterioration condition validation for real structural elements.	37
Figure 4.1	Example of a relation between covariates z_1 , z_2 and true response \dot{x}_0 , along with 2D grid defined by $M^Q = 6^2$ reference points with coordinates of z_c^1 , z_c^2 and \dot{x}_z represented by the expected value $\dot{\mu}_z$	41
Figure 4.2	SSM-KR framework for estimating the deterioration state of structural element e_p^j from time t to time T.	42
Figure 4.3	Histogram of synthetic structural attribute z	45
Figure 4.4	Comparison between the updated estimates $\dot{\mu}_z$ (iteration #3) at each reference point $z_c \in z$ and the true relation between the synthetic structural attribute z and the deterioration speed \dot{x}_z	46
Figure 4.5	Recursive estimation of the state $\dot{x}_{0,p}^j$ illustrated by the probability density function (PDF) with the true speed represented by the vertical line and the SSM model represented by a dashed line.	46
Figure 4.6	Comparison between the SSM-KR model errors histogram (right) and the SSM model errors histogram (left), with the errors determined by the difference between the true initial speed and the smoothed estimate of the initial speed.	47
Figure 4.7	Estimation results for synthetic inspectors parameters $\sigma_V(I_i)$ (total: 223 inspectors) with dashed line referring to the initial estimate for all $\sigma_V(I_i)$ parameters.	47

Figure 4.8	Deterioration condition estimate for synthetic structural element e_1^{191} , with the <i>circle</i> marker representing the SSM-KR estimates, the <i>square</i> marker representing SSM estimates, the dashed line representing the true condition, and the shaded area representing the forecast period.	48
Figure 4.9	Deterioration speed of synthetic structural element e_1^{191} , with the <i>circle</i> marker representing the SSM-KR estimates, the <i>square</i> marker representing SSM estimates, the dashed line representing the true state, and the shaded area representing the forecast period.	48
Figure 4.10	Average error estimate of the SSM-KR model represented by the expected value (<i>circle marker</i>) and confidence interval ($\pm 2\sigma$) for the condition and speed, compared to the error estimates of the SSM model represented by the expected value (<i>square marker</i>).	49
Figure 4.11	Frequency of structural attributes from real data	50
Figure 4.12	Histogram for the estimated parameters $\sigma_V(I_i)$ of real inspectors (total: 223 inspectors) with the dashed line referring to the initial estimate for all $\sigma_V(I_i)$	51
Figure 4.13	Deterioration condition estimate for real structural element e_{10}^{244} with the <i>circle</i> marker representing the SSM-KR estimates, the <i>square</i> marker representing SSM estimates, and the shaded area representing the forecast period.	51
Figure 4.14	Deterioration speed of structural element e_{10}^{244} with the <i>circle</i> marker representing the SSM-KR estimates, the <i>square</i> marker representing SSM estimates, and the shaded area representing the forecast period.	52
Figure 4.15	Deterioration condition estimate for real structural element e_1^{1599} with the <i>circle</i> marker representing the SSM-KR estimates, the <i>square</i> marker representing SSM estimates, and the shaded area representing the forecast period.	52
Figure 4.16	Deterioration speed of structural element e_1^{1599} with the <i>circle</i> marker representing the SSM-KR estimates, the <i>square</i> marker representing SSM estimates, and the shaded area representing the forecast period.	53
Figure 5.1	Recursive estimation for the network-scale change in the deterioration condition δ and speed $\dot{\delta}$ based on data from $E_1 = 139$ structural elements underwent intervention h_1 , $E_2 = 141$ elements underwent intervention h_2 , and $E_3 = 134$ elements underwent intervention h_3	61
Figure 5.2	The effect of the number of observations per time series T_p on the state estimate of $\dot{\delta}_\tau$ under the same intervention h_3 at time $\tau \approx \frac{T_p}{2}$	61

Figure 5.3	Deterioration state analysis for the condition and the speed based on the observations $\tilde{\mathbf{y}}_{t,1}^{184} \in [25, 100]$ of the synthetic structural element e_1^{184} with an intervention h_1 at time $\tau = 2018$, error bars representing the inspectors' uncertainty estimates, and the shaded area representing the forecast period.	62
Figure 5.4	Deterioration state analysis for the condition and the speed based on the observations $\tilde{\mathbf{y}}_{t,1}^{53} \in [25, 100]$ of the synthetic structural element e_1^{53} with an intervention h_2 at time $\tau = 2017$, error bars representing the inspectors' uncertainty estimates, and the shaded area representing the forecast period.	62
Figure 5.5	Deterioration state analysis for the condition and the speed based on the observations $\tilde{\mathbf{y}}_{t,1}^{314} \in [25, 100]$ of the synthetic structural element e_1^{314} with an intervention h_3 at time $\tau = 2015$, error bars representing the inspectors' uncertainty estimates, and the shaded area representing the forecast period.	63
Figure 5.6	Recursive estimation for the network-scale change in the deterioration condition and speed of the front wall structural elements, using data from $E_2 = 26$ elements that underwent intervention h_2 , and $E_3 = 58$ elements that underwent intervention h_3	65
Figure 5.7	Deterioration state analysis for the condition and the speed based on the observations $\tilde{\mathbf{y}}_{t,1}^{2773} \in [25, 100]$ of the front wall structural element e_1^{2773} with an intervention h_2 at time $\tau = 2016$, error bars representing the inspectors' uncertainty estimates, and the shaded area representing the forecast period.	65
Figure 5.8	Deterioration state analysis for the condition and the speed based on the observations $\tilde{\mathbf{y}}_{t,1}^{541} \in [25, 100]$ of the front wall structural element e_1^{541} with an intervention h_3 at time $\tau = 2011$, error bars representing the inspectors' uncertainty estimates, and the shaded area representing the forecast period.	66
Figure 5.9	Recursive estimation for the network-scale change in the deterioration condition and speed based on $E_3 = 80$ beam structural elements that underwent intervention h_3	67

Figure 5.10	Deterioration state analysis for the condition and the speed based on the observations $\tilde{\mathbf{y}}_{t,1}^{520} \in [25, 100]$ of the beam structural element e_1^{520} with an intervention h_3 at time $\tau = 2011$, error bars representing the inspectors' uncertainty estimates, and the shaded area representing the forecast period.	67
Figure 6.1	Primary \mathcal{G}_1 and secondary \mathcal{G}_2 structural elements categories without interventions represented by the light blue colour and with interventions represented by the red colour, with the categories sorted in a descending order based on the number of elements.	70
Figure 6.2	Relative annual aggregated costs of interventions for the set $\mathcal{B}_c \subset \mathcal{B}$, with $B_c = 2999$ bridges, which represent all bridges with reported costs.	71
Figure 6.3	Hierarchy of the structural components in bridge b_j , with their corresponding deterioration states, with each level in the hierarchy differentiated using a unique colour.	73
Figure 6.4	Deterioration state analysis for the condition and the speed based on the $\tilde{\mathbf{y}}_{t,1}^{2905} \in [25, 100]$ of <i>front-wall</i> element, error bars representing the inspectors' uncertainty estimates, and the shaded area representing the forecast period.	76
Figure 6.5	Deterioration state analysis for the condition and the speed based on the $\tilde{\mathbf{y}}_{t,1}^{2905} \in [25, 100]$ of <i>front-wall</i> element, with an intervention automatically triggered at $\tau = 2012$, error bars representing the inspectors' uncertainty estimates, and the shaded area representing the forecast period.	77
Figure 6.6	Primary and secondary structural elements categories in bridge b_{990}	79
Figure 6.7	Deterioration state analysis for the condition and the speed based on the deterioration state estimates of <i>external-sides</i> elements $e_{1:20}^{990}$, with the aggregated observations $\tilde{\mathbf{y}}_{op,t}^{990} \in [25, 100]$, and their corresponding uncertainty estimates represented by the error bars, with the shaded area representing the forecast period.	79
Figure 6.8	Deterioration state analysis for the condition and the speed of group \mathcal{G}_1^{990} , based on the deterioration state estimates of primary categories $\mathcal{S}_{1,1:8}^{990}$, with the aggregated observations $\tilde{\mathbf{y}}_{gp,t}^{990} \in [25, 100]$, and their corresponding uncertainty estimates represented by the error bars, with the shaded area representing the forecast period.	80

Figure 6.9	Deterioration state analysis for the condition and the speed based on the deterioration state estimates of <i>wheel guard</i> elements $e_{1:20}^{990}$, with the aggregated observations $\tilde{y}_{os,t}^{990} \in [25, 100]$, and their corresponding uncertainty estimates represented by the error bars, with the shaded area representing the forecast period.	81
Figure 6.10	Deterioration state analysis for the condition and the speed of group \mathcal{G}_2^{990} , based on the deterioration state estimates of secondary categories $\mathcal{S}_{2,1:16}^{990}$, with the aggregated observations $\tilde{y}_{gs,t}^{990} \in [25, 100]$, and their corresponding uncertainty estimates represented by the error bars, with the shaded area representing the forecast period.	81
Figure 6.11	Primary and secondary structural elements categories of bridge b_{3348} without interventions represented by the blue colour, with interventions represented by the red colour, and with uncategorized interventions in the orange.	82
Figure 6.12	Deterioration state analysis for the condition and the speed based on the deterioration state estimates of <i>concrete slab</i> elements $e_{1:3}^{3348}$, with the interventions at time $\tau = 2015$, the aggregated observations $\tilde{y}_{op,t}^{3348} \in [25, 100]$, with their corresponding uncertainty estimates represented by the error bars, and the shaded area representing the forecast period. .	83
Figure 6.13	Deterioration state analysis for the condition and the speed based on the deterioration state estimates of the primary categories $\mathcal{S}_{1,1:8}^{3348}$, with the interventions at time $\tau = 2015$, the aggregated observations $\tilde{y}_{gp,t}^{3348} \in [25, 100]$, with their corresponding uncertainty estimates represented by the error bars, and the shaded area representing the forecast period. .	84
Figure 6.14	Deterioration state analysis for the condition and the speed based on the deterioration state estimates of <i>pavement</i> elements $e_{1:3}^{3348}$, with the interventions at time $\tau = 2015$, the aggregated observations $\tilde{y}_{os,t}^{3348} \in [25, 100]$, with their corresponding uncertainty estimates represented by the error bars, and the shaded area representing the forecast period.	84
Figure 6.15	Deterioration state analysis for the condition and the speed based on the deterioration state estimates of the secondary categories $\mathcal{S}_{2,1:15}^{3348}$, with $\tilde{y}_{gs,t}^{3348} \in [25, 100]$ representing the aggregation for a subset of observations, with their corresponding uncertainty estimates represented by the error bars, and the shaded area representing the forecast period.	85

Figure 6.16	Deterioration state analysis for the network's condition and speed based on the average state of the primary structural elements from $B \approx 7000$ bridges, with the shaded area representing the forecast period.	86
Figure 6.17	Deterioration state analysis for the network's condition and speed based on the average state of the secondary structural elements from $B \approx 7000$ bridges, with the shaded area representing the forecast period.	87
Figure 6.18	Deterioration state analysis for the network's condition and speed based on the average state of the primary structural elements from $B \approx 7000$ bridges, with automatically triggered interventions, and the shaded area representing the forecast period.	88
Figure 6.19	Deterioration state analysis for the network's condition and speed based on the average state of the secondary structural elements from $B \approx 7000$ bridges, with automatically triggered interventions, and the shaded area representing the forecast period.	88
Figure 6.20	Cumulative ratio for the total number of elements with intervention E_r to the total number of visually inspected elements E , in each structural group \mathcal{G}_1 and \mathcal{G}_2	89
Figure 6.21	Comparison between the costs, number of interventions E_r , and the network-scale expected condition improvement $\mathbb{E}[\mu^\delta]$ for interventions performed on the primary and secondary structural elements from $B = 2999$ bridges.	90
Figure D.1	Categories for the health condition and the priority index.	109
Figure E.1	Scatter plots for the normalized annual average of daily traffic vs. the normalized annual average of daily truck-traffic vs. and the normalized length associated with each bridge in the network.	110
Figure E.2	Expected values for the network's deterioration condition and speed based on a weighted average of $B \approx 7000$ according to: number of bridges, AADT, bridge length and number of trucks for the primary and secondary groups.	111

LIST OF SYMBOLS AND ACRONYMS

Symbols

A	Transition matrix
\mathbf{A}_κ	Array of normalized kernel regression weights
<i>A</i>	Category of Little damage
<i>a</i>	Vector of normalized kernel regression weights
\mathcal{B}	Set of bridges
B	Total number of bridges
B_{tr}	Total number of bridges in the training set
B_v	Total number of bridges in the validation set
B_t	Total number of bridges in the testing set
B_r	Total number of bridges that underwent interventions
<i>B</i>	Category of medium damage
<i>b</i>	Bridge identification
C	Total number of material categories
C	Observation matrix
<i>C</i>	Category of important damage
<i>c</i>	Intervention cost
\mathcal{D}	Database of inspections
<i>D</i>	Category of very important damage
<i>d</i>	Structural element quantity
\mathcal{E}	Set of structural elements in a bridge
E	Total number of structural elements
E_r	Number of structural elements with interventions
E_t	Number of structural elements in the testing set
E_{tr}	Number of structural elements in the training set
E_v	Number of structural elements in the validation set
<i>e</i>	Structural element identification
<i>F</i>	Cumulative distribution function
<i>f</i>	Probability density function
\mathcal{G}_1	Primary structural element group
\mathcal{G}_2	Secondary structural element group
G	Number of structural categories in a group

g	Transformation function
g^{-1}	Inverse transformation function
H	Constraints coefficient matrix
h	Intervention category
\mathcal{I}	Set of inspectors
I	Total number of inspectors
\mathbf{I}	Identity matrix
I	Inspector identification
i	Index of inspectors
\mathbf{J}	Kalman smoother gain matrix
j	Index of bridges
\mathbf{K}	Kalman gain matrix
\mathbf{k}	Multivariate kernel function
k	Univariate kernel function
\mathcal{L}	Network-scale log-likelihood
l	Lower bound of health condition
ℓ	Kernel length
M	Number of reference points in one dimension
m	Structural attributes index or structural element category index
\mathcal{N}	Normal distribution
n	Transformation function parameter
\mathbf{o}	Vector of hidden states of the deterioration in a structural category
P	Number of structural elements in a structural category
p	Transition probability or index of structural elements
$p_{1:2}$	Deterioration speed model parameters
Q	Number of covariates
\mathbf{Q}	Model process error covariance matrix
\mathbf{Q}^{ki}	Kinematic model process error covariance matrix
\mathbf{Q}^r	Element-level interventions error
q	Deterioration state of the network
\mathcal{R}	Intervention set
R	Number of intervention categories
\mathbf{R}	Observation error covariance matrix
r	Interventions category index
\mathcal{S}	Structural element category
S_j	Number of structural categories in a bridge

s	Vector of hidden states of the deterioration in a structure
T_p	Total number of observations
T	Total number of time stamps
t	Time stamp
t_ϕ	Outlier timestamp
\mathcal{U}	Uniform distribution
u	Upper bound of health condition
v	Observation error
w	Transition model process error
w_0	Kernel regression model error
w_r	Element-level interventions error
\mathcal{X}	Set of discrete deterioration states
X	Number of discrete deterioration states
x	Vector of hidden states in the unconstrained space
\tilde{x}	Vector of hidden states in the constrained space
\dot{x}_z	Vector of hidden states associated with covariates
x	State of deterioration condition in the unconstrained space
\tilde{x}	State of deterioration condition in the constrained space
\dot{x}	State of deterioration speed in the unconstrained space
$\tilde{\dot{x}}$	State of deterioration speed in the constrained space
\ddot{x}	State of deterioration acceleration in the unconstrained space
$\tilde{\ddot{x}}$	State of deterioration acceleration in the constrained space
y	Condition observation in the unconstrained space
\tilde{y}	Condition observation in the constrained space
y_a	Condition observation of little damage category
y_b	Condition observation of medium damage category
y_c	Condition observation of important damage category
y_d	Condition observation of very damaged category
y_{op}	Expected observation in a primary structural category
y_{os}	Expected observation in a secondary structural category
y_{gp}	Expected observation in a primary structural group
y_{gs}	Expected observation in a secondary structural group
\mathbb{Z}^+	Set of positive integers
Z	Transition probability matrix
Z_c	Matrix of reference points
z	Structural attribute

z_c	Vector of reference points for a single covariate
α	Gamma distribution parameter
β	Gamma distribution parameter
δ	Vector of hidden states of change in deterioration
δ	State of change in deterioration condition
$\dot{\delta}$	State of change in deterioration speed
$\ddot{\delta}$	State of change in deterioration acceleration
Δt	Time-step duration
ϵ	Error state estimate of the deterioration post-interventions
η	Convergence tolerance
Γ	Gamma function
γ	Skewness of normal distribution
λ	Mixture weight in gaussian mixture approach
μ	Expected value
μ	Vector of expected values
ν	Iteration limit per parameter
ω	Weight associated with the discrete deterioration state
ρ	Stall limit
σ	Standard deviation
Σ	Covariance matrix
τ	Intervention time
θ	Vector of model parameters
θ^m	Subset of model parameters
θ^s	Vector of initial model parameters
θ^κ	Vector of kernel regression parameters
ζ	Initial stall
∞	Infinity

Acronyms

AADT	Annual Average of Daily Traffic
AADTT	Annual Average of Daily Truck-Traffic
ANN	Artificial Neural Network
CPU	Central Processing Unit
DMM	Discrete Markov Model
GPU	Graphics Processing Unit

IDW	Inverse Distance Weighted Interpolation
KF	Kalman Filter
KR	Kernel Regression
KS	Kalman Smoother
MLE	Maximum Likelihood Estimation
NR	Newton-Raphson
PDF	Probability Density Function
SHM	Structural Health Monitoring
SSM	State-Space Model
SSM-KR	Hybrid Model of State-Space Model & Kernel Regression

LIST OF APPENDICES

Appendix A	Parameter Estimation Framework for SSM Deterioration Model	106
Appendix B	Parameter Estimation Framework for SSM-KR Deterioration Model	107
Appendix C	Kernel Functions:	108
Appendix D	Decision Making for Synthetic Interventions	109
Appendix E	Network-Scale Deterioration Analysis Based on Bridges' Attributes	110
Appendix F	Categories of Structural Elements	112
Appendix G	Network-Scale Effect of Interventions on Structural Categories	114
Appendix H	Network-Scale Characteristics of Structural Categories	116

CHAPTER 1 Introduction

1.1 Motivation

The levels of serviceability and safety associated with the transportation infrastructures are often linked with the economical growth of a society [1, 2]. As an asset, transportation infrastructure has to be monitored and maintained on a regular basis. Hence, structural health monitoring (SHM) of bridges has gained an increasing attention from researchers and infrastructure managers [3]. Bridge SHM systems encompass many techniques and practices, which can be categorized into three general schemes [4]. These schemes are: a) sensor-based monitoring systems, b) visual inspections, c) combination of visual inspections and sensor-based monitoring [4]. Each of the aforementioned systems has advantages and disadvantages that justifies its use. Sensor-based monitoring systems can provide continuous feedback about specific phenomena or behaviour associated with structural elements. However, the capacity of turning sensor-based data into useful information for managers currently limits the large-scale applicability of such systems. On the other hand, visual inspections consists in on-site inspections performed by teams of inspectors. Visual Inspections have the main advantage of providing direct information about the health state of a structure. These information are based on broad structural evaluations that do not target a specific damage or structural component [4]. As a result, visual inspections have been considered by many infrastructures owners as the primary option for network-scale monitoring [5–7].

Although visual inspections is a popular monitoring approach, along with many advantages, this monitoring system suffers from shortages that limit its efficiency. First, visual inspections are performed by different inspectors over time, so that it is common to have inconsistencies in the data. These inconsistencies introduce difficulties in differentiating between measurement errors and legitimate changes in a structure's condition. Second, the frequency of visual inspections varies among bridges, typically ranging from one inspection per year to one inspection every four years. Hence, there is typically few monitoring data available over long periods of time, which presents difficulties in interpreting this data [4].

The uncertainty and insufficiency of monitoring data lead to difficulties and challenges in developing accurate structural deterioration models. These models are essential for interpreting the inspection data and improving its utility in maintenance planning and decision making. The need for a better decision making systems has been emphasized by a report from Canadian Centre for Policy Alternatives [8], in addition to reports by international organizations, such as the Organization for Economic Co-operation and Development OECD [9].

This research project presents new data-driven methods that enhance the interpretability of network-scale visual inspection data. The outcome of this thesis is a collection of methods that will help monitoring and maintaining existing transportation infrastructure. These techniques enable tracking the performance of structural elements, forecasting the deterioration state, assessing the change in deterioration rate, and quantifying the effect of interventions.

1.2 Network-Scale Monitoring of Bridges

Figure 1.1 illustrates the information hierarchy for a transportation network database. The levels identified in this hierarchy are: the *network level*, the *bridge level* and the *element level*. The network level defines the transportation network regional properties which include information about the country, the province and the inspection code used in evaluating the structures. The bridge level is defined by the set of bridges $\mathcal{B} = \{b_1, b_2, \dots, b_{\mathcal{B}}\}$, with each bridge b_j described by $\mathbf{z}_j \in \mathcal{Z}$ structural attributes. The structural attributes \mathbf{z}_j include the geolocations (latitude, longitude), traffic loads (e.g., annual average daily traffic), construction year and other structure related properties. The last level is the structural elements level, defined by the set $\mathcal{E}_j = \{\mathcal{S}_1^j \cup \dots \cup \mathcal{S}_{\mathcal{S}_j}^j\} = \{e_1^j, e_2^j, \dots, e_{\mathcal{E}_j}^j\}$, where a structural element e_p^j represents the p -th structural element associated with the m -th structural category \mathcal{S}_m^j in the bridge b_j . Here, a structural category \mathcal{S} refers to the set of structural elements with similar characteristics or role in the bridge (e.g., beams). The structural element level contains information about the element material and type, inspection data, within-bridge location, and other element-related properties. The inspection data provides information about the deterioration process, which includes the inspection time t , the inspector I_i from the set of inspectors $\mathcal{I} = \{I_1, I_2, \dots, I_{\mathcal{I}}\}$ responsible for evaluating bridges in \mathcal{B} , and the deterioration condition of the structural element $\tilde{y} \in [l, u]$, with l representing the worst possible condition and u representing the best condition. The symbol (\sim) in \tilde{y} is utilized to differentiate between observations in the bounded space $[l, u]$ and unbounded space \mathbb{R} . The inspection data support the main bulk of the deterioration analysis, nonetheless, other information related to the bridge can also contribute to the analysis, by identifying deterioration patterns exhibited within common attributes in the network of bridges.

The information about maintenance and intervention for bridges within \mathcal{B} is maintained in a separate database. This segment of information is defined by $\mathcal{R}^* = \{\mathcal{R}_1, \dots, \mathcal{R}_j, \dots, \mathcal{R}_{\mathcal{B}_r}\}$, where \mathcal{R}_j represents the interventions performed on bridge b_j , and \mathcal{B}_r is the number of bridges that underwent interventions. Each intervention is defined by $\mathcal{R}_j = \{\mathbf{h}^j, \tau_j\}$, with $\mathbf{h}^j = [h_1^j \dots h_r^j \dots h_{\mathcal{R}}^j]^\top$ is a vector of \mathcal{R} intervention categories and τ_j is the intervention time. An intervention category h_r can be applied to one or multiple structural elements in

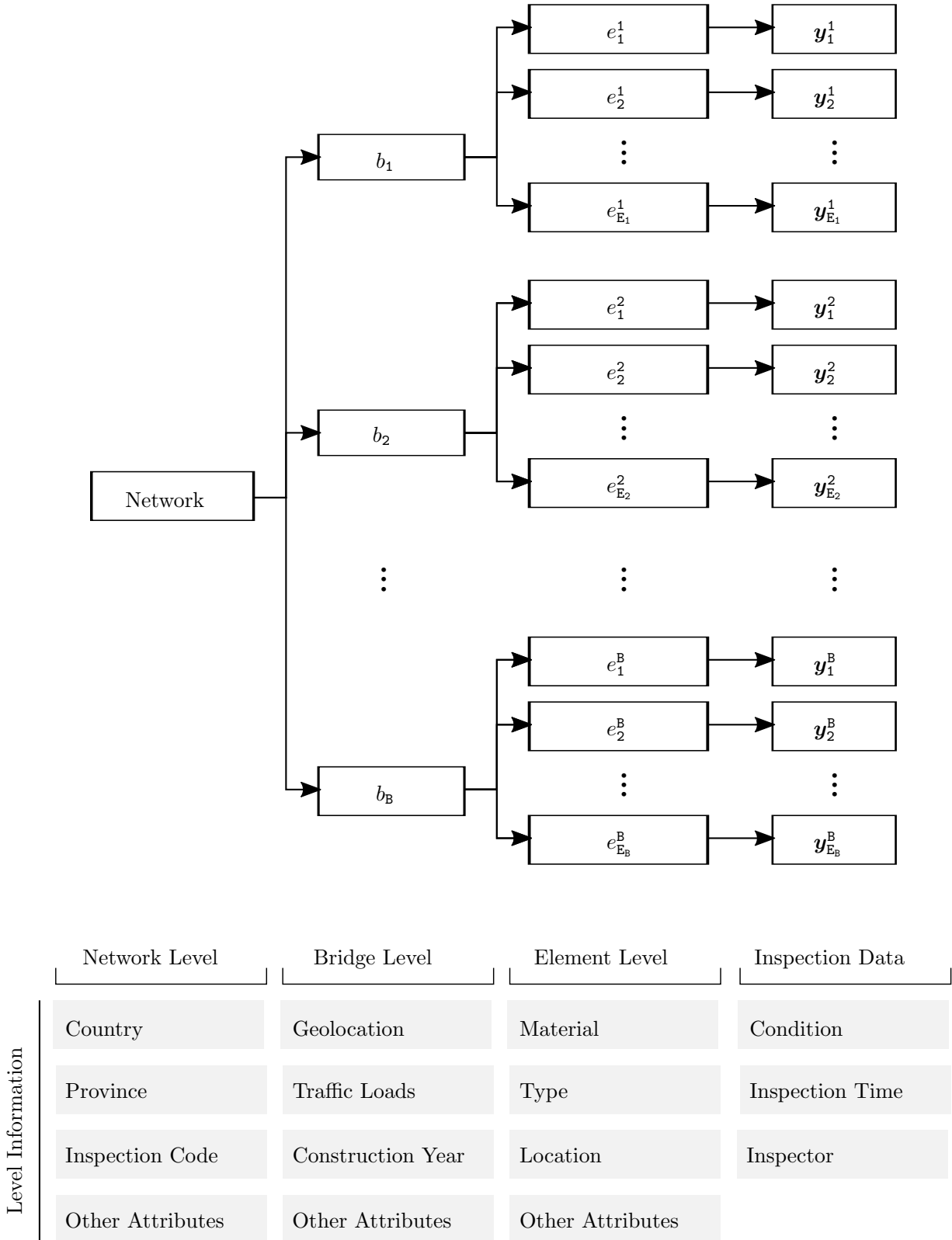


Figure 1.1 Information hierarchy for network-scale database

different bridges. In the context of this study, each structural element in the dataset has underwent a single intervention in the time-window of the available data.

1.3 Research Objectives

This research project aims at developing data-driven methods that are well suited for the network-scale analyses of inspection and intervention data of transportation infrastructure. The core objectives of this work are:

- Modelling infrastructures deterioration from network-scale visual inspections while accounting for the subjective nature of these inspections.
- Quantifying the local and the network-scale effects of interventions based on visual inspections.
- Validating and verifying the proposed methods with real and synthetic datasets.

1.4 Thesis Outline

The content of this thesis is organized as follows: Chapter 2 presents a literature review that compiles the strengths and limitations of existing methods for modelling the deterioration behaviour based on visual inspections, in addition to presenting the theoretical foundations of state-space models (SSM), which is utilized in performing the deterioration analysis in this thesis. Chapter 3 outlines the formulation of SSM as a deterioration model, along with describing the main characteristics of visual inspection data. Chapter 4 presents a hybrid framework that combines SSM with kernel regression (KR), in order to take advantage of the structural similarity between bridges, and exploit it to improve the deterioration model performance. Chapter 5 describes a new approach that allows quantifying the effects of interventions, along with the integration of this approach within the SSM-KR deterioration model. This is followed by estimating the overall deterioration states for bridges and the entire network in Chapter 6, which is done using the proposed methods. Finally, Chapter 7 provides the thesis conclusions, existing limitations and future research directions.

1.5 Co-Authored Papers

The majority of the work presented in this thesis has been already published or submitted for publication. The list of co-authored papers is composed of,

- Hamida, Z. and Goulet, J.-A. (2020). Modeling Infrastructure Degradation from Visual Inspections Using Network-Scale State-Space Models. *Structural Control and Health Monitoring*. 27(9):e2582.
- Hamida, Z. and Goulet, J.-A. (2020). Network-Scale Deterioration Modelling Based on Visual Inspections and Structural Attributes. *Structural Safety*. 88:102024
- Hamida, Z. and Goulet, J.-A. (Submitted, 2020). Quantifying the Effects of Interventions Based on Visual Inspections of Bridges Network. *Structure and Infrastructure Engineering*.

CHAPTER 2 Literature Review

This chapter presents a brief introduction about network-scale bridge management and its components, followed by a review for state-of-the-art techniques utilized in modelling infrastructure degradation and the effect of interventions. The review identifies the limitations of existing methods and justifies the thesis' objectives presented in Chapter 1.

2.1 Bridge Management System (BMS)

Bridge management systems (BMS) are utilized in managing the information and sustaining the long-term health of bridges network under budgetary constraints [10]. A basic BMS is composed of modules dealing with data storage, maintenance costs, deterioration models, optimization and analysis models, and updating functions [10,11]. One of the essential roles of a BMS is supporting decision making for maintenance and planning. Hence, the success of a BMS depends on the capacity of interpreting the inspection data and estimating the future condition of structures [12,13]. In this thesis, the primary focus will be on methods utilized in interpreting visual inspection data in order to model the deterioration behaviour and quantify the effect of maintenance interventions in bridges.

2.2 Network-Scale Monitoring Using Visual Inspections

Visual inspections are hands-on inspections performed on site by teams of inspectors. The evaluation method in visual inspection is mainly based on visual observation, and in some cases these observations can be validated by an instrument or tool (e.g., using a hammer to examine concrete delamination) [7]. Thus, visual inspections are known to be subjective, as they rely on the experience and judgment of the inspector [64]. An example that provides an insight about the visual inspection process is shown in Figure 2.1. In this example, Figure 2.1a shows a structural element with a rust stain on the concrete surface, and Figure 2.1b shows an apparent rusty reinforcement in a structural element. Both cases imply a corrosion in the reinforcement, and the level of damage severity in both cases is *Medium*, according to the standards specified by the Manual of Inspections from MTQ [7]. While the damage cases appear to be different, however, the reduction of the section in Figure 2.1b is considered negligible, therefore, it is treated in the same way as the case shown in Figure 2.1a. Further details about the evaluation method are provided in §3.5.1. The inspector during visual inspections is required to determine the type and the level of damage severity of each defect,

in addition to the percentage of the structural element area affected by the damage [7].

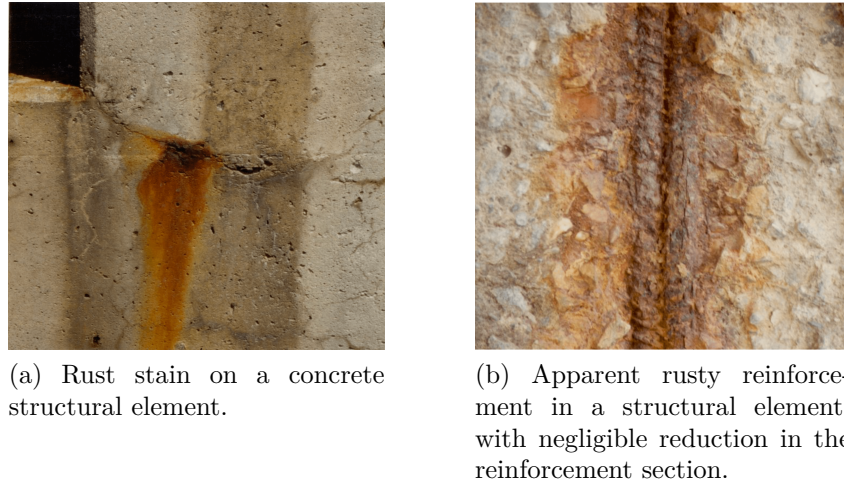


Figure 2.1 Examples for corrosion of reinforcement in structural elements taken from the Manual of Inspection [7].

Applying visual inspections on a network-scale denotes that the inspections are performed on a number of bridges, using the same inspection standards. The frequency of inspections on each bridge can vary, and is determined based on different factors, such as the age of the bridge and the annual average of daily traffic (AADT) [7]. Commonly the inspections are performed on a yearly scale ranging from one inspection every four years up to one inspection per year. During the network-scale inspections, the inspector may or may not inspect the same bridge she/he inspected before.

2.3 Modelling Deterioration & Time Series Data

Different methods exist in the literature to describe the deterioration behaviour of structural elements based on visual inspections [6, 12, 14–19]. The majority of these methods are divided between two approaches: Markov deterioration models and regression-based models. Nonetheless, *Discrete Markov Models* (or *Markov Process*) represents the largest proportion of the literature in the context of bridge visual inspections [6, 14–17]. This section elaborates on the basic concepts of DMM and regression-based models along with their existing limitations. The last part of this section presents the theoretical foundations of state-space models (SSM), which is utilized as the primary deterioration framework in this thesis.

2.3.1 Discrete Markov Model (DMM)

A DMM model describes the time-evolution of stochastic systems in which, the next future state is only dependent on the present state [20]. The main components of DMM are a set of system states $\mathcal{X} = \{x_1, x_2, \dots, x_{\mathbf{x}}\}$ and a set of transition probabilities represented by the transition matrix $\mathbf{Z} \in [0, 1]^{\mathbf{x} \times \mathbf{x}}$. A generic transition matrix in DMM can be written as,

$$\mathbf{Z} = \begin{bmatrix} x_1^{t+1} & \cdots & x_j^{t+1} & \cdots & x_{\mathbf{x}}^{t+1} \\ p_{11} & \cdots & p_{1j} & \cdots & p_{1\mathbf{x}} \\ \vdots & \ddots & \vdots & \ddots & \vdots \\ p_{i1} & \cdots & p_{ij} & \cdots & p_{i\mathbf{x}} \\ \vdots & \ddots & \vdots & \ddots & \vdots \\ p_{\mathbf{x}1} & \cdots & p_{\mathbf{x}j} & \cdots & p_{\mathbf{x}\mathbf{x}} \end{bmatrix} \begin{bmatrix} x_1^t \\ x_i^t \\ \vdots \\ x_{\mathbf{x}}^t \end{bmatrix}.$$

Each component $p_{ij} \in [0, 1]$ in \mathbf{Z} represents the conditional probability of transitioning from state x_i at time t to state x_j at time $t + 1$ such that, $p_{ij} = \Pr(x_j^{t+1} | x_i^t)$. In the context of modeling structural deterioration, each system state represents a qualitative state of deterioration. Figure 2.2 illustrates a deterioration model with four deterioration states: *Excellent* (x_1), *Good* (x_2), *Damaged* (x_3) and *Seriously Damaged* (x_4). The arrows in the graph represent the possible transitions across the states associated with the transition probabilities which collectively form the transition matrix,

$$\mathbf{Z} = \begin{bmatrix} x_1^{t+1} & x_2^{t+1} & x_3^{t+1} & x_4^{t+1} \\ p_{11} & p_{12} & p_{13} & p_{14} \\ 0 & p_{22} & p_{23} & p_{24} \\ 0 & 0 & p_{33} & p_{34} \\ 0 & 0 & 0 & p_{44} \end{bmatrix} \begin{bmatrix} x_1^t \\ x_2^t \\ x_3^t \\ x_4^t \end{bmatrix}.$$

The terms under the diagonal in \mathbf{Z} are equal to 0 because the deterioration process is monotonic over time (i.e. non-increasing). The time interval between t and $t + 1$ is generally considered as 1 year in the case of visual inspections, therefore, it would be unexpected for a structural element to skip a deterioration state from time t to time $t + 1$ [14, 21]. Hence,

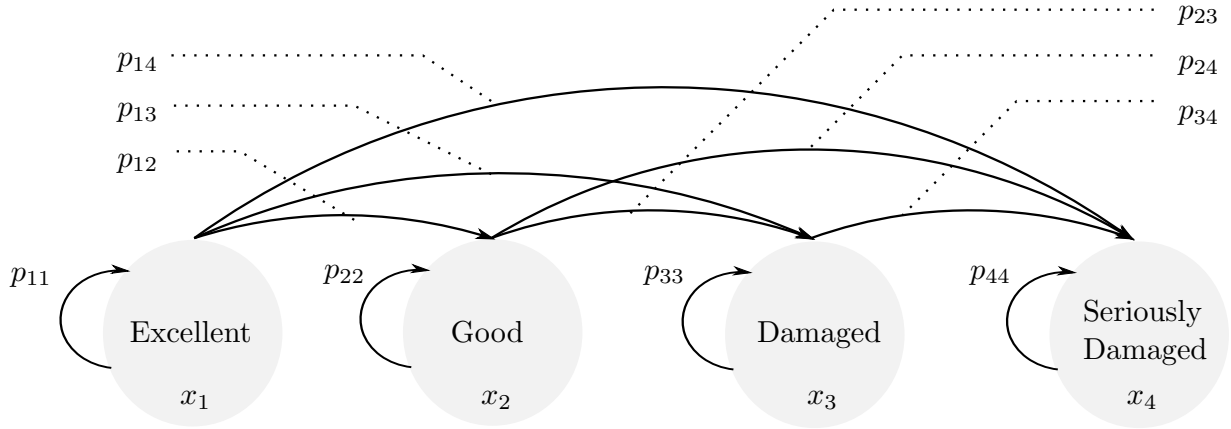


Figure 2.2 Discrete Markov model states with the arrows representing all the possible transitions in a deterioration model.

the transition matrix can be further simplified into,

$$\mathbf{Z} = \begin{bmatrix} x_1^{t+1} & x_2^{t+1} & x_3^{t+1} & x_4^{t+1} \\ p_{11} & 1 - p_{11} & 0 & 0 \\ 0 & p_{22} & 1 - p_{22} & 0 \\ 0 & 0 & p_{33} & 1 - p_{33} \\ 0 & 0 & 0 & 1 \end{bmatrix} \begin{bmatrix} x_1^t \\ x_2^t \\ x_3^t \\ x_4^t \end{bmatrix}. \quad (2.1)$$

The aforementioned assumption reduces the number of transition probabilities to be estimated for the model. Estimating the transition probabilities \$p_{ij}\$ is done based on the inspection data, and by using the *Maximum Likelihood Estimation* (MLE) [22], expressed by,

$$\mathcal{L}(p) = \sum_{i,j}^{\mathbf{x}} N_{ij} \log(p_{ij}),$$

where \$\mathcal{L}(\cdot)\$ is the log-likelihood function and \$N_{ij}\$ is the number of observed transitions from state \$x_i^t\$ to state \$x_j^{t+1}\$. Maximizing \$\mathcal{L}(\cdot)\$ is carried out while maintaining the constraint, \$\sum_{j=1}^{\mathbf{x}} p_{ij} = 1\$. One approach to solve this maximization is by using the *Lagrange multiplier* [22], which leads to the estimate,

$$\hat{p}_{ij} = \frac{N_{ij}}{\sum_{j=1}^{\mathbf{x}} N_{ij}}.$$

The estimate for \$p_{ij}\$ is further improved using different formulations and methods that adapt to the context of visual inspections [14, 21, 23–25]. These methods have relied mainly on

recursively minimizing the difference between the predicted and observed deterioration condition of structural elements [21]. Further extensions to the DMM framework are introduced in a variety of studies to improve its performance [6, 26, 27]. Zhang et al. [27] modified the transition matrix into a stochastic transition matrix to incorporate the epistemic uncertainty in DMM. For that end, an error term $\epsilon \sim \text{Beta}(\alpha, \beta)$ is added to the diagonal of the transition matrix Z . Van Erp and Orcesi [26] combined Markov process with nested sampling to improve parameters estimation and assign confidence bounds on Markov transition matrices. Soetjipto et al. [6] developed a hybrid approach of *Markov-System Dynamic* (MSD), which allows analyzing the interdependence of different facets on the system reliability.

While many studies have adopted *Discrete Markov Models*, the use of such models is subject to many limitations. Current DMM models have accommodated some of the *epistemic* uncertainty and the *aleatory* uncertainty in the inspection data [27]; However, the inspectors uncertainty is typically overlooked. The inspectors uncertainty is regarded in many studies as one of the main sources of variability in visual inspections due to the subjective nature of the evaluation [4, 5]. Theoretically, the inspector uncertainty can be estimated in a *Hidden Markov Model* (HMM) [28] with an *observation matrix* for each inspector. However, in practice, given the large number of inspectors, estimating an *observation matrix* for each inspector is seldom feasible. This is because the amount of data required for the model parameters estimation is unattainably large, in addition to being computationally expensive. Another limitation in the DMM models is attributed to the discretization aspect. Relying on discrete states in representing a naturally continuous physical process can introduce approximation errors. These approximation errors can result in additional flaws in forecasting the deterioration process [29]. In addition, the speed of deterioration over time can't be directly quantified, as quantifying the speed requires representing the deterioration by a continuous process. The importance of quantifying the speed of deterioration arise from the prospect of enabling further analysis such as modeling the effect of interventions. Further factors that add up to the limitations in Markov models are the stationarity of the transition probabilities and the interpretability which are detailed in the work of Zambon et al. [30]. Recent studies have addressed the stationarity and discretization issues by using a semi-Markov process model [18, 31, 32], nonetheless, this type of Markov models may require having an analytical deterioration model to enhance its performance [30].

2.3.2 Regression Methods

Another perspective on modeling the deterioration based on visual inspections is by using regression-based methods [12, 19, 33]. Regression is the task of modeling the relationship between the system response y and one or more system attributes (or covariates) z . This

type of model is described mathematically by, $\mathbf{y} = g(\mathbf{z})$. The data utilized in building regression models is defined by pairs of observations and covariates $\mathcal{D} = \{(z_i, y_i), \forall i = 1 : D\}$, whereby y_i is an observation associated with covariates $\mathbf{z}_i = [z_1, z_2, \dots, z_q]_i^T$. Various regression techniques are employed in solving structural health monitoring problems [34]. Within the confines of visual inspections, Artificial Neural Network (ANN) is the most common approach [12, 19, 33].

The use of ANN for modeling structural deterioration through visual inspections data has been demonstrated in different studies [12, 19]. Huang [19] identified significant structural attributes through statistical analysis (ANOVA) and utilized ANN model to predict future deterioration of concrete decks. Lee et al. [12] employed an ANN model to predict deterioration by relying on traffic volumes and population growth around the bridge area. Their study demonstrated that non-bridge factors (e.g. population growth around the bridge area) can explain structural deterioration patterns in bridges.

From the literature, it is noted that the application of regression models is generally limited in comparison with the DMM models. This is mainly attributed to the incompatibility of these models with the context of visual inspections. For example, in cases where few observations are available, it becomes challenging for a regression-based model to capture the temporal dependence in the time-series and provide a reliable prediction [35, 36]. In addition, the performance of regression methods is subject to the quality of the selected attributes utilized in training the model. The quality of a dataset can be measured by: completeness, uniqueness, timeliness, validity, accuracy and consistency [37]. From a real world standing point, these requirements are challenging to meet. Further requirements in regression analysis are related to the generality of the sample or the balanced representation of the system responses. In the context of structural health monitoring, this means having an equal representation for structural elements at all deterioration levels. The aforementioned property is challenging in practice, because the majority of structures are maintained at a good health and rarely structural elements have a poor condition. The aforementioned shortages related to the data can significantly impact the model performance, therefore, additional efforts are required to reduce the effect of these limitations. Finally, training and validating regression-based models are in most cases offline processes. Hence, at any point in time, when new inspection data becomes available, it is required to repeat the training and the validation of the model. Nonetheless, from the survey of regression-based studies, it is perceivable that some of the structural attributes can convey information about the structural deterioration pattern over time [19].

2.3.3 State-Space Models

State-space models (SSM) are well suited for time series data and allow estimating the hidden states of a system from imperfect observations. The term *hidden states* refers to the unobservable states of the system. A state-space model is composed of two models: an *observation model* and a *transition model*. The formulas describing each model are,

$$\overbrace{\mathbf{y}_t = \mathbf{C}\mathbf{x}_t + \mathbf{v}_t, \underbrace{\mathbf{v}_t : \mathbf{V} \sim \mathcal{N}(\mathbf{v}; \mathbf{0}, \mathbf{R}_t)}_{\text{observation errors}}}_{\text{observation model}} \quad (2.2)$$

$$\overbrace{\mathbf{x}_t = \mathbf{A}\mathbf{x}_{t-1} + \mathbf{w}_t, \underbrace{\mathbf{w}_t : \mathbf{W} \sim \mathcal{N}(\mathbf{w}; \mathbf{0}, \mathbf{Q}_t)}_{\text{process errors}}}_{\text{transition model}} \quad (2.3)$$

where \mathbf{y}_t represents the observations, \mathbf{C} is the observation matrix, \mathbf{x}_t is the state vector at time t : $\mathbf{x}_t : \mathbf{X} \sim \mathcal{N}(\mathbf{x}, \boldsymbol{\mu}_t, \Sigma_t)$, \mathbf{A} is the state transition matrix, \mathbf{v}_t , \mathbf{w}_t are the observation and process errors and \mathbf{R}_t , \mathbf{Q}_t represent respectively the observations and transition error covariance matrices. Different algorithms for estimating hidden states exist in the literature for different types of problems [39–41]. In this review, the mathematical formulation of *Kalman Filter* (KF), *Kalman Smoother* (KS), and constrained state estimation are described in details as this thesis build upon them in developing the proposed network-scale deterioration framework.

Kalman Filter & Kalman Smoother

The Kalman Filter (KF) is a framework for estimating the hidden states of a linear dynamical system [42]. The hidden states are estimated in the KF at time t through the *prediction step* and the *update step*. The *prediction step* is described by,

$$\begin{aligned} \mathbb{E}[\mathbf{X}_t | \mathbf{y}_{1:t-1}] &\equiv \boldsymbol{\mu}_{t|t-1} = \mathbf{A}\boldsymbol{\mu}_{t-1|t-1} \\ \text{cov}[\mathbf{X}_t | \mathbf{y}_{1:t-1}] &\equiv \Sigma_{t|t-1} = \mathbf{A}\Sigma_{t-1|t-1}\mathbf{A}^\top + \mathbf{Q}_t. \end{aligned} \quad (2.4)$$

The term $\mathbb{E}[\mathbf{X}_t | \mathbf{y}_{1:t-1}]$ refers to the expected value of the state vector \mathbf{x}_t at time t given all the observations $\mathbf{y}_{1:t-1}$ up to time $t - 1$. If an observation is available at time t , the expected value and covariance estimates are updated with the observation information using the *update step*. The update step relies on the conditional probability for estimating the posterior expected value and covariance at time t . The equations describing the update step

are,

$$\begin{aligned}
f(\mathbf{x}_t | \mathbf{y}_{1:t}) &= \mathcal{N}(\mathbf{x}_t; \boldsymbol{\mu}_{t|t}, \boldsymbol{\Sigma}_{t|t}) \\
\boldsymbol{\mu}_{t|t} &= \boldsymbol{\mu}_{t|t-1} + \mathbf{K}_t (\mathbf{y}_t - \mathbf{C}\boldsymbol{\mu}_{t|t-1}) \\
\boldsymbol{\Sigma}_{t|t} &= (\mathbf{I} - \mathbf{K}_t \mathbf{C}) \boldsymbol{\Sigma}_{t-1|t-1} \\
\mathbf{K}_t &= \boldsymbol{\Sigma}_{t-1|t-1} \mathbf{C}^\top \mathbf{G}_t^{-1} \\
\mathbf{G}_t &= \mathbf{C} \boldsymbol{\Sigma}_{t-1|t-1} \mathbf{C}^\top + \mathbf{R},
\end{aligned} \tag{2.5}$$

where $\boldsymbol{\mu}_{t|t} \equiv \mathbb{E}[\mathbf{X}_t | \mathbf{y}_{1:t}]$ the posterior expected value and $\boldsymbol{\Sigma}_{t|t} \equiv \text{cov}[\mathbf{X}_t | \mathbf{y}_{1:t}]$ the posterior covariance at time t , conditional to the observations up to time t , \mathbf{K}_t is the Kalman gain matrix, \mathbf{I} is the identity matrix and \mathbf{G}_t is the innovation covariance matrix. The KF algorithm is expressed in the short form as,

$$(\boldsymbol{\mu}_{t|t}, \boldsymbol{\Sigma}_{t|t}, \mathcal{L}_t) = \text{Kalman filter}(\boldsymbol{\mu}_{t-1|t-1}, \boldsymbol{\Sigma}_{t-1|t-1}, \mathbf{y}_t, \mathbf{A}_t, \mathbf{Q}_t, \mathbf{C}_t, \mathbf{R}_t), \tag{2.6}$$

where \mathcal{L}_t represent the log-likelihood for observation \mathbf{y}_t . In addition to KF, the Kalman smoother (KS) is utilized to improve the KF estimates retrospectively based on information from the entire time series. The *RTS Kalman Smoother* [43] equations are defined by,

$$\begin{aligned}
f(\mathbf{x}_t | \mathbf{y}_{1:T}) &= \mathcal{N}(\mathbf{x}_t; \boldsymbol{\mu}_{t|\mathbb{T}}, \boldsymbol{\Sigma}_{t|\mathbb{T}}) \\
\boldsymbol{\mu}_{t|\mathbb{T}} &= \boldsymbol{\mu}_{t|t} + \mathbf{J}_t (\boldsymbol{\mu}_{t+1|\mathbb{T}} - \boldsymbol{\mu}_{t+1|t}) \\
\boldsymbol{\Sigma}_{t|\mathbb{T}} &= \boldsymbol{\Sigma}_{t|t} + \mathbf{J}_t (\boldsymbol{\Sigma}_{t+1|\mathbb{T}} - \boldsymbol{\Sigma}_{t+1|t}) \mathbf{J}_t^\top \\
\mathbf{J}_t &= \boldsymbol{\Sigma}_{t|t} \mathbf{A}^\top \boldsymbol{\Sigma}_{t+1|t}^{-1}.
\end{aligned} \tag{2.7}$$

Constrained State Estimation

In some applications, it is required to constrain the state estimates of the state-space models, in order to prevent relying on state estimates that are incompatible with the physics of the problem. Different approaches are described in the literature for imposing constraints in the KF framework [44, 45]. In this study, the PDF truncation method [45] is utilized for handling the model state constraints. For a state vector \mathbf{x}_t with an expected value $\boldsymbol{\mu}_{t|t} \in \mathbb{R}^{n \times 1}$ and a coefficient matrix $\mathbf{H} \in \mathbb{R}^{1 \times n}$, the hidden state vector is constrained as in,

$$l \leq \mathbf{H}\mathbf{x}_t \leq u, \tag{2.8}$$

where l and u represent the lower and upper bounds respectively. The first step to apply the constraints is to transform the state vector \mathbf{x}_t into a space where the constraints are

decoupled and only a single component in \mathbf{x}_t is constrained as,

$$\bar{l} \leq \bar{x}_t \leq \bar{u}, \quad (2.9)$$

where \bar{x}_t is the transformed state corresponding to the constrained component in the original state vector, \bar{l} and \bar{u} are the transformed lower and upper bounds, respectively. Imposing the constraints in Equation 2.9 can be done by approximating a truncated PDF with an expected value $\hat{\mu}_{t|t}$ and variance $\hat{\sigma}_{t|t}^2$ estimated using the equations below,

$$\begin{aligned}\hat{\mu}_{t|t} &= \bar{\alpha} \left[\exp\left(\frac{-\bar{l}^2}{2}\right) - \exp\left(\frac{-\bar{u}^2}{2}\right) \right], \\ \hat{\sigma}_{t|t}^2 &= \bar{\alpha} \left[\exp\left(\frac{-\bar{l}^2}{2}\right) (\bar{l} - 2\hat{\mu}_{t|t}) - \exp\left(\frac{-\bar{u}^2}{2}\right) (\bar{u} - 2\hat{\mu}_{t|t}) \right] + \hat{\mu}_{t|t}^2 + 1.\end{aligned}$$

Calculating $\bar{\alpha}$, \bar{l} and \bar{u} is done according to,

$$\bar{l} = \frac{l - (\mathbf{H}\boldsymbol{\mu}_{t|t})}{\sqrt{(\mathbf{H}\boldsymbol{\Sigma}_{t|t}\mathbf{H}^\top)}}, \quad \bar{u} = \frac{u - (\mathbf{H}\boldsymbol{\mu}_{t|t})}{\sqrt{(\mathbf{H}\boldsymbol{\Sigma}_{t|t}\mathbf{H}^\top)}}, \quad \bar{\alpha} = \frac{1}{\sqrt{\pi/2 \left[\operatorname{erf}\left(\frac{\bar{u}}{\sqrt{2}}\right) - \operatorname{erf}\left(\frac{\bar{l}}{\sqrt{2}}\right) \right]}},$$

where $\operatorname{erf}(.)$ represents the error function. The constrained expected value of the state $\boldsymbol{\mu}_{t|t}$ and covariance $\boldsymbol{\Sigma}_{t|t}$ in the original state vector are updated as,

$$\begin{aligned}\boldsymbol{\mu}_{t|t} &= \mathbf{T}\mathbf{W}^{1/2}\mathbf{S}^\top [\hat{\mu} \ 0 \ \dots \ 0] + \boldsymbol{\mu}_{t|t}, \\ \boldsymbol{\Sigma}_{t|t} &= \mathbf{T}\mathbf{W}^{1/2}\mathbf{S}^\top \operatorname{diag}([\hat{\sigma}^2 \ 1 \ \dots \ 1]) \mathbf{S}\mathbf{W}^{1/2}\mathbf{T}^\top.\end{aligned}$$

The matrices \mathbf{T} and \mathbf{W} are obtained from the *Jordan* canonical decomposition of $\boldsymbol{\Sigma}_{t|t}$ and the matrix \mathbf{S} is obtained through the *Gram-Schmidt* orthogonalization [46]. Figure 2.3 illustrates an example of the PDF truncation method applied on a state vector with two components $\mathbf{x} = [x_t, \dot{x}_t]$ with $-10 < \dot{\mu}_{t|t} < 0$. In this figure, the original state in Figure 2.3a is constrained using the PDF truncation, which results in the state shown in Figure 2.3b. In addition, Figure 2.3c illustrates the transformation of the bounds and the approximation of the PDF for this example. The constraints in the transformed space becomes $\bar{u} = 0$ and $\bar{l} = -2.44$ with the transformed truncated PDF defined by $\hat{\mu} = -0.77$ and $\hat{\sigma} = 0.56$.

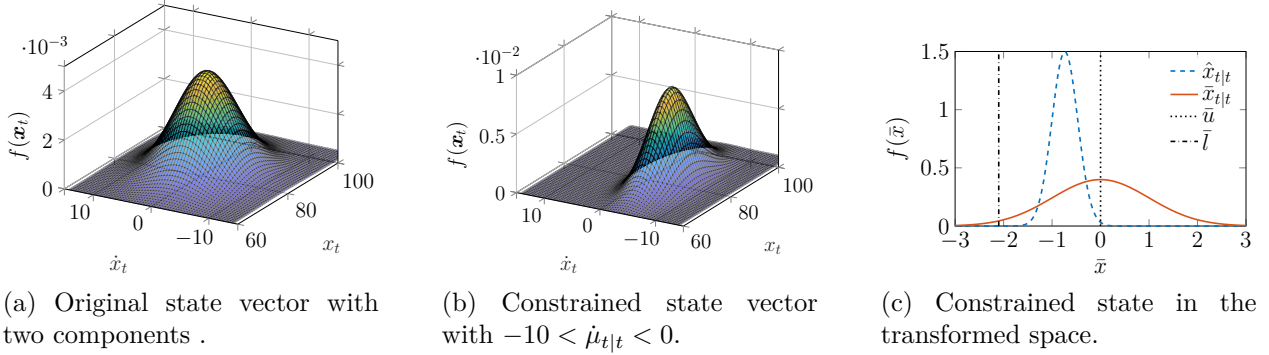


Figure 2.3 Example of applying the PDF truncation method for a state vector with a single constraint $\dot{\mu}_{t|t} < 0$.

2.4 Effect of Interventions

In the context of network-scale bridge maintenance, an intervention can be classified into three categories: *preventive maintenance*, *rehabilitation*, and *replacement* [47, 48]. While one can expect a greater improvement from a rehabilitation compared to a preventive maintenance, it is important to empirically quantify the effect of each intervention strategy on the condition of structural elements. This is because the network-scale planning of interventions is subject to budgetary constraints that require effective resource allocation [49, 50]. In addition, quantifying the effect of interventions is essential for maintaining the accuracy of deterioration analyses, as it is likely to have multiple interventions during the lifetime of structural elements. In order to quantify the effect of interventions, it is required to have information about the deterioration state of structures before and after applying interventions. Quantifying the effect of interventions based on visual inspections is traditionally done within a *Discrete Markov Model* (DMM) [14, 49, 51–53]. The effect of interventions is addressed by two metrics: the improvement in the condition, and the time delay in the deterioration [14, 53]. These quantities are determined by either relying on the expert judgment [14, 54], or through direct estimation from the inspection data [49, 51, 53]. In either cases, the effect of intervention is characterized by a deterministic value or by three values of minimum, maximum and mode [54, 55]. These representations are insufficient, as applying the same intervention on different structural elements may yield different outcomes [56]. In addition, quantifying the effect of interventions directly from the observations implies disregarding the inspectors uncertainty which is also the case in DMM deterioration models. Overall, there is currently a lack of methods where the effect of interventions on structural deterioration is explicitly quantified.

2.5 Bridge Deterioration State & Network-Scale Analyses

Performing network-scale analyses such as prioritizing maintenance of bridges under budgetary constraints, requires an overall estimate for the deterioration state of each bridge [50, 57–60]. This is done by aggregating the deterioration information of many structural elements and systems into a single metric \tilde{s}_t^j that allows performing comparisons across bridges. However, the aggregation comes at the cost of some loss in information [61]. In addition, there is a large spectrum of roles that bridges can take in the network, which implies that some bridges have more value to the network than others. For example, some bridges contribute to the traffic resilience of the network, while others contribute more to the resilience of commercial services. Therefore, it is important to consider different factors when assessing the overall deterioration estimate of bridges [62]. There exists different approaches for estimating the overall deterioration state of a bridge [57]. The ratio-based method relies mainly on the ratio of the current deterioration state $\tilde{x}_{t,p}^j$ to the perfect state u_p^j of structural elements [57, 63], represented by,

$$\tilde{s}_t^j = \frac{\sum_p^{\mathbf{E}_j} (\tilde{x}_{t,p}^j \times c_p^j)}{\sum_p^{\mathbf{E}_j} (u_p^j \times c_p^j)} \times 100,$$

where \tilde{s}_t^j is the overall estimate of the deterioration state of bridge b_j and c_p^j is the replacement cost of structural element e_p^j . The replacement cost in this approach represent the weights which emphasize the relative importance of the element to the bridge. These weights can be considered on a linear scale, or nonlinear scale that amplifies weights of elements in a poor structural condition [63]. The latter is useful in assessing the vulnerability of bridges in case of extreme events or hazards [57]. One of the limitations in the ratio-based approach is that it is challenging to estimate the actual replacement cost of elements which induce additional uncertainties on the overall estimate of the bridge deterioration state [57].

Other approaches for estimating the overall deterioration state of bridges suggest aggregating the deterioration states of the structural components based on weighted averaging of different importance factors. Importance factors can be assigned at the element-level to amplify the criticality of some elements in the bridge (e.g. the extent of damage in an element), or at the network-level to amplify the importance of some bridges over others (e.g. average annual daily traffic of a bridge). Determining the weights associated with each importance factors is a subjective task, that mainly relies on the expert judgement [57, 62]. Therefore, it is more convenient to assess each factor independently, which can convey information about the deterioration state of the network without prior hypothesis.

2.6 Conclusions from the Literature Review

The literature review has covered the main methods employed in modelling the deterioration of structures using visual inspections data. Specifically, the review examined the discrete Markov models and some of the regression-based methods. In the context of deterioration analysis using DMM, the inspectors' uncertainty is disregarded in the analyses. This is because incorporating the inspector uncertainty is associated with a significant increase in the number of model parameters that need to be estimated, which also coincides with the amount of data required for the estimation process. Furthermore, factoring information from structural attributes in DMM is challenging and comes at the expense of less data being available for estimating the transition probabilities. For example, in order to factor the structure's age, it is required to discretize the data into subsets of age groups, where each subset is represented by a set of transition probabilities. Similarly, factoring other structural attributes (i.e. material, structure type, . . . , etc.) in a Markov model will result in increasing the number of model parameters and decreasing the amount of data available for estimating each parameter. This explains why the majority of studies that use a DMM deterioration model have overlooked the dependency between the transition matrix and structural attributes. Finally, representing an intrinsically continuous process with a discrete model can result in approximation flaws, which eventually weakens the deterioration model predictive capacity and limit the potential of further deterioration analysis, such as the estimation of the deterioration speed. Considering the aforementioned limitations of the discrete models, the review has also covered the theoretical foundations of state-space models, which offers a continuous modelling alternative to DMM. The next chapters present the sub-components of a framework that relies on state-space models (SSM) to describe the deterioration behaviour using a kinematic model. The SSM allows estimating the deterioration speed and effectively quantifying the inspectors uncertainty. The use of SSM also offers compatibility with regression-based methods, which allows exploiting the common information among structures for improving the deterioration model performance. In addition, using SSM enables the stochastic modelling of the effect of interventions on structural elements as well as on a network-scale.

CHAPTER 3 Modelling Deterioration Using State-Space Models

3.1 Introduction

This chapter presents a method for modelling the deterioration behaviour of structural elements based on network-scale visual inspections. The chapter starts with a discussion about the essential modelling prerequisites associated with visual inspection data in §3.2, followed by the mathematical formulation of the proposed deterioration model based on state-space models (SSM) in §3.3. Thereafter, the details and properties of real visual inspections and synthetic data are presented in §3.5. The synthetic data is utilized to verify the SSM model performance while the real data is utilized for validation. Numerical analyses and results that demonstrate the predictive capacity of the proposed SSM deterioration model are shown in §3.5, and finally a discussion and summary of findings is presented in §3.6. The main contributions in this chapter are:

- A method for quantifying the uncertainty of the inspectors that are performing visual inspections.
- A method for quantifying inspections uncertainty based on the deterioration state of the structural element and the inspectors uncertainty.
- A validation and verification of the proposed model with real and synthetic datasets, respectively.

3.2 Visual Inspections Characteristics

This section presents existing challenges in modelling visual inspection data along with the proposed solutions that account for these challenges.

3.2.1 Inspectors Uncertainty

Visual inspections are performed by different individuals $I_i \in \mathcal{I} = \{I_1, I_2, \dots, I_{\mathcal{I}}\}$ over time, therefore, it is common to observe variability in the recorded data [10, 64, 65]. This variability is mainly attributed to the subjective nature of the evaluation. The uncertainty of observations is commonly quantified in state-space models by estimating a single standard deviation parameter σ_V common for all observations such that, for any structural element e_p^j in bridge b_j , the observation error is defined by a gaussian random variable $v_{t,p}^j : V \sim \mathcal{N}(v; 0, \sigma_V^2)$. In

order to account for the inspectors uncertainty, each inspector I_i is assigned a standard deviation parameter $\sigma_V(I_i)$. The standard deviations $\sigma_V(I_i)$ are considered as model parameters to be estimated from the data as detailed in §3.4. Such formulation allows characterizing inconsistencies that exist in sequences of observations obtained from different inspectors.

3.2.2 State-Dependant Uncertainty

In addition to considering the observations uncertainty $\sigma_V(I_i)$ as a function of the inspector, it is required to take into account that inspection uncertainty can also be dependant on the structural element condition [64]. For example, if the structural element $e_p^j \subset \mathcal{B}$ is in a perfect condition ($\tilde{x}_p^j = u$), then an inspector I_i is less likely to misjudge its condition. Such hypothesis also holds for structural elements with a poor condition ($\tilde{x}_p^j = l$). On the other hand, for structural elements with a partial damage (e.g. $\tilde{x}_p^j = \frac{l+u}{2}$), the possibility of misjudging the structural element condition becomes higher, due to the subjective nature of the evaluation. In order to accommodate the aforementioned uncertainty characteristics, a non-linear space transformation is applied on the data. Space transformation is done by using a transformation function that maps each point from the original space to a point in the transformed space (i.e. $g : [l, u] \rightarrow \mathbb{R}$).

Applying a proper transformation in this context allows the observation and transition uncertainty to become a function of the structural element's deterioration state \tilde{x} . In addition, space transformation can enable constraining the deterioration state estimate \tilde{x} within the feasible interval of the deterioration condition $[l, u]$. Acquiring both of the aforementioned properties is possible by using a step function that has two characteristics: a linear middle span with $1 : 1$ slope ratio (i.e. $\frac{dx}{d\tilde{x}} = 1$), and non-linear end, for which the first derivative is known. The proposed transformation function $g(\cdot)$ and its inverse $g^{-1}(\cdot)$ are derived from the CDF of the *Gamma distribution* defined by,

$$F(x; \alpha, \beta) = \frac{1}{\beta^\alpha \Gamma(\alpha)} \int_0^x t^{\alpha-1} e^{-\frac{t}{\beta}} dt. \quad (3.1)$$

where $\Gamma(\cdot)$ is the gamma function and $\{\alpha, \beta\}$ are the Gamma distribution parameters. By assigning the parameter $\beta = 1$, the CDF function becomes the *incomplete gamma* function [66], which is written as,

$$F(x, a) = \frac{1}{\Gamma(a)} \int_0^x t^{a-1} e^{-t} dt. \quad (3.2)$$

This function is defined for the domain $x \in (0, \infty]$; in order to have a function defined for $x \in [-\infty, \infty]$, Equation 3.2 is modified into,

$$\tilde{x} = g^{-1}(x) = \begin{cases} \frac{1}{\Gamma(\alpha)} \int_0^{x^{\frac{1}{\alpha}}} t^{\alpha-1} e^{-t} dt, & x > \frac{u+l}{2}, \\ x, & x = \frac{u+l}{2}, \\ -\frac{1}{\Gamma(\alpha)} \int_0^{x^{\frac{1}{\alpha}}} t^{\alpha-1} e^{-t} dt, & x < \frac{u+l}{2}, \end{cases} \quad (3.3)$$

where \tilde{x} represents the state in the constrained space $\tilde{x} \in [l, u]$. The transformation function $g(\cdot)$ mapping the state $\tilde{x} \in [l, u]$ to $x \in [-\infty, \infty]$ is defined by,

$$x = g(\tilde{x}) = \begin{cases} \left[\frac{1}{\Gamma(\alpha)} \int_0^{\tilde{x}} t^{\alpha-1} e^{-t} dt \right]^{\alpha}, & \frac{u+l}{2} < \tilde{x} \leq u, \\ \tilde{x}, & \tilde{x} = \frac{u+l}{2}, \\ -\left[\frac{1}{\Gamma(\alpha)} \int_0^{\tilde{x}} t^{\alpha-1} e^{-t} dt \right]^{\alpha}, & l \leq \tilde{x} < \frac{u+l}{2}, \end{cases} \quad (3.4)$$

where the parameter α is given by: $\alpha = 2^{-n}$, with n is a positive integer $n \in \mathbb{Z}^+$. The role of the parameter n is to control the curvature at the transformation function ends. Figure 3.1 illustrates the transformation function $g(\tilde{x})$ with different n values. For $n = 1$, the transformation function has a low curvature, and as the value for n increases, the curvature becomes higher. However, for any n , the slope ratio of the middle span remains fixed at 1 : 1. Moreover, it is noted that for $n \geq 4$, the change in the shape of the transformation function is insignificant, so that $n = 5$ is roughly equivalent to a linear transformation. Therefore, the possible values for the parameter n can be limited to $n \in \{1, 2, 3, 4, 5\}$. Identifying the parameter n that best suit the problem context is done through the parameter estimation framework described in §3.4. An example that demonstrates the role of the transformation function is shown in Figure 3.2. In this figure, two cases for the application of space transformation function $g^{-1}(x)$ on a Normal PDF are examined. The first case is shown in the

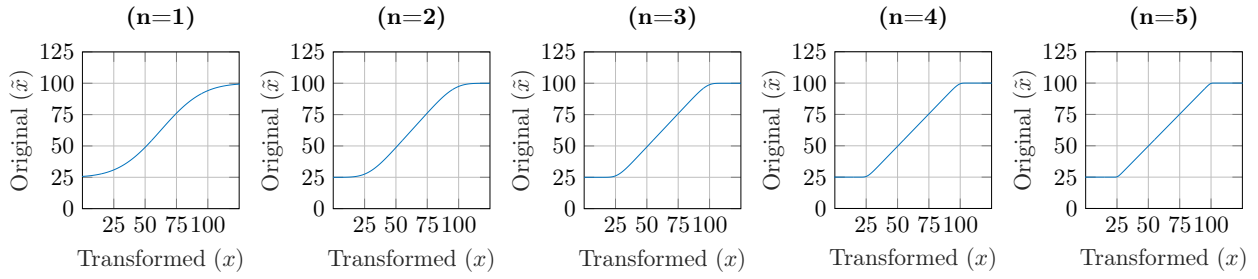


Figure 3.1 Transformation function $g(\cdot)$ with different n values.

dashed-line PDFs in Figure 3.2a and 3.2b. This example illustrates how the probability content is adjusted when the expected value of the state in the unbounded space ($x \in [-\infty, \infty]$) has a value near the lower bound $l = 25$ of the bounded space ($\tilde{x} \in [25, 100]$). On the other hand, the second example illustrated by continuous-line PDFs in Figure 3.2a and 3.2b, shows that when the expected value of the state is near the middle span of $g(.)$, the PDF in the bounded space reflects subtle differences from the PDF in the unbounded space. In sum-

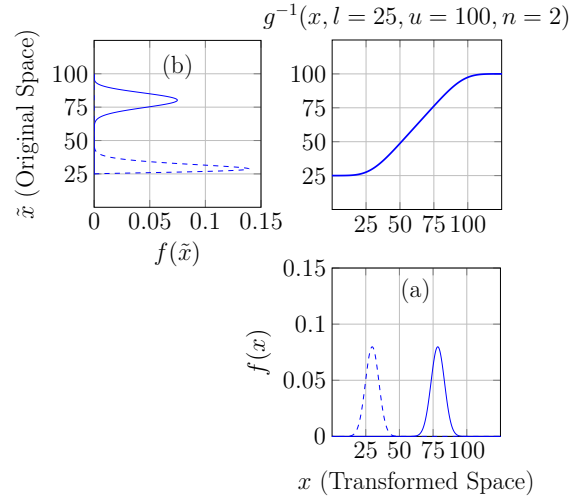


Figure 3.2 Examples of state transformation with the proposed transformation function.

mary, the purpose of introducing the transformation function $g(.)$ is to enable the inspections uncertainty to be dependent on the deterioration state of the structural element and restrict the estimated deterioration state within the feasible deterioration condition bounds $[l, u]$.

3.2.3 Monotonicity and State Constraints

The uncertainty and insufficiency of the inspection data for each structural element may result in unrealistic trends in the time series. For example, a set of observations may wrongfully indicate that an element's condition is improving over time without interventions being made on the structure. In order to prevent such a problem, constraints are applied for each time step. The constraint ensures that the deterioration condition between any consecutive time steps t and $t + 1$ is not improving. This is achieved by constraining the speed to be negative through the following criterion: $\dot{\mu} + 2\dot{\sigma} \leq 0$, where $\dot{\mu}$ and $\dot{\sigma}$ are respectively the expected value and the standard deviation of the speed \dot{x} . The PDF truncation method [45] is employed if the aforementioned constraint is violated in the proposed model.

3.3 Modelling Deterioration Using State-Space Models

The framework proposed for modelling the deterioration process in structural elements is based on the state-space models theory presented in §2.3.3. The goal of this framework is to model the deterioration behaviour with a *kinematic model* [67], that includes the element's deterioration condition x , speed \dot{x} , and acceleration \ddot{x} as defined by,

$$\underbrace{\begin{bmatrix} x_t \\ \dot{x}_t \\ \ddot{x}_t \end{bmatrix}}_{\mathbf{x}_t} = \underbrace{\begin{bmatrix} 1 & \Delta t & \frac{\Delta t^2}{2} \\ 0 & 1 & \Delta t \\ 0 & 0 & 1 \end{bmatrix}}_{\mathbf{A}} \cdot \underbrace{\begin{bmatrix} x_{t-1} \\ \dot{x}_{t-1} \\ \ddot{x}_{t-1} \end{bmatrix}}_{\mathbf{x}_{t-1}} + \underbrace{\begin{bmatrix} w_t \\ \dot{w}_t \\ \ddot{w}_t \end{bmatrix}}_{\mathbf{w}_t}, \quad (3.5)$$

where \mathbf{x}_t and \mathbf{x}_{t-1} are the state vector at time t and $t - 1$, \mathbf{A} describes the model kinematics for transitioning from \mathbf{x}_{t-1} to \mathbf{x}_t and \mathbf{w}_t is the model-error vector. The kinematic model in Equation 3.5 is employed to characterize the deterioration behaviour in bridges \mathcal{B} . Therefore, for each structural element $e_p^j \in \mathcal{E} \subset \mathcal{B}$, the *transition model* that describes the deterioration process from time $t - 1$ to time t is,

$$\mathbf{x}_{t,p}^j = \mathbf{A}\mathbf{x}_{t-1,p}^j + \mathbf{w}_t, \quad (3.6)$$

where $\mathbf{x}_{t,p}^j$ is the state vector at time t consisting of the condition $x_{t,p}^j$, the speed of degradation $\dot{x}_{t,p}^j$ and the acceleration $\ddot{x}_{t,p}^j$. The expected value of each component in the state vector $\mathbf{x}_{t,p}^j$ is represented by $\mu_{t,p}^j$ for the condition, $\dot{\mu}_{t,p}^j$ for the speed and $\ddot{\mu}_{t,p}^j$ for the acceleration. The matrix \mathbf{A} in the transition model represents the transition matrix and $\mathbf{w}_t : \mathbf{W} \sim \mathcal{N}(\mathbf{w}; \mathbf{0}, \mathbf{Q}_t)$ represents the model-error vector with the model error covariance [67] \mathbf{Q}_t defined by,

$$\mathbf{Q}_t = \sigma_W^2 \times \begin{bmatrix} \frac{\Delta t^5}{20} & \frac{\Delta t^4}{8} & \frac{\Delta t^3}{6} \\ \frac{\Delta t^4}{8} & \frac{\Delta t^3}{3} & \frac{\Delta t^2}{2} \\ \frac{\Delta t^3}{6} & \frac{\Delta t^2}{2} & \Delta t \end{bmatrix}.$$

The observation model for this SSM is described by,

$$y_{t,p}^j = \mathbf{C}\mathbf{x}_{t,p}^j + v_{t,p}^j, \quad (3.7)$$

where $y_{t,p}^j$ is the observation in the transformed space, \mathbf{C} is the observation matrix defined by $\mathbf{C} = [1 \ 0 \ 0]$, and $v_{t,p}^j : V \sim \mathcal{N}(v; 0, \sigma_V^2(I_i))$ is the observation error with $\sigma_V(I_i)$ being the standard deviation of the error associated with the observations of an inspector $I_i \in \mathcal{I}$. Figure

3.3 illustrates the details and the steps of the proposed degradation model for predicting and forecasting the deterioration behaviour of a single structural element e_p^j from time t up to time T . In this context, time T represents the time step associated with the last inspection point.

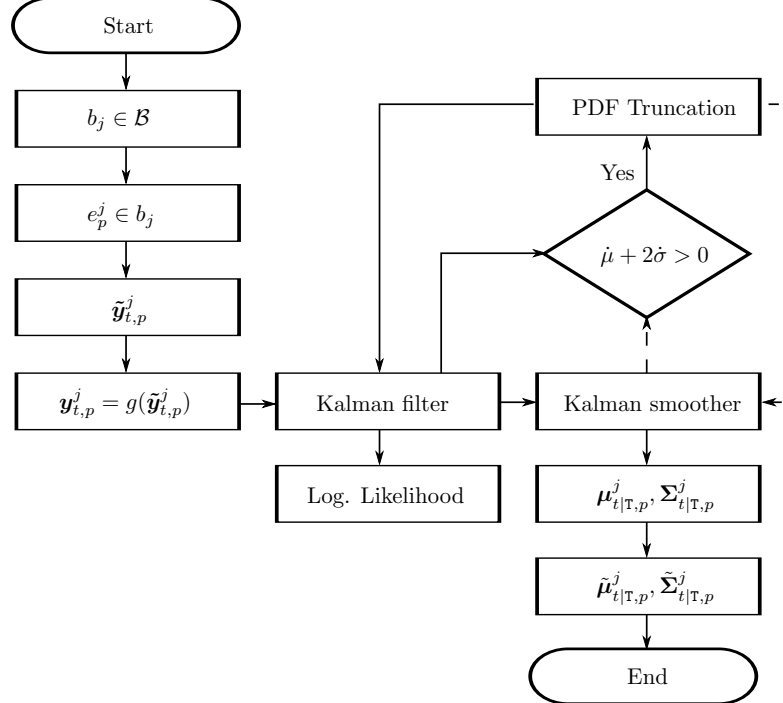


Figure 3.3 Structural degradation model for predicting and forecasting the deterioration state of structural element e_p^j from time t to time T .

The framework starts with the observation $\tilde{y}_{t,p}^j \in [l, u]$ representing the condition of structural element $e_p^j \in \mathcal{E} \subset \mathcal{B}$. The observation $\tilde{y}_{t,p}^j$ is passed in the transformation function $g(\cdot)$ presented in Equation 3.3 to obtain the transformed state observation $y_{t,p}^j \in \mathbb{R}$. Following the transformation step, the observations are ready for the time series analysis through the Kalman filter and smoother. For any time series data $\mathbf{y}_{t,p}^j$, the Kalman filter starts at time $t = 0$ with an initial estimate for the state expected value vector $\boldsymbol{\mu}_{0,p}^j = [\mu_{0,p}^j \dot{\mu}_{0,p}^j \ddot{\mu}_{0,p}^j]^\top$ and the covariance matrix $\boldsymbol{\Sigma}_{0,p}^j = \text{diag}[\sigma_{0,p}^j \dot{\sigma}_{0,p}^j \ddot{\sigma}_{0,p}^j]^2$. In the covariance matrix, the variance of the initial speed is described by the function,

$$(\dot{\sigma}_0)^2 = p_1^2(u - \tilde{\mu}_1) + p_2^2, \quad (3.8)$$

where p_1, p_2 are model parameters to be estimated from the inspection data and $\tilde{\mu}_1$ is the expected value of the condition at time $t = 1$. Initially $\tilde{\mu}_1$ is considered equal to the first

observation $\tilde{\mu}_1 = \tilde{y}_1$, however, after obtaining the smoothed states, $\tilde{\mu}_1$ is set equal to the expected value of the smoothed state $\tilde{\mu}_1 = \tilde{\mu}_{1|\text{T}}$. The function in Equation 3.8 is chosen based on the *maximum likelihood estimate* (MLE) method in the real data and direct experimentation with synthetic data. This variance model is employed to facilitate the estimation of the initial speed, given that few observations are available in each time series. Furthermore, the initial estimate for the expected condition $\mu_{0,p}^j$ is assumed to be equal to the average of the first three observations, while the initial expected speed and acceleration are considered as $\dot{\mu}_{0,p}^j = \ddot{\mu}_{0,p}^j = 0$. The initial state $\boldsymbol{\mu}_{0,p}^j$, $\boldsymbol{\Sigma}_{0,p}^j$ is propagated over time using the *prediction step* and the *update step* of the Kalman filter (see §2.3.3). After each update step, the constraint $\dot{\mu}_{t|t,p}^j + 2\dot{\sigma}_{t|t,p}^j \leq 0$ is examined as described §3.2.3. If the aforementioned constraint is violated, the PDF truncation method is employed to constrain the estimate of the speed $\dot{x}_{t|t,p}^j$ within the feasible bounds. Following the filtering step, the Kalman smoother is utilized to refine the state estimates and the initial state at time $t = 0$. Provided that the number of observations per structural element is limited, the estimate of the initial state $\boldsymbol{x}_{0,p}^j$ can be further improved in the parameter estimation framework, which is detailed in the next section. After the smoothing step, the outputs $\boldsymbol{\mu}_{t|\text{T},p}^j$, $\boldsymbol{\Sigma}_{t|\text{T},p}^j$ are back-transformed to the original space $\tilde{\boldsymbol{\mu}}_{t|\text{T},p}^j$, $\tilde{\boldsymbol{\Sigma}}_{t|\text{T},p}^j$ for interpretation and analysis. This back-transformation step is done using the inverse transformation function $g^{-1}(.)$ described in Equation 3.3. The next section describes the unknown model parameters and the estimation method.

3.4 Model Parameter Estimation

The unknown model parameters to be estimated from the inspection data are: the inspectors standard deviations $\sigma_V(I_i)$, the standard deviation of the transition model error σ_W , the transformation function parameter n and the initial state parameters $\{\sigma_0, \ddot{\sigma}_0, p_1, p_2\}$. These parameters are grouped in the following set:

$$\boldsymbol{\theta} = \left\{ \underbrace{\sigma_V(I_{1:1})}_{\text{Inspectors std's.}}, \underbrace{\sigma_W}_{\text{Process error std.}}, \underbrace{n}_{\text{Transform. Param.}}, \underbrace{\sigma_0, \ddot{\sigma}_0, p_1, p_2}_{\text{Initial state.}} \right\}. \quad (3.9)$$

The parameter estimation framework for the parameters $\boldsymbol{\theta}$ is based on the *maximum likelihood estimate* (MLE) method. The MLE estimate is obtained through maximizing the joint prior probability of observations while assuming the observations to be conditionally independent given the state x . Thus, the likelihood for a sequence of observations can be obtained through the product,

$$f(y_{1:\text{T}}|\boldsymbol{\theta}) = \prod_{t=1}^{\text{T}} f(y_t|y_{1:t-1}, \boldsymbol{\theta}). \quad (3.10)$$

In order to avoid numerical instabilities, the natural logarithm is taken for the likelihood estimate. Hence, Equation 5.10 becomes the *log-likelihood* estimate described by,

$$\ln f(y_{1:T}|\boldsymbol{\theta}) = \sum_{t=1}^T \ln f(y_t|y_{1:t-1}, \boldsymbol{\theta}). \quad (3.11)$$

Because the analysis in the proposed framework are performed on a network-scale, the *log-likelihood* estimate is taken for the inspection sequences of all the structural elements $e_p^j \forall j, p$ combined. Therefore, the network-scale *log-likelihood* becomes,

$$\mathcal{L}(\boldsymbol{\theta}) = \sum_{j=1}^B \sum_{p=1}^{E_j} \sum_{t=1}^{T_p} \ln f(y_{t,p}^j | y_{1:t-1,p}^j, \boldsymbol{\theta}), \quad (3.12)$$

whereby B is the total number of bridges, E_j is the total number of structural elements in the j -th bridge and T_p is the total number of observations for the p -th structural element. From Equation 3.12, in order to identify the set of parameters $\boldsymbol{\theta}^*$ that maximizes the *log-likelihood* estimate, the following optimization problem is to be solved,

$$\begin{aligned} \boldsymbol{\theta}^* &= \arg \max_{\boldsymbol{\theta}} \mathcal{L}(\boldsymbol{\theta}), \\ \text{subject to: } &\sigma_W, \sigma_0, \ddot{\sigma}_0, p_1, p_2 > 0, \\ &\sigma_V(I_i) > 0, \forall I_i \in \mathcal{I}, \\ &n \in \{1, 2, 3, 4, 5\}. \end{aligned} \quad (3.13)$$

Solving this optimization problem is achieved through an iterative gradient-based optimization framework. The steps of the estimation framework are illustrated in the pseudocode shown in Appendix A [68]. In this framework, the model parameters $\boldsymbol{\theta}$ are optimized initially with the assumption that the standard deviation σ_V of the observation uncertainty is equal across all inspectors, $\sigma_V(I_1) = \sigma_V(I_2) = \dots = \sigma_V(I_I) = \sigma_V$. Therefore, the initial optimization step is performed on the set of parameters $\boldsymbol{\theta}^s = \{\sigma_W, \sigma_V, \sigma_0, \ddot{\sigma}_0, p_1, p_2\}$. This step provides an initial value for the model parameters along with an initial value for the standard deviation associated with each inspector $\sigma_V(I_{1:1}) = \sigma_V$. Thereafter, the optimization algorithm iterates over the $\sigma_V(I_i)$ parameters while keeping other model parameters in $\boldsymbol{\theta}$ fixed. The framework keeps iterating over the inspectors parameters $\sigma_V(I_i)$ until the improvements in the objective function $\mathcal{L}(.)$ are less than the tolerance threshold ϵ or the stall limit is met. The stall limit is a predefined number of iterations where improvements in the objective function $\mathcal{L}(.)$ are less than 5%. Following the convergence of the parameters $\sigma_V(I_i)$, the optimization algorithm revisits the model parameters in the subset $\boldsymbol{\theta}^m = \{\sigma_W, \sigma_0, \ddot{\sigma}_0, p_1, p_2\} \subset \boldsymbol{\theta}$. The it-

erative framework keeps alternating between the $\sigma_V(I_i)$ parameters and the parameters in the subset $\boldsymbol{\theta}^m$ until the global convergence criteria is met. As for the parameter n , since the number of possible values for n is limited, the full optimization procedure is repeated with different n values in order to identify the value that maximizes the objective function. In this optimization scheme, the upper and lower bounds for the model parameters are defined as follows: $\sigma_W \in [10^{-3}, 0.01]$, $\sigma_V \in [1, 10]$, $\sigma_0 \in [1, 10]$, $\ddot{\sigma}_0 \in [10^{-3}, 0.05]$, $p_1 \in [0, 0.05]$, $p_2 \in [0, 0.15]$. The aforementioned bounds were obtained from experimentation with real and synthetic inspection data in order to ensure the deterioration model is consistent with realistic structural deterioration curves, especially in cases that have either insufficient data and/or highly noisy data.

3.5 Case Studies

Evaluating the SSM deterioration model performance is done using synthetic data for verification and real data for validation. This section presents the main characteristics of visual inspection datasets, followed by the deterioration analyses on structural elements from each dataset.

3.5.1 Visual Inspections and Synthetic Data

In this section, a detailed description of the real visual inspections dataset and the evaluation method is presented. Thereafter, the characteristics of synthetic data are outlined along with the equations utilized for generating it.

Visual Inspection Data

The real dataset includes information from a network of approximately $B \approx 10000$ structures $\mathcal{B} = \{b_1, b_2, \dots, b_B\}$, located in the province of Quebec, Canada. Visual inspections in this dataset are performed on a yearly basis with dates ranging from late 2007 up to early 2020. During that time-window, the majority of bridges have been inspected from 3 to 5 times. Each structural element e_p^j is evaluated according to a codified procedure [7]. The evaluation method requires the inspectors to break down the health condition into four categories according to the damage severity. The categories are: A: *Nothing to little*, B: *Medium*, C: *Important* and D: *Very Important*. An example of a structural element inspection data at a given time t is: $y_a = 80\%$, $y_b = 20\%$, $y_c = 0\%$, $y_d = 0\%$. In the example, the inspection data implies that 80% of the structural element area has no damages (category A), while the remaining 20% of the element area has medium damages (category B). Accordingly, the sum

of the values under each category (A, B, C, and D) for a single element must be equal to 100% (i.e. $y_a + y_b + y_c + y_d = 100\%$), and the evaluation in each category must pertain to $0\% \leq y_a, y_b, y_c, y_d \leq 100\%$.

Representing the deterioration level using four interdependent metrics increases the complexity of the analysis. This is because of the need to model the deterioration according to each metric while accounting for the dependency across other metrics. Therefore, data aggregation is applied to transform the four metrics of any inspection point into a single metric. The data aggregation method is similar in concept to the expected utility theory approach [69], where the weights ω_i are assigned to each state category. Hence, the aggregation formula for any inspection data is,

$$\tilde{y} = \omega_1 y_a + \omega_2 y_b + \omega_3 y_c + \omega_4 y_d, \quad (3.14)$$

whereby \tilde{y} is the aggregated observation representing the inspection data (y_a, y_b, y_c, y_d) . In this study, the values proposed for the weights are: $\omega_1 = 1$, $\omega_2 = 0.75$, $\omega_3 = 0.5$, $\omega_4 = 0.25$. Employing the aforementioned weights restrain the aggregated measure within the range $\tilde{y} \in [25, 100]$. Hence, a structural element with $(\tilde{y} = 100)$ corresponds to the state undamaged ($y_a = 100\%, y_b = 0\%, y_c = 0\%, y_d = 0\%$), while a structural element with $(\tilde{y} = 25)$ corresponds to the state *Very Important* damage ($y_a = 0\%, y_b = 0\%, y_c = 0\%, y_d = 100\%$). All numerical analysis are carried out using the aggregated observation \tilde{y} .

Synthetic Visual Inspection Data

A synthetic dataset is generated to be quantitatively and qualitatively representative of the real inspection database. The total number of structural elements e_p^j in the synthetic dataset is $E = 10827$. The structural elements considered in this analysis are for the element type *beam*, with an average service-life of $T = 60$ years. The health condition of the structural elements is represented by a continuous numerical value within the range $\tilde{y} \in [25, 100]$.

To start generating the synthetic data, the true state of deterioration is generated for each synthetic structural element e_p^j through the transition model in Equation 3.6. The true state of the deterioration has to maintain the qualitative characteristics of a real deterioration, which is done by examining several criteria. These criteria are obtained through empirical experiments and analyses with real and synthetic data. The criteria are,

1. Slow deterioration: $x_{\frac{T}{2}} > 0.85 \times x_1$.
2. Plateau in the deterioration curve: $x_T > 0.5 \times x_1$.
3. Speed threshold: $\dot{x}_1 < 0.01 \times x_1 - 1.3$.
4. Acceleration threshold: $\ddot{x}_1 < 0.001 \times x_1 - 0.13$.

A deterioration curve with any of the above-mentioned conditions is rejected and excluded from the synthetic database. After generating the true deterioration curves, a set of 194 synthetic inspectors $\mathcal{I} = \{I_1, I_2, \dots, I_{194}\}$ is generated. Each synthetic inspector is assumed to have a zero-mean error with $v_t : V \sim \mathcal{N}(0, \sigma_V^2(I_i))$. The standard deviation $\sigma_V(I_i)$ is generated for each synthetic inspector from a uniform distribution $\sigma_V(I_i) \sim U(v_1, v_2)$. The parameters considered in this study are $v_1 = 1$ and $v_2 = 6$ representing the minimum and maximum values of a uniform distribution. Thereafter, the observation model described in Equation 3.7 is utilized to generate an observation sample from the true deterioration state. Figure 3.4 illustrates the true deterioration curve for a synthetic structural element e_1^{623} and the set of synthetic inspections associated with it. The number of observations per synthetic

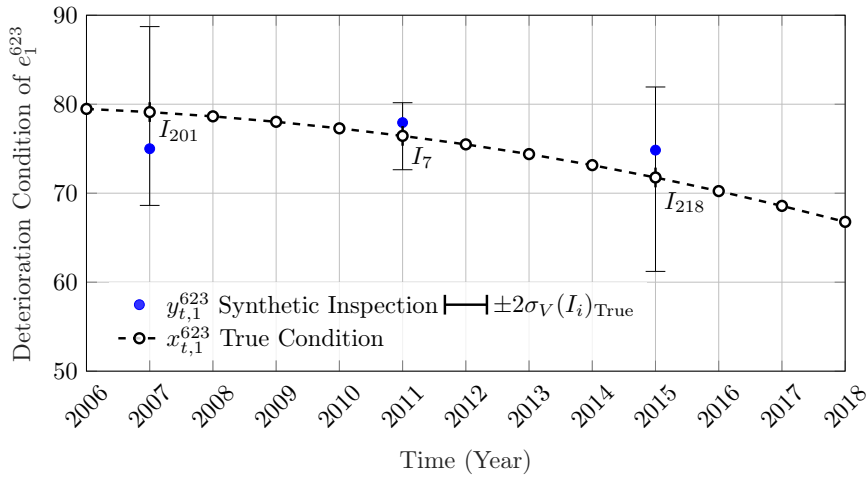


Figure 3.4 Sample of synthetic inspections $y_{t,1}^{623}$ taken from a true deterioration condition of synthetic structural element e_1^{623} using synthetic inspectors I_i .

structural element is determined in accordance with the real dataset, which is 3 to 5 observations $\mathbf{y}_{t,p}^j$ per structural element for the majority of structures, while few structures have 6 to 8 observations per structural element. Accommodating this property is done using weighted sampling, with the weights determined from the real dataset.

The true state and the observations are generated in the transformed space with a transformation function parameter $n = 3$. The standard deviation of the process error is assumed to be $\sigma_W = 5 \times 10^{-3}$.

3.5.2 SSM Model Verification & Analyses with Synthetic Data

The main goal of performing analysis with synthetic data is to verify the predictive capacity of the proposed deterioration model with a dataset that is representative of the real dataset.

The use of synthetic data can also enable verifying the performance of the parameter estimation framework since the model parameters are known in the synthetic case. Estimating the model parameters based on the synthetic data is done as described in §3.4. The set of model parameters θ estimated through the parameter estimation framework is shown in Table 3.1, while Figure 3.5 shows the estimation results of the $\sigma_V(I_i)$ parameters.

Table 3.1 Estimated model parameters from synthetic inspection data.

σ_W	σ_0	σ_V	$\ddot{\sigma}_0$	p_1	p_2	n
2.1×10^{-3}	1.241	3.001	0.0498	0.0421	0.0611	3

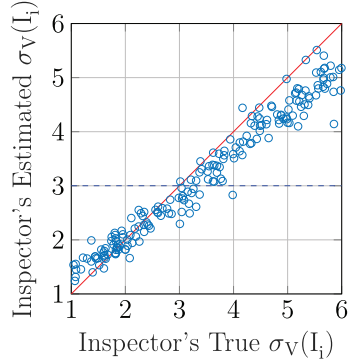


Figure 3.5 Scatter plot of inspectors true $\sigma_V(I_i)$ vs. estimated $\sigma_V(I_i)$ with a dashed line representing the initial value at the start of the optimization.

In Figure 3.5, the horizontal dashed line corresponds to σ_V , which is the initial estimate for all $\sigma_V(I_i)$, $\forall I_i \in \mathcal{I}$. By considering the alignment among the true and estimated $\sigma_V(I_i)$, the scatter plot in Figure 3.5 confirms that the proposed parameter estimation method is capable of estimating the standard deviations $\sigma_V(I_i)$ associated with the inspectors from network-scale inspection data.

Following the assessment of the estimated model parameters θ^* , the performance of the deterioration model is examined at the structural element-level. Examples that examine the predictive capacity of the deterioration model for structural elements are shown in Figures 3.6-3.8. These examples demonstrate the deterioration-model performance for different cases, verified by the true deterioration for the synthetic structural element. The deterioration forecast in the examples is considered for a period of 10 years. The first example shows a low variability case represented by the set of observations $\hat{y}_{t,1}^{837}$ from the synthetic structural element e_1^{837} . The deterioration model performance in this example is illustrated in Figure 3.6, where it can be noticed that the model estimates are consistent with the true deterioration

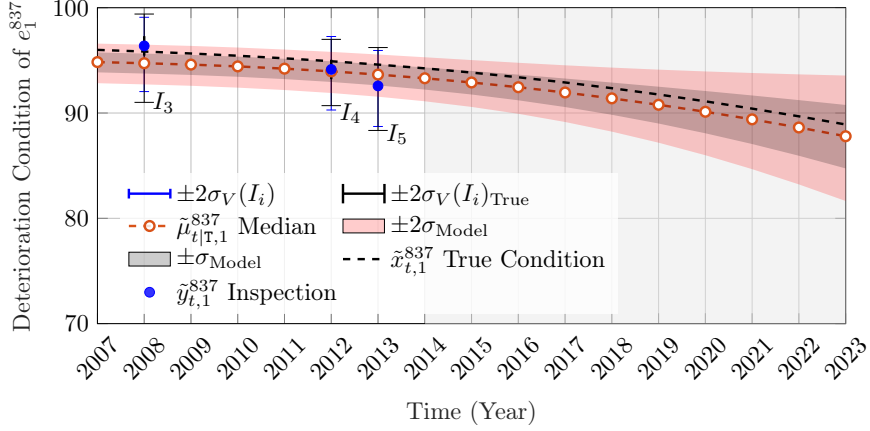


Figure 3.6 Condition deterioration analysis based on the observations $\tilde{y}_{t,1}^{837} \in [25, 100]$ of the synthetic structural element e_1^{837} , with error bars representing the inspectors true (wide whiskers) & estimated (narrow whiskers) uncertainties, and the shaded area representing the forecast period.

during the prediction phase and stays consistent throughout the total forecast period. The good performance in this case can be attributed to having inspectors with relatively small uncertainties along with consistent inspection data. The speed estimates associated with this case are shown in Figure 3.7a. The speed estimate starts with a low uncertainty when the de-

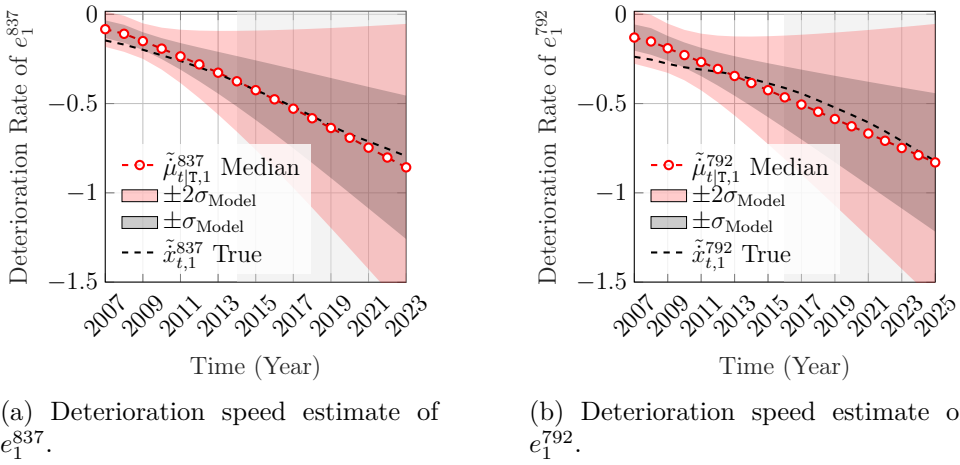


Figure 3.7 Deterioration speed estimate for synthetic structural elements, with the shaded area representing the forecast period.

terioration speed is near zero due to the model constraints, thereafter, the uncertainty grows larger as the deterioration speed increases. The true deterioration speed nearly overlaps with the model estimate throughout the forecast period which demonstrates an excellent forecast

performance.

The second example illustrates the deterioration model performance with a series of inspections that has high variability. This case is demonstrated by the set of observations $\mathbf{y}_{t,1}^{792}$ of synthetic structural element e_1^{792} . The model performance in forecasting the deterioration condition is shown in Figure 3.8. The three observations in this time-series came from inspec-

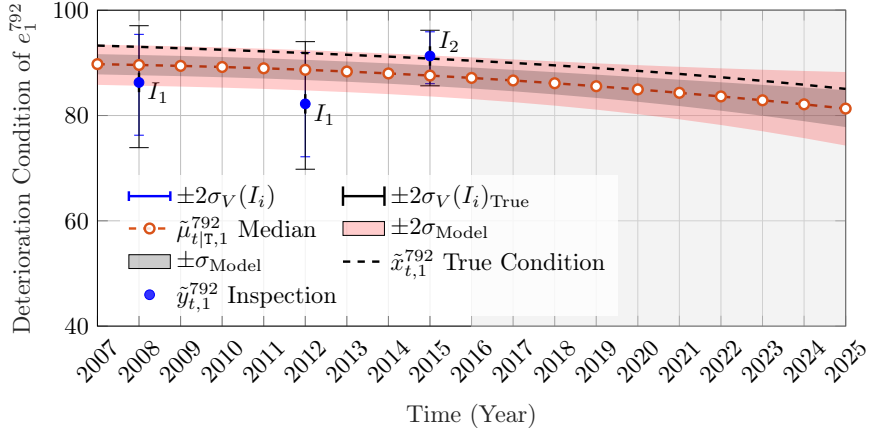


Figure 3.8 Condition deterioration analysis based on the observations $\tilde{\mathbf{y}}_{t,1}^{792} \in [25, 100]$ of the synthetic structural element e_1^{792} with error bars representing the Inspectors true (wide whiskers) & estimated (narrow whiskers) uncertainties, and the shaded area representing the forecast period.

tors that have high uncertainties. This justifies the deviation of the deterioration model from the true state in the prediction phase. In addition, this case emphasizes the importance of estimating the inspectors uncertainties $\sigma_V(I_i)$, given that the model estimate puts more weight on the data from the inspector I_2 because he has a lower uncertainty. The deterioration speed estimate along with the true speed are shown in Figure 3.7b. The deterioration-speed estimates, as shown in Figure 3.7b, shows a similar performance to the deterioration condition prediction phase with the true speed being within the $\pm 2\sigma_{\text{Model}}$ interval. It can be noticed that the poor initial speed estimate is associated with an inferior model performance in estimating the deterioration condition. This asserts the importance of having a good initial state estimate for the deterioration model especially in short time-series data.

In order to examine the overall performance of the deterioration model, a dataset of $E_s = 3250$ ($\approx 30\%$ of E) structural elements e_p^j are analyzed. The deterioration forecast is assessed for a period of 10 years for each structural element $e_p^j \in \mathcal{E}$. The yearly average of the forecast absolute error in the expected condition $\mu_{t|\mathbf{T},p}^j$, the expected speed $\dot{\mu}_{t|\mathbf{T},p}^j$ and the expected acceleration $\ddot{\mu}_{t|\mathbf{T},p}^j$ are shown in Figure 3.9. In this graph, it can be noticed that the yearly average of the absolute errors in each category increases over the forecast time except for

the acceleration; because the condition and the speed are changing monotonically, the errors can accumulate during the forecast; however, the acceleration is locally constant over time so that the errors has the possibility to average out. Moreover, the bias in the expected

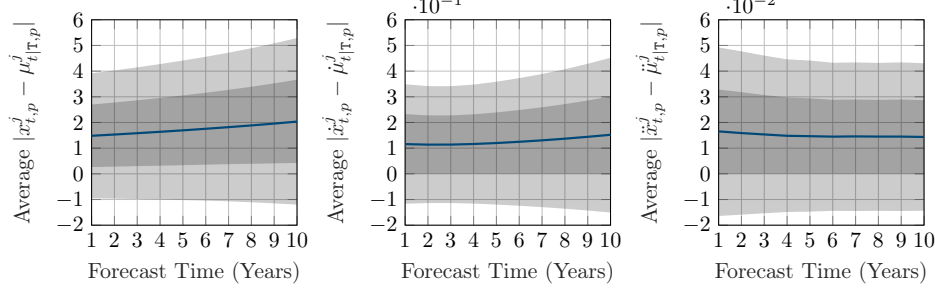


Figure 3.9 Absolute average error in forecast time for the expected condition, speed and acceleration based on the true condition, speed and acceleration respectively, with the 95% confidence interval ($\pm 2\sigma$) for each error.

condition of the forecast is examined with scatter plots generated at different years. The graphs shown in Figure 3.10 illustrates the true condition $\tilde{x}_{t,p}^j$ versus the model expected condition $\tilde{\mu}_{t|T,p}^j$ generated at forecast years {1, 5, 10}. It is noticed from Figure 3.10 that the deterioration model maintains a good predictive capacity over time for the majority of structural elements. Furthermore, in analyses with synthetic data, the model has sustained a good performance for longer periods > 10 year, however, the results obtained from these analyses are not conclusive. This is because the number of experiments was limited, and the experiments performed did not take into account the effect of external factors such as the effect of climate change.

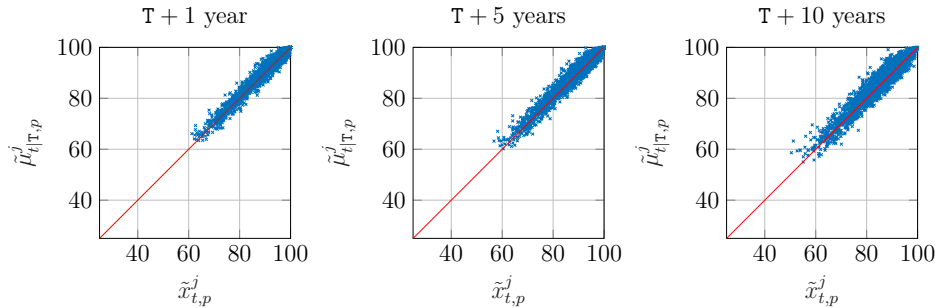


Figure 3.10 Scatter plot for the model estimate of the condition $\tilde{\mu}_{t|T,p}^j$ vs. the true condition $\tilde{x}_{t,p}^j$ at forecast years 1, 5 and 10.

Further analysis includes assessing the confidence interval of the model estimates. Specif-

ically, the probability of the true deterioration condition being within the 95% confidence interval (i.e. $\mu \pm 2\sigma$) of the model state estimate. For that end, the probability of the true state being within the range of $\mu_{t|\mathbf{T},p}^j \pm 2\sigma_{t|\mathbf{T},p}^{x,j}$ is computed at each year and for all structural elements e_p^j . Figure 3.11 illustrates the aforementioned probability of the model state estimate over the forecast time. In Figure 3.11, the dashed line represents the average probability

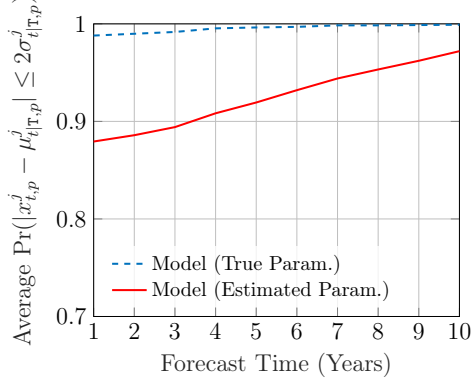


Figure 3.11 The probability of the true condition being within the 95% confidence interval of the model predicted state for the model with the true parameters (dashed) and the estimated parameters.

of $x_{t,p}^j$ being within $\mu_{t|\mathbf{T},p}^j \pm 2\sigma_{t|\mathbf{T},p}^{x,j}$ for a deterioration model with true parameters (including the true initial speed and acceleration for each time series) while the solid line represents the average probability of $x_{t,p}^j$ being within $\mu_{t|\mathbf{T},p}^j \pm 2\sigma_{t|\mathbf{T},p}^{x,j}$ for a deterioration model with estimated parameters. It can be noticed that the model with the estimated parameters achieves a probability of $\approx 87\%$ when forecasting one year ahead, while the same model with the true parameters has a probability of $\approx 98\%$.

3.5.3 SSM Model Validation & Analyses with Real Data

Following the verification step, the proposed deterioration model is validated using real inspection data. The dataset considered in the analyses is the inspection dataset for structural elements of type *Beam* taken from bridges $\mathcal{B} = \{b_1, b_2, \dots, b_j\}$. The total number of structural elements employed in the estimation is $E = 10827$ structural elements representing a sample of 2593 bridges. The majority of the selected structural elements has 3 to 5 inspections per element, performed by different inspectors (a total of 194 inspectors). In this dataset, the health condition of the structural elements is represented by a continuous numerical value within the range $\tilde{y} \in [25, 100]$. It should be noted that the number of structural elements is obtained after excluding time series data that is identified as excessively noisy or insuffi-

cient. In this study, an excessively noisy or insufficient time series of a structural element is identified by:

1. The total number of observations in the time series is less than three.
2. The number of observations that indicate significant improvement $y_{t+\Delta t} - y_t > 5$ in the structural element is greater than the number of observations indicating otherwise. Δt here refers to the time span between two consecutive observations.
3. The time series has excessively high observation errors $|y_{t+\Delta t} - y_t| > 15$.

The parameter estimation results for the deterioration model are shown in Table 3.2 except for the estimated $\sigma_V(I_i)$ values which are represented in a histogram shown in Figure 3.12.

Table 3.2 Estimated model parameters from real inspection data.

σ_W	σ_0	σ_V	$\ddot{\sigma}_0$	p_1	p_2	n
5.236×10^{-3}	1	4.021	0.049	0.045	0.002	4

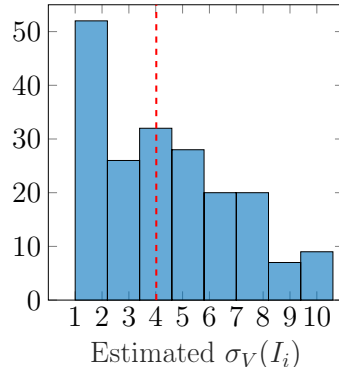


Figure 3.12 Histogram for the estimated $\sigma_V(I_i)$ values in the transformed space for real inspectors (total: 194 inspectors) with a dashed line representing the initial value at the start of the optimization.

In order to validate the deterioration model performance, different examples for patterns of inspection data are analyzed. The first example for the real inspection data considers the model performance in the case where the set of inspections has a low variability. This case is illustrated with the inspection data shown in Figure 3.13 for structural element e_1^{14} in bridge b_{14} . In Figure 3.13, the model estimate has a small uncertainty in the prediction phase. This is attributed to the structural element e_1^{14} being in a near perfect condition according to the inspection data as well as having consistency and low uncertainty in the inspection data. It

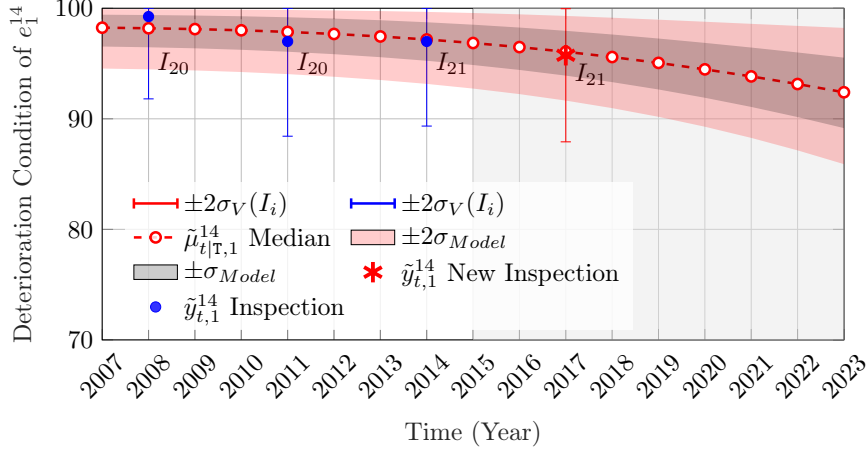


Figure 3.13 Condition deterioration analysis based on observations $\tilde{y}_{t,1}^{14} \in [25, 100]$ of the real structural element e_1^{14} with error bars representing the inspectors estimated uncertainties, and the shaded area representing the forecast period.

can be noticed that inspector I_{20} appears to have two different $\sigma_V(I_i)$, as shown in the first and the second inspection points. This is because the uncertainty associated with each observation is dependent on the structural element deterioration state $x_{t,p}^j$ as previously detailed in §3.2.2. Moreover, the inspection data point at year 2017 (represented by the asterisk symbol) is a validation point which is not included when estimating the model parameters $\boldsymbol{\theta}^*$ nor the update step of KF. It can be noticed that the deterioration model forecast is consistent with this new inspection data. The deterioration speed associated with this condition estimate is shown in Figure 3.14a. The next example, shown in Figure 3.15, demonstrates the model

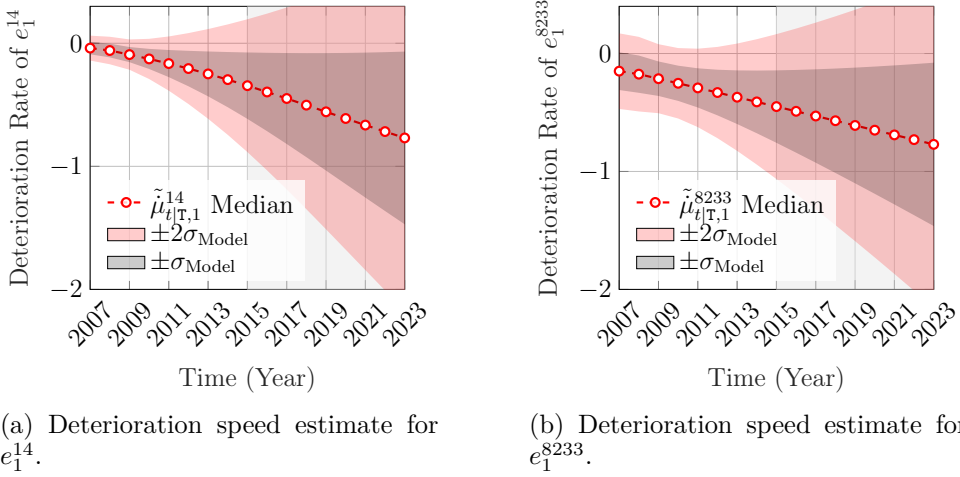


Figure 3.14 Deterioration speed estimate for real structural elements, with the shaded area representing the forecast period.

performance in the case where the inspection data display high variability. The deterioration

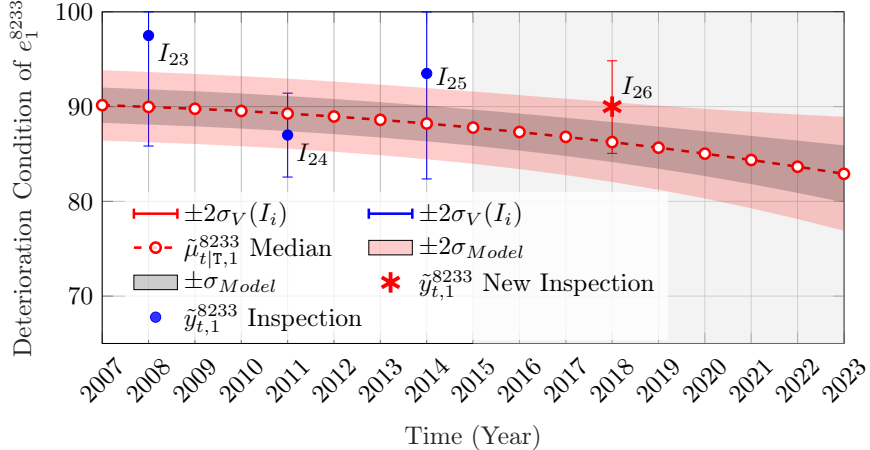


Figure 3.15 Condition deterioration analysis based on observations $\hat{y}_{t,1}^{8233} \in [25, 100]$ of the real structural element e_1^{8233} with error bars representing the inspectors estimated uncertainties, and the shaded area representing the forecast period.

model in this case maintains a downward deterioration curve while accounting for the inspections data according to their respective estimated uncertainties. Moreover, and similarly to the previous example, the model forecast stays consistent with the new inspection data point at year 2018. The deterioration speed associated with the condition estimate for e_1^{8233} is shown in Figure 3.14b.

In order to assess the bias in the deterioration model for the real database, a scatter plot for the model forecast versus new inspection data points is presented in Figure 3.16a. The term *new inspections* refers to observations that were never used in training the deterioration model. Each point in Figure 3.16a represent a model forecast $\tilde{\mu}_{t|T}$ versus a new inspection \tilde{y}_t at time t for a population of structural elements e_p^j . The symbol associated with each point represents the number of years until the new inspection data (observation) has arrived. For example, in a structural element e_p^j , a duration of 4 years refers to the time between two consecutive inspections, in which one of them is the new inspection point. It should be noted that the model forecast is not required to perfectly match the observations due to the presence of observations uncertainties. Considering the same scatter plot, the uncertainty associated with each new observation can be illustrated by the symbol size as shown in Figure 3.16b. In Figure 3.16b, the points with the lowest uncertainty are the closest to the diagonal, however, for points with the uncertainty $\sigma_V > 4$, the scatter tend to spread away from the diagonal. Furthermore, it can be noticed that the model does not show any significant sign of bias toward overestimating or underestimating the deterioration condition. In order to further assess the bias, a normalized histogram is shown in Figure 3.16c in order to examine

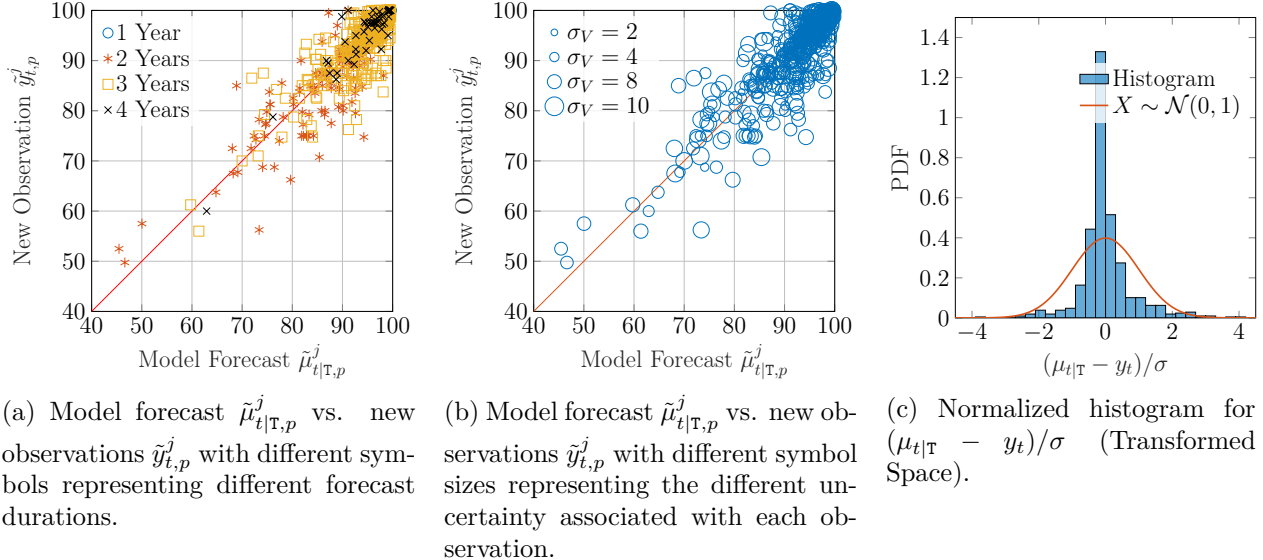


Figure 3.16 Deterioration condition validation for real structural elements.

the difference between the model forecast and the new observations. The histogram shows that the normalized bias and dispersion in the deterioration model forecast are compatible with the PDF of standard Normal distribution. From the analyses above, the deterioration model have displayed a performance similar to the analyses with the synthetic inspection data, which validates the conclusions taken from the analyses with the synthetic data.

3.6 Conclusion

This chapter presented a network-scale SSM deterioration model for the visual inspections of a bridge-network. The model enables quantifying the uncertainty of visual inspections through estimating the standard deviation associated with each inspector as well as considering the inspection uncertainty dependent on the deterioration state. The analyses with synthetic data have demonstrated a good performance for the model in estimating the uncertainty associated with each inspector (a total of 194 inspectors). In addition, the deterioration analyses with the synthetic data have shown a good predictive capacity for the proposed framework. The assessment considered a forecast period of 10 years for each synthetic structural element. From the analyses, the probability of the true condition being within the confidence interval $\mu \pm 2\sigma$ of the model forecast is estimated at 87%. The deterioration model has been also validated with real inspection data. The analyses included validation with inspection data that were not included at the model parameter estimation phase nor the update step of KF. The assessment have shown that the model is unbiased towards overestimating or underestimating

the structural elements condition. Overall, the deterioration analyses have shown that the proposed framework has a consistent and robust performance with respect to highly noisy data. Future improvements to the proposed framework can include examining the inspectors bias, as well as a Bayesian framework for the estimation of the model parameters. Including the inspector bias can be done through estimating the mean parameter in the observations error term. Furthermore, the analyses with the deterioration speed and acceleration have shown that further improvements on the model are required, specifically, improving the initial state estimate of the speed. This can directly result in improving the overall predictive capacity on a network-scale. Improving the state estimate of the deterioration speed can be done by analyzing the relationship between the deterioration speed and the structural attributes of structures using regression analysis. This is achieved by formulating a hybrid framework that combines SSM with kernel regression (KR), which is presented in the next chapter.

CHAPTER 4 Integrating Structural Attributes in Deterioration Analysis

4.1 Introduction

The SSM deterioration model presented in Chapter 3 relies only on the inspection data and does not take into account the structural attributes of structures, such as the material, the location and other structural-related attributes. Structural attributes are important because they can be used to explain and learn some of structural deterioration patterns across the network. For example, different regions may impose different external factors (e.g. cold vs. warm climate), which can affect the deterioration rate, not to mention also that each material has a unique aging process. Furthermore, the capacity for estimating the deterioration speed is limited in SSM, which may impact the long-term forecast and in some cases the short-term forecast if there are not enough inspection data. In this chapter, the aim is to improve the short and long term forecast of the SSM deterioration model by taking advantage of the structural similarities across the network of bridges. This is done by deriving a hybrid framework that combines the SSM deterioration model with a kernel regression model, in order to incorporate structural attributes in the deterioration analysis.

The layout of this chapter is organized as follows. §4.2 presents a review of kernel regression (KR) theory. This is followed by the mathematical formulation of a hybrid deterioration model that combines SSM with KR in §4.3. This section includes also the steps toward estimating the hidden states and parameters/hyper-parameters associated with SSM-KR. Thereafter, deterioration analyses with synthetic and real data using SSM-KR model are presented in §4.4. Finally, §4.5 presents the conclusions obtained from the analyses in this chapter. The main contributions of this chapter are:

- A framework for modelling the deterioration based on visual inspections and structural attributes.
- An overall improvement in the estimation for the deterioration speed.
- A verification and validation using synthetic and real datasets respectively.

4.2 Kernel Regression (KR)

Kernel methods are well-known and frequently used for pattern detection and discrimination problems [70]. Kernel regression relies on a kernel function that provides information about the similarity between pairs of covariates. In this context, the purpose of employing KR is

to incorporate information from the structural attributes \mathbf{z} in the deterioration analysis of structural elements. KR is utilized to estimate the initial deterioration speed $\dot{x}_{0,p}^j$ associated with each structural element e_p^j . This estimation is based on the *Nadaraya-Watson* model [71],

$$\dot{x}_{0,p}^j = (\mathbf{a}_p^j)^\top \dot{\mathbf{x}}_z + w_0 : W_0 \sim \mathcal{N}(w_0; 0, \sigma_{w_0}^2), \quad (4.1)$$

with the vector \mathbf{a}_p^j obtained by,

$$\mathbf{a}_p^j = \frac{\mathbf{k}(\mathbf{z}_j, \mathbf{Z}_{c(m)}, \boldsymbol{\ell})}{\sum_{m=1}^M \mathbf{k}(\mathbf{z}_j, \mathbf{Z}_{c(m)}, \boldsymbol{\ell})}, \quad m = 1, \dots, M, \quad (4.2)$$

where \mathbf{z}_j is a vector of Q covariates associated with the j -th bridge and \mathbf{Z}_c is a matrix that encodes a Q -dimensional grid of reference points. The Q -dimensional grid is obtained from discretizing the range of each covariate with an equal number of M reference points, such that $\mathbf{Z}_c = [\mathbf{z}_c^1 \dots \mathbf{z}_c^Q] \in \mathbb{R}^{M^Q \times Q}$. The function $\mathbf{k}(\cdot)$ is a multivariate kernel function $\mathbf{k} : \mathbb{R}^Q \rightarrow \mathbb{R}$ representing the multiplicative kernel,

$$\mathbf{k}(\mathbf{z}_j, \mathbf{Z}_{c(m)}, \boldsymbol{\ell}) = k\left(\frac{z_j^1 - z_{c(m)}^1}{\ell_1}\right) \cdot \dots \cdot k\left(\frac{z_j^Q - z_{c(m)}^Q}{\ell_Q}\right), \quad m = 1, \dots, M. \quad (4.3)$$

where $k(\cdot)$ is the univariate kernel function and $\boldsymbol{\ell} = [\ell_1 \dots \ell_Q]$ represents the kernel length parameter associated with each covariate. Estimating $\boldsymbol{\ell}$ parameters as well as the noise parameter σ_{w_0} can be done using the parameter estimation framework described in §4.3.1.

Figure 4.1 illustrates an example for the relationship between the covariates $\mathbf{z}_j \in \mathcal{Z}$, the response \dot{x}_0 , and the reference points \mathbf{Z}_c . In this graph, the true relation between the covariates z_1, z_2 and the response \dot{x}_0 is illustrated by the surface on top, while the reference points are represented by a 2D grid, which is defined by $\mathbf{z}_c^1, \mathbf{z}_c^2$ and the state $\dot{\mathbf{x}}_z$ represented by the expected value $\dot{\mu}_z$. Estimating the hidden states $\dot{\mathbf{x}}_z$, such that each \dot{x}_z matches or approaches the true response \dot{x}_0 associated with the coordinates \mathbf{z}_c^1 and \mathbf{z}_c^2 is done using the recursive framework detailed in §4.3.2.

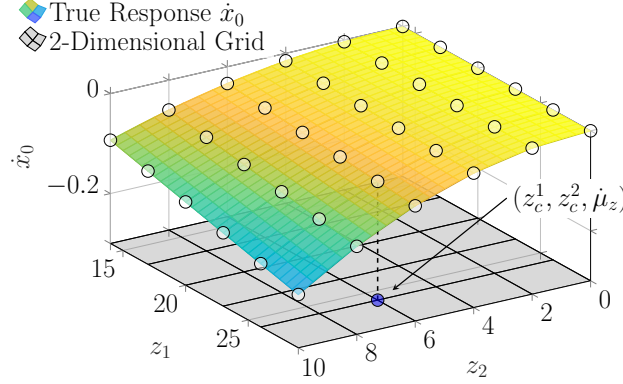


Figure 4.1 Example of a relation between covariates z_1 , z_2 and true response \dot{x}_0 , along with 2D grid defined by $M^q = 6^2$ reference points with coordinates of z_c^1 , z_c^2 and \dot{x}_z represented by the expected value $\dot{\mu}_z$.

4.3 Integrating Structural Attributes in Deterioration Analysis

The full framework for estimating the deterioration state $\mathbf{x}_{t,p}^j$ over time is illustrated in Figure 4.2. For any structural element e_p^j in bridge $b_j \in \mathcal{B}$, the inspection data $\tilde{\mathbf{y}}_{t,p}^j$ and the structural attributes \mathbf{z}_j are considered in the analyses. The structural attributes \mathbf{z}_j are utilized in the KR model to obtain an initial estimate for the deterioration speed $\dot{x}_{0,p}^j$, while the inspection data are transformed from the bounded space $\tilde{\mathbf{y}}_{t,p}^j \in [l, u]$ to the unbounded space $\mathbf{y}_{t,p}^j \in \mathbb{R}$ using the transformation function defined in Equation 3.4. Furthermore, the expected initial deterioration condition is considered as $\mu_{0,p}^j = y_{1,p}^j$ with the variance $\sigma_{0,p}^{j,2} = \sigma_0^2$, and the expected initial acceleration is $\ddot{\mu}_{0,p}^j = 0$ with the variance $\ddot{\sigma}_{0,p}^{j,2} = \ddot{\sigma}_0^2$. Following the initialization step, the Kalman filter is utilized for propagating the initial state $\mathbf{x}_{0,p}^j$ forward in time through the prediction step and the update step up to time T. Similarly, the Kalman smoother is applied to refine the KF estimates from $t = T - 1$ to $t = 0$. At each time step t in KF and KS, the state estimate is examined with the following constraint $\dot{\mu}_{t,p}^j + 2\dot{\sigma}_{t,p}^j \leq 0$. The aforementioned constraint ensures the state estimate does not allow the structural element health to improve over time. If the constraint is violated, the PDF truncation method described in §2.3.3, is applied. The outcome of the SSM-KR framework is denoted by $\tilde{\mu}_{t|T,p}^j \in [l, u]$ which represents the smoothed expected values for the deterioration state and $\tilde{\Sigma}_{t|T,p}^j$ representing the smoothed variances at each time step t .

4.3.1 Model Parameters & Estimation Framework

In addition to the SSM model parameters defined in Equation 3.9, the SSM-KR model parameters include the kernel length parameters ℓ and the kernel process error σ_{w_0} . The

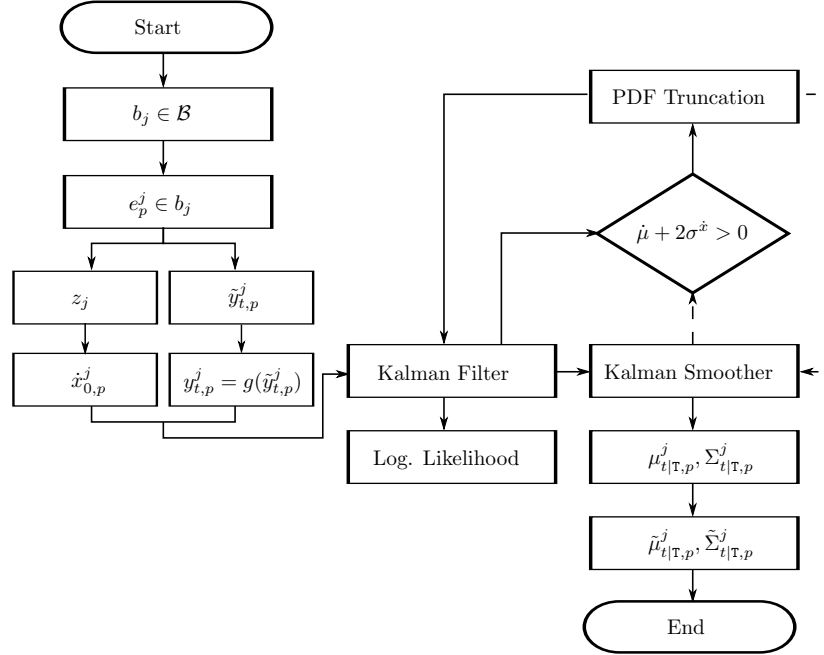


Figure 4.2 SSM-KR framework for estimating the deterioration state of structural element e_p^j from time t to time T .

SSM-KR model parameters are grouped in the set,

$$\boldsymbol{\theta} = \left\{ \underbrace{\sigma_V(I_{1:\mathbb{I}})}_{\text{Inspectors Std.}} , \underbrace{\widehat{\sigma_W}}_{\text{Transform. Param.}} , \underbrace{n}_{\text{Initial state}} , \underbrace{\sigma_0, \ddot{\sigma}_0, p_1, p_2}_{\text{KR process error}} , \underbrace{\widehat{\ell}}_{\text{Kernel length}} \right\}, \quad (4.4)$$

where $\sigma_V(I_{1:\mathbb{I}})$ refers to the standard deviations associated with each inspector $I_i \in \mathcal{I}$, σ_w is the kinematic model process noise, n is the transformation function parameter, and $\{\sigma_0, \ddot{\sigma}_0, p_1, p_2\}$ are the parameters associated with the covariance of the initial state $\Sigma_{0,p}^j = \text{diag}[\sigma_0^2 \, \ddot{\sigma}_0^2 \, \ddot{\sigma}_0^2]$, with $\ddot{\sigma}_0^2$ is defined by a linear function in Equation 3.8.

All model parameters in Equation 4.4 are estimated using the *Maximum Likelihood Estimate* (MLE) which is defined by the network-scale log-likelihood described in Equation 3.12. The parameters estimation procedure is formulated as an optimization problem with the following constraints,

$$\begin{aligned} \boldsymbol{\theta}^* &= \arg \max_{\boldsymbol{\theta}} \mathcal{L}(\boldsymbol{\theta}), \\ \text{subject to: } & \sigma_w, \sigma_{w_0}, \sigma_0, \ddot{\sigma}_0, p_1, p_2, \ell > 0, \\ & \sigma_V(I_i) > 0, \forall I_i \in \mathcal{I}, \\ & n \in \{1, 2, 3, 4, 5\}. \end{aligned} \quad (4.5)$$

The optimization problem above is solved by using a gradient-based optimization framework for all parameters $\boldsymbol{\theta}$, which is detailed in §4.3.2. In order to ensure that the deterioration model is not overfitting, the database is split into a training, validation, and testing sets. The split of the data is done randomly and bridge-wise such that the structural elements of one bridge can not exist in the training set and the validation/testing set at the same time.

4.3.2 Recursive Estimation for the Deterioration Speed

The estimation of the hidden states $\dot{\mathbf{x}}_z$ is done recursively by relying on the Kalman smoother estimates. At the beginning, $\dot{\mathbf{x}}_z$ is initialized with an expected value $\dot{\boldsymbol{\mu}}_{z=0}$ and a variance $\dot{\Sigma}_z = \text{diag}(4)$ so that it represents a weakly informative prior. Estimating $\dot{\mathbf{x}}_z$ is done based on the structural elements in the training set as in,

$$\begin{aligned} \mathbf{J}_z &= \dot{\Sigma}_z \mathbf{A}_\kappa^\top \dot{\Sigma}_{0|z}^{-1}, \\ \dot{\boldsymbol{\mu}}_{z|\mathcal{T}} &= \dot{\boldsymbol{\mu}}_z + \mathbf{J}_z (\dot{\boldsymbol{\mu}}_{0|\mathcal{T}} - \dot{\boldsymbol{\mu}}_{0|z}), \\ \dot{\Sigma}_{z|\mathcal{T}} &= \dot{\Sigma}_z + \mathbf{J}_z (\dot{\Sigma}_{0|\mathcal{T}} - \dot{\Sigma}_{0|z}) \mathbf{J}_z^\top, \end{aligned} \quad (4.6)$$

where \mathbf{A}_κ is an array of vectors \mathbf{a}_p^j as in $\mathbf{A}_\kappa = [\mathbf{a}_1^1 \cdots \mathbf{a}_p^j]^\top$, $\dot{\boldsymbol{\mu}}_{0|z}$ and $\dot{\Sigma}_{0|z}$ are the expected value and the covariance matrix for the speed at time $t = 0$, as predicted by Equation 4.1, for all structural elements. The expected value vector $\dot{\boldsymbol{\mu}}_{0|\mathcal{T}}$ and the covariance matrix $\dot{\Sigma}_{0|\mathcal{T}}$ represent the SSM smoothed estimates for the deterioration speed at time $t = 0$ and for all structural elements. At the beginning, the SSM estimation of the deterioration speed is based on the initial values $\dot{\mu}_{0,p}^j = 0$ and $\dot{\sigma}_{0,p}^{j,2} = \dot{\sigma}_0^2$. After each update of $\dot{\mathbf{x}}_z$, the expected value $\dot{\mu}_{0,p}^j$ of the SSM is updated by Equation 4.1 with $\dot{\mu}_{0,p}^j = \dot{\mu}_{0,p|z}^j$, while the KR variance is reinitialized with $\Sigma_z = \text{diag}(4)$. The SSM variance $\dot{\sigma}_{0,p}^{j,2}$ is not updated because the KR model has a large variance initially which negatively affect the SSM model performance. The update processes in Equation 4.6 and in the SSM prior are repeated recursively until the MLE estimate of the validation set is no longer improving. Thereafter, the KR model is utilized in providing the full prior estimate of the speed $\dot{x}_{0,p}^j$ for any structural element e_p^j .

Parameters & Hidden State Estimation Framework

The gradient optimization algorithm employed in this framework is the *Newton-Raphson* algorithm, which is similar to the optimization framework presented in §3.4. The estimation framework starts with optimizing the initial set of model parameters $\boldsymbol{\theta}^s = \{\sigma_w, \sigma_V, \sigma_0^x, \sigma_0^{\ddot{x}}, p_1, p_2\}$, where σ_V is the observation uncertainty parameter common for all inspectors $\sigma_V(I_{1:\mathbf{I}}) = \sigma_V$. Following this step, the optimization framework updates the inspectors parameters by iter-

tively optimizing each parameter $\sigma_V(I_i)$, while keeping the rest of model parameters $\boldsymbol{\theta}$ fixed. The convergence for $\sigma_V(I_i)$ parameters is determined by either having the difference in \mathcal{L} (validation set) less than the tolerance ϵ , or if the *stall limit* is reached. The stall is the number of iterations with no significant improvements in the objective function. Upon the convergence of $\sigma_V(I_i)$, the model parameters in $\boldsymbol{\theta}^m = \{\sigma_w, \sigma_0^x, \sigma_0^{\ddot{x}}, p_1, p_2\} \subset \boldsymbol{\theta}$ are updated by the optimization algorithm. Thereafter, the recursive estimation for $\dot{\mathbf{x}}_z$ is carried out using the framework presented in §4.3.2. The initial estimation of $\dot{\mathbf{x}}_z$ is done based on the initial KR model parameters $\boldsymbol{\theta}^\kappa = \{\sigma_{w_0}, \boldsymbol{\ell}\} \subset \boldsymbol{\theta}$. Following the optimization of $\boldsymbol{\theta}^\kappa$, the state $\dot{\mathbf{x}}_z$ is refined in accordance with the new KR parameters. The estimation procedure for the inspectors' parameters, the parameters in $\{\boldsymbol{\theta}^m, \boldsymbol{\theta}^\kappa\}$ and the state $\dot{\mathbf{x}}_z$ is repeated recursively until the global convergence criteria is met. Finally, the parameter $n \in \{1, 2, 3, 4, 5\}$ is identified by repeating the full optimization procedure for each value of n . The pseudo code which describe the details of the aforementioned framework is shown Appendix B.

Determining Hyper-Parameters

The number of covariates Q and the number of reference points associated with each covariate M can affect the computational cost associated with the recursive estimation framework presented in §4.3.2. This is because increasing Q or M will result in increasing the size of the state vector $\dot{\mathbf{x}}_z$ represented by $\dot{\boldsymbol{\mu}}_{z|T} \in \mathbb{R}^{M^Q \times 1}$ and $\dot{\boldsymbol{\Sigma}}_{z|T} \in \mathbb{R}^{M^Q \times M^Q}$, which consequently increases the computational demand for computing the KR equations. Determining Q and M is done based on numerical experimentation using MLE, while taking into account the computational cost. For example, if two cases $M_2^{Q_2} \gg M_1^{Q_1}$, have $\mathcal{L}_2 > \mathcal{L}_1$, where $\mathcal{L}_2 - \mathcal{L}_1 = \eta$, and η is negligible, then $M_1^{Q_1}$ is considered in the analysis. Nonetheless, resolving the computational complexity in cases with large M^Q is possible by either utilizing dimensionality reduction approaches, such as principal components analyses (PCA) [72], or other low rank approximation methods [73,74], or by using parametric regression methods instead of a non-parametric approach.

4.4 Deterioration Analyses with SSM-KR

This section presents the analyses performed using the SSM-KR framework on synthetic and real inspection datasets.

4.4.1 Model Verification Using Synthetic Data

The synthetic data used in verifying the SSM-KR model have the same characteristics described in §3.5.1. In order to add a synthetic structural attribute to this dataset, it is assumed

that the true deterioration speed exhibit the following relation with z_j ,

$$z_j = \log(|\dot{x}_0^j|) + w_0 : W_0 \sim \mathcal{N}(w_0; 0, 0.1^2). \quad (4.7)$$

Generating the synthetic attribute z_j allows verifying the performance of the recursive estimation framework presented in Section 4.3.2. The synthetic training dataset consists in $E = 16500$ structural elements with a total of $I = 223$ inspectors providing the observations in each time-series. The synthetic structural attribute z_j associated with each structural element is illustrated in the histogram shown in Figure 4.3, where it can be noticed that

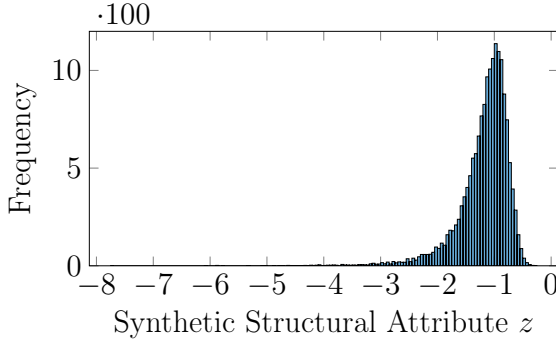


Figure 4.3 Histogram of synthetic structural attribute z .

the distribution of z values has a long tail with the majority of the values concentrated within the range $[-2, -0.5]$. Factoring the information from the structural attribute z in the deterioration analyses is done through the KR model. The kernel function utilized in this case is the *radial basis function* (RBF) [75]. The total number of reference points \mathbf{z}_c is $M = 20$, which is also equivalent to the total number of hidden states in $\dot{\mathbf{x}}_z$. The estimation of $\dot{\mathbf{x}}_z$ in Equation 4.1 is done based on the recursive framework presented in §4.3.2. Figure 4.4 illustrates the initial expected value $\dot{\mu}_z$ and the updated state $\dot{\mathbf{x}}_z$ following convergence after 3 iterations in the recursive framework. In Figure 4.4, it can be noticed that the $\dot{\mathbf{x}}_z$ estimates are deviating from the true curve when $z < -2$. This is because the range of values $z \in [-8, -2]$ is associated with the tail of the distribution (Figure 4.3), where few or no data is available. An example for the effect of the state $\dot{\mathbf{x}}_z$ convergence on the KR model performance is presented in Figure 4.5. In this example, it is shown that after each $\dot{\mathbf{x}}_z$ update, the expected value from KR $\dot{\mu}_{0,p}^j$ is approaching the true speed $\dot{x}_{0,p}^j$.

In order to assess the network-scale improvement in estimating the initial deterioration speed, a comparison between the error histogram of the SSM-KR model and the SSM model is shown in Figure 4.6. The errors are determined by the difference between the true initial speed and the smoothed estimate of the initial speed from each model. From the two histograms in Fig-

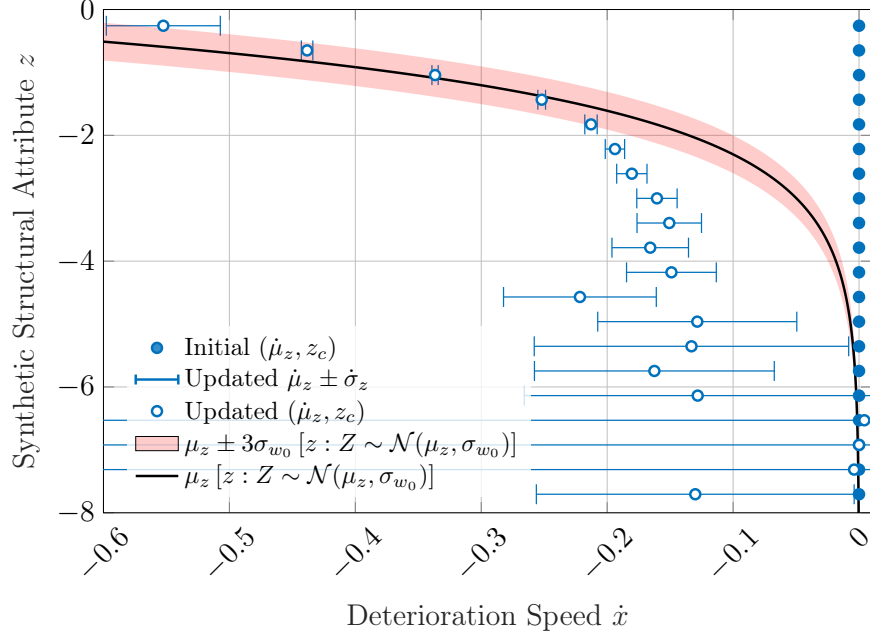


Figure 4.4 Comparison between the updated estimates $\hat{\mu}_z$ (iteration #3) at each reference point $z_c \in z$ and the true relation between the synthetic structural attribute z and the deterioration speed \dot{x}_z .

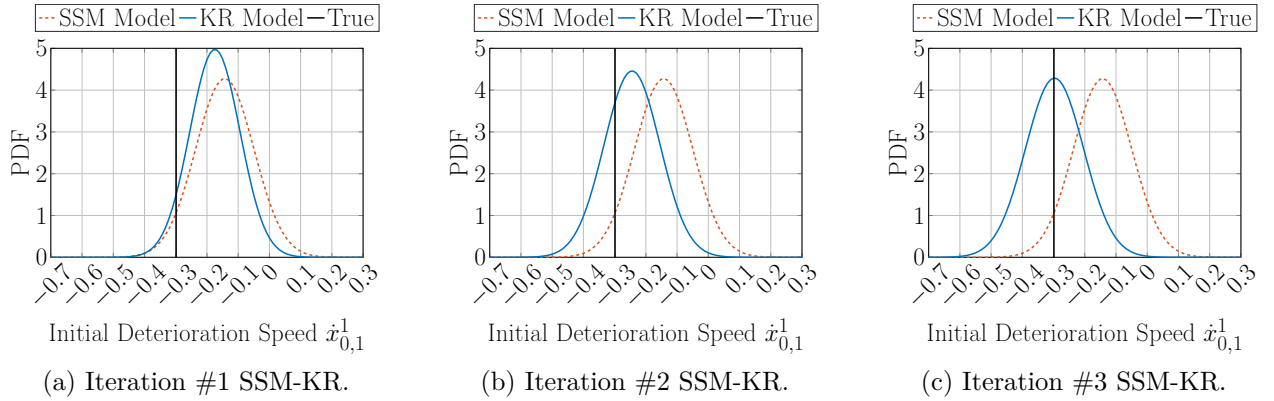


Figure 4.5 Recursive estimation of the state $\dot{x}_{0,p}^j$ illustrated by the probability density function (PDF) with the true speed represented by the vertical line and the SSM model represented by a dashed line.

ure 4.6, it is noticed that the new formulation reduces the bias in the initial speed estimate. The parameter estimation for the SSM-KR model is done using the gradient-based optimization framework detailed in §3.4. The estimated model parameters are shown in Figure 4.7 for the inspectors parameters and Table 4.1 for the rest of model parameters. In Figure 4.7, the alignment of the scatter with the diagonal verifies the capacity of the optimization

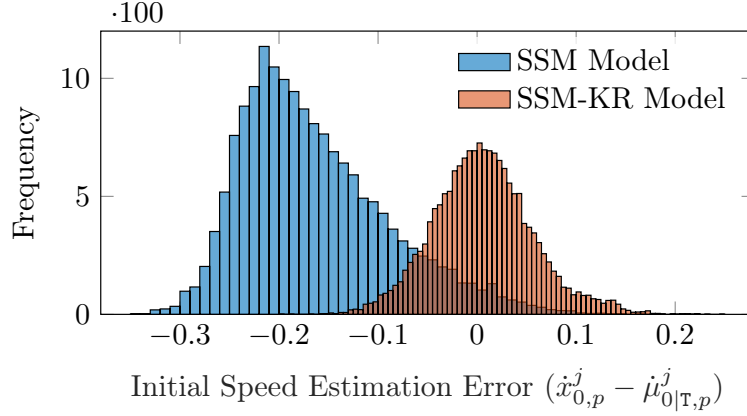


Figure 4.6 Comparison between the SSM-KR model errors histogram (right) and the SSM model errors histogram (left), with the errors determined by the difference between the true initial speed and the smoothed estimate of the initial speed.

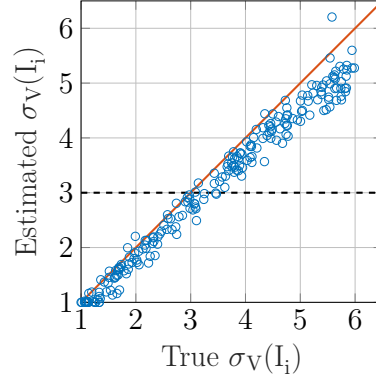


Figure 4.7 Estimation results for synthetic inspectors parameters $\sigma_V(I_i)$ (total: 223 inspectors) with dashed line referring to the initial estimate for all $\sigma_V(I_i)$ parameters.

Table 4.1 Estimation results of model parameters for synthetic data.

σ_w	σ_0^x	σ_V	$\sigma_0^{\tilde{x}}$	p_1	p_2	n	σ_{w_0}	ℓ^{RBF}
3.787×10^{-3}	1.001	3.001	0.0498	0.0499	0.1488	4	0.1238	0.1933

framework in estimating the inspectors' parameters, where the dashed line represents the initial estimate σ_V for all the inspectors' parameters $\sigma_V(I_i)$.

Examples of time-series analyses using the SSM-KR model are shown in Figures 4.8 and 4.9. In this example, both SSM-KR and SSM (without factoring the structural attribute) are utilized in producing the deterioration estimates of the condition and the speed. From Figure 4.8, the condition estimates of SSM-KR and SSM are overlapping initially, however,

these estimates starts to diverge over time due to the difference in the initial speed estimate of each model. It can be noticed in this example that the true state represented by a dashed line is within the confidence interval of the SSM-KR model. The speed estimate associated

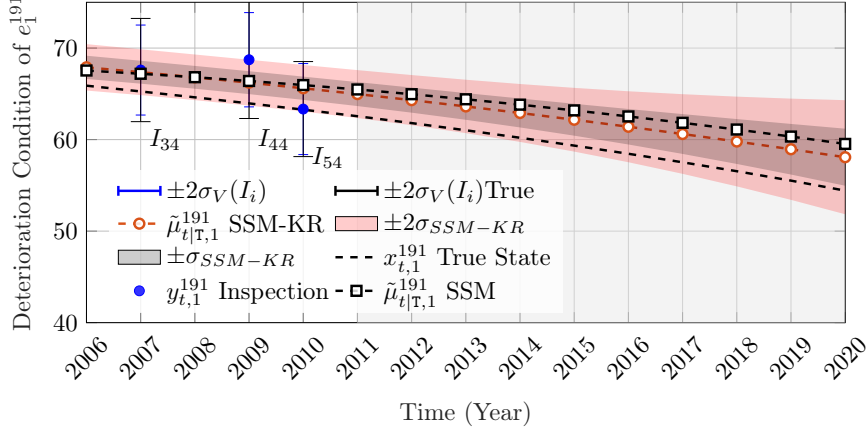


Figure 4.8 Deterioration condition estimate for synthetic structural element e_1^{191} , with the *circle* marker representing the SSM-KR estimates, the *square* marker representing SSM estimates, the dashed line representing the true condition, and the shaded area representing the forecast period.

with the aforementioned example is shown in Figure 4.9. It can be noticed that the overall estimate for the speed in the SSM-KR model is better than the SSM.

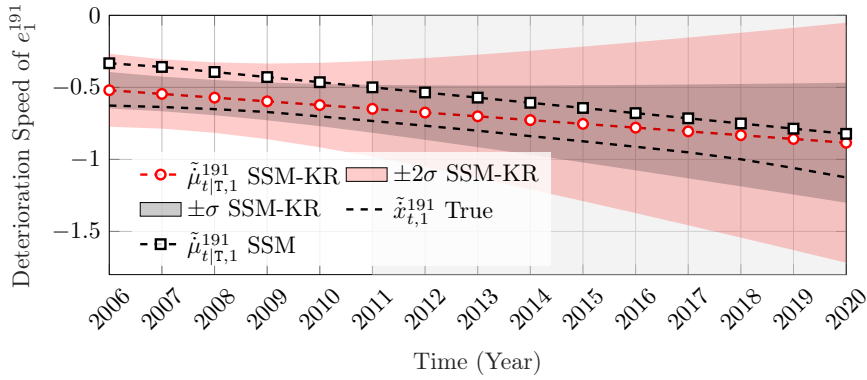


Figure 4.9 Deterioration speed of synthetic structural element e_1^{191} , with the *circle* marker representing the SSM-KR estimates, the *square* marker representing SSM estimates, the dashed line representing the true state, and the shaded area representing the forecast period.

In order to examine the network-scale improvements, Figure 4.10 illustrates the average error in forecast time for the condition and the speed based on the SSM-KR model and the SSM model. From Figure 4.10a, it can be noticed that the average error in SSM-KR condition

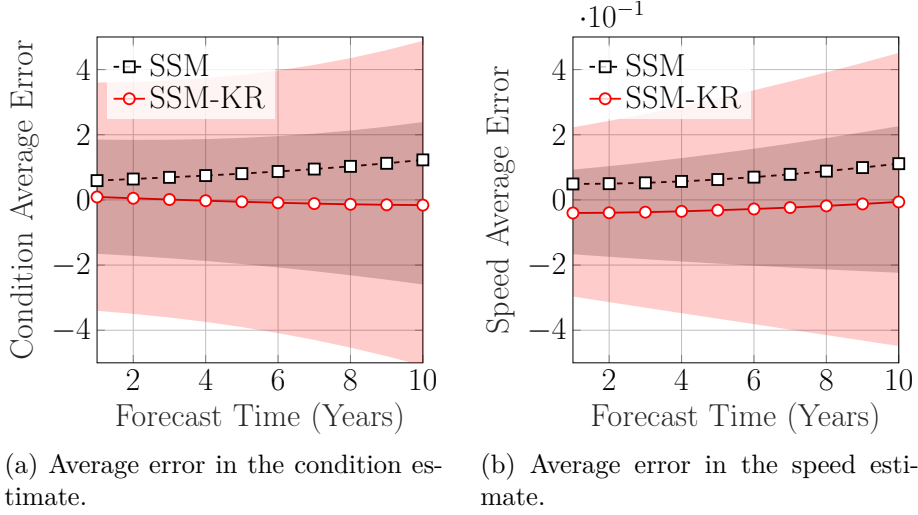


Figure 4.10 Average error estimate of the SSM-KR model represented by the expected value (*circle marker*) and confidence interval ($\pm 2\sigma$) for the condition and speed, compared to the error estimates of the SSM model represented by the expected value (*square marker*).

estimate is near zero throughout the time-window of analyses, while the average error in SSM is diverging monotonically away from zero. From this, it can be concluded that factoring information about the structural attribute has reduced the overall bias in estimating the deterioration condition. On the other hand, in Figure 4.10b, the speed estimates in both models are changing monotonically with the SSM model speed estimates diverging similarly to the SSM condition estimates.

4.4.2 Model Validation Using Real Data

The validation analyses with real data are performed using the real inspection data presented in §3.5.1. The structural element category utilized in the analysis is *Beams*. A structural element is considered in the deterioration analyses if it has 3 or more inspections without interventions. The total number of beam elements that are considered in the deterioration analyses is: $E = 16689$ elements taken from $B = 2133$ bridges. The number of inspectors involved in this dataset is $I = 223$. The inspections dataset is divided into a training set with $E_{tr} = 13639$ structural elements from $B_{tr} = 1915$ bridges, validation set with $E_v = 2034$ structural elements from $B_v = 142$ bridges and a testing set having $E_t = 1016$ structural elements from $B_t = 76$ bridges.

The structural attributes z_j considered in the analyses are: z_j^1 the structure's material, z_j^2 the age of the structure and z_j^3 the structure's location represented by the latitude. The selection of attributes is based on the kernel bandwidth parameters in ℓ , which are estimated based on

the inspection data and using the MLE approach [76, 77]. If an estimated kernel bandwidth ℓ converges to a large value relative to the range of the covariate, then the inverse of ℓ will result in the covariate z being almost independent of the response [77]. The histogram for each of the aforementioned attributes is shown in Figure 4.11. It should be noted that the

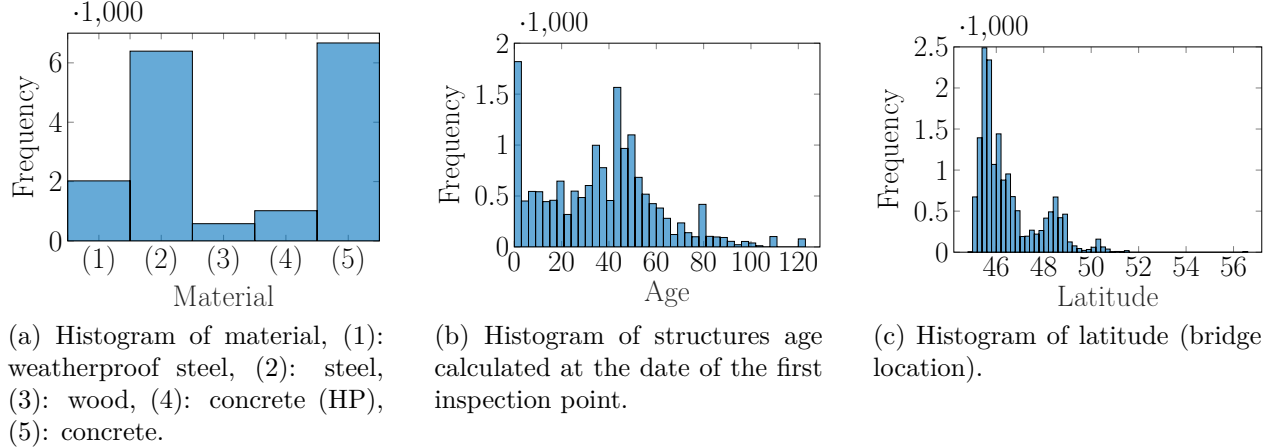


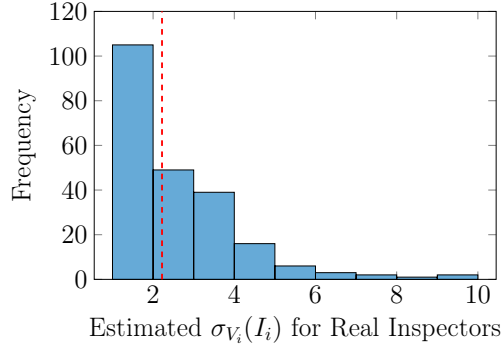
Figure 4.11 Frequency of structural attributes from real data

age of the bridge is determined by deducting the date of the first inspection point from the construction date of the bridge. The multivariate KR analyses involve different types of kernel functions. The selection of the kernel function is done based on the type of data (i.e. categorical or continuous) and the MLE estimate. In this case study, the structure's material is assumed to be unordered categorical data, which can be modelled using the Aitchison and Aitken [78] (AAK) kernel function. The kernel length in the AAK function is bounded by $0 \leq \ell \leq \frac{C-1}{C}$, where C is the number of categories [79]. The structure's age and latitude are analyzed using the Matérn 12 (M12) kernel function [77]. In addition to the structural attributes, the condition of the structural element at the first inspection point is also included as a covariate in the multivariate KR. The kernel function utilized for the condition is the Matérn 52 (M52) [77]. The equations for each of the aforementioned kernel functions are available in Appendix 2. The estimated SSM-KR model parameters are shown in Table 4.2, while the inspectors parameters are shown in Figure 4.12. In order to demonstrate the performance of SSM-KR in the real case, two examples are considered from the test set. The first example is for the structural element e_{10}^{244} from bridge b_{244} . This bridge was $z_{244}^2 = 61$ years of age at the time of the first inspection, located at a latitude $z_{244}^3 \approx 48$, with the material of the beam elements in it is $z_{244}^1 = \text{steel}$.

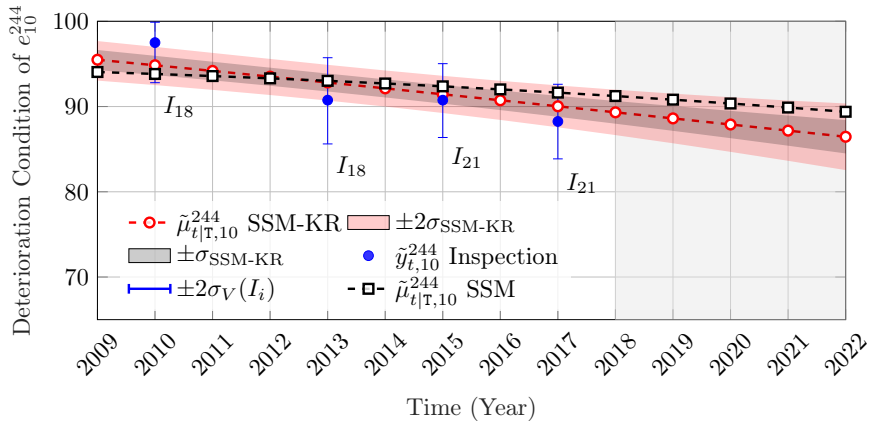
The deterioration analyses for the structural element e_{10}^{244} from b_{244} are shown in Figures 4.13 and 4.14. Figure 4.13 illustrates a comparison between the condition estimates of SSM-KR represented by the *circle* marker and the SSM represented by the *square* marker. It can be

Table 4.2 Estimation results of SSM-KR parameters for real data.

σ_w	σ_0^x	σ_V	$\sigma_0^{\ddot{x}}$	p_1	p_2	n
5.451×10^{-3}	1.025	2.220	0.0499	0.0096	0.1473	4
σ_{w_0}	ℓ^{AAK}	ℓ^{M12}	ℓ^{M12}	ℓ^{M52}		
0.1292	0.0166	12.6064	1.4309	7.2166		

Figure 4.12 Histogram for the estimated parameters $\sigma_V(I_i)$ of real inspectors (total: 223 inspectors) with the dashed line referring to the initial estimate for all $\sigma_V(I_i)$.

noticed that SSM-KR estimates adapt in a better way to the recorded observation compared to the SSM estimates. Furthermore, the same comparison is performed for the deterioration

Figure 4.13 Deterioration condition estimate for real structural element e_{10}^{244} with the *circle* marker representing the SSM-KR estimates, the *square* marker representing SSM estimates, and the shaded area representing the forecast period.

speed estimates from each model. From Figure 4.14, throughout the prediction time, the speed estimates of SSM-KR shows a consistent progression in comparison to the SSM speed

estimates.

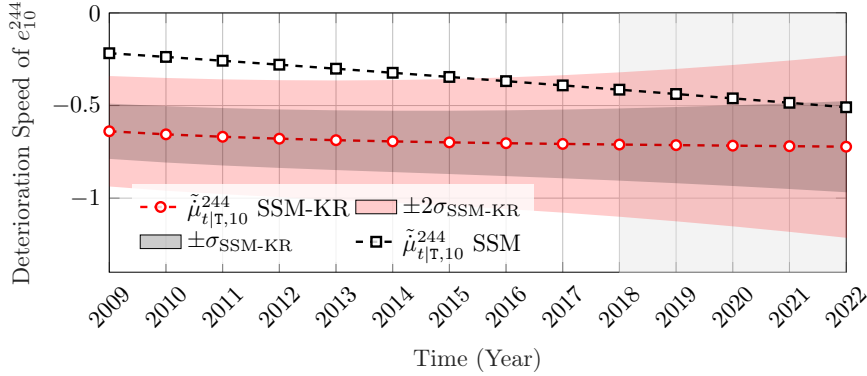


Figure 4.14 Deterioration speed of structural element e_{10}^{244} with the *circle* marker representing the SSM-KR estimates, the *square* marker representing SSM estimates, and the shaded area representing the forecast period.

The second example is taken from a bridge b_{1599} located at $z_{1599}^3 \approx 46$ with $z_{1599}^2 = 65$ years of age at the time of the first inspection. The structural element e_1^{1599} material is $z_{1599}^1 = \text{concrete}$. The inspection data $\tilde{y}_{t,1}^{1599}$ exhibit a higher variability compared to the first example as shown in Figure 4.15. Similarly, the SSM-KR estimates show a better adaption to the inspection data in comparison with the SSM model estimates. The deterioration speed

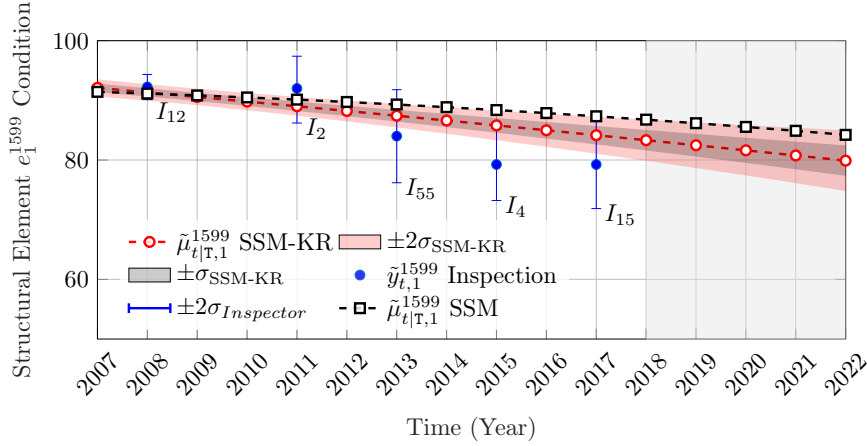


Figure 4.15 Deterioration condition estimate for real structural element e_1^{1599} with the *circle* marker representing the SSM-KR estimates, the *square* marker representing SSM estimates, and the shaded area representing the forecast period.

estimates associated with e_1^{1599} are shown in Figure 4.16. The steady estimates of the speed in SSM-KR imply a coherent prior estimate, in comparison to the steep changes in the SSM speed estimates.

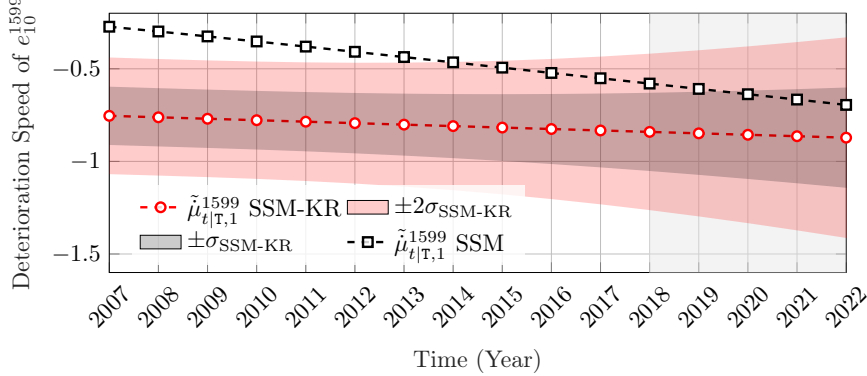


Figure 4.16 Deterioration speed of structural element e_1^{1599} with the *circle* marker representing the SSM-KR estimates, the *square* marker representing SSM estimates, and the shaded area representing the forecast period.

The network-scale improvement in the real case is quantified in Table 4.3, where the log-likelihood associated with the training, the validation and the testing sets are reported. From Table 4.3, SSM-KR shows a better log-likelihood in each dataset compared to the SSM model.

Table 4.3 Comparison between SSM-KR and SSM based on the log-likelihood in the training, validation and testing sets

Model	Training	Validation	Testing
SSM	-121175	-17187	-8822
SSM-KR	-116223	-16822	-8482

4.5 Conclusion

In this chapter, a hybrid framework based on state-space models and kernel regression is proposed for modelling the deterioration behaviour of a bridge network. The SSM-KR model relies on visual inspection data and takes into account the structural attributes of each bridge. The role of KR is to model patterns between the deterioration speed and the structural attributes. The performance of SSM-KR is verified with synthetic data and benchmarked against a SSM model that does not account for structural attributes. The results have shown that the overall bias in the condition estimates is lower for the SSM-KR, compared to the SSM, as demonstrated by the average error in the forecast time. In addition, the SSM-KR does not show any significant bias toward overestimating or underestimating the initial speed. The analyses also included a validation with real inspections database. Two test cases are

considered to demonstrate the model performance. In both cases, the SSM-KR showed a better adaption to the inspection data in comparison with the SSM model. Furthermore, the SSM-KR deterioration speed estimates have a better consistency throughout the analyses time-window. The SSM and SSM-KR are also compared based on the log-likelihood in the training, validation, and testing sets. The SSM-KR has an overall better log-likelihood in each subset of data which emphasizes the importance of factoring structural attributes. Although SSM-KR has a better performance, the model can be computationally demanding, when the number of structural attributes is increased $Q > 5$, the number of reference points in the KR model becomes significantly large. Nonetheless, overcoming such problem is possible through dimensionality reduction approaches or by using a parametric regression method instead of the non-parametric regression approach. Overall, factoring structural attributes has improved the deterioration model predictive capacity, especially when few inspection points are available. This enables further analyses such as quantifying the effect of interventions which is tackled in the next chapter.

CHAPTER 5 Quantifying the Effects of Interventions on Structural Elements

5.1 Introduction

Interventions are an intrinsic part of any structural element service life. In the context of network-scale bridge maintenance, an intervention can be classified into three categories: *preventive maintenance*, *rehabilitation* and *replacement* [47, 48]. Quantifying the effect of interventions is commonly based on either expert judgement and reference values or ad hoc estimation from visual inspection data [14, 49, 51, 53, 54]. In this chapter the effect of interventions is modelled as random variables within the network-scale deterioration model SSM-KR. The proposed formulation enables estimating the local effect of interventions at the structural-element level as well as the network-scale effect for a population of structures. In addition, the proposed formulation allows accommodating the inspectors uncertainty in the aforementioned estimates. This allows quantifying the effect of different types of interventions on a network-scale, which lays out the groundwork for enhanced planning and allocation of maintenance funds.

This chapter is organized as follows. In §5.2 different types of interventions are presented along with details about the real interventions database and the simulation of synthetic interventions. This is followed by §5.3, which provides the mathematical formulation of the proposed framework for quantifying the effect of interventions. Analyses and results using the proposed framework with real and synthetic data are presented in §5.4. Finally, a summary of findings derived from the results are presented in §5.5. The main contributions in this chapter are:

- A method for quantifying the effect of interventions while taking into account the inspectors uncertainty.
- A verification and validation of the proposed model with synthetic and real datasets, respectively.
- An estimation of the local effect of interventions at the structural-element level as well as the network-scale effect for a population of structural elements.

5.2 Interventions Database

In this section, the real interventions dataset is presented followed by a description of synthetic interventions generated in order to verify the model performance.

5.2.1 Interventions in the Real Case Study

In addition to the inspection database described in §3.5.1, a network-scale interventions database is also available. In this database, the network-scale interventions are classified into 3 categories [7]. These categories are, h_1 : preventive maintenance, h_2 : routine maintenance and h_3 : repairs. Each of the aforementioned categories encompass a set of actions. For example, the intervention actions associated with the *beam* structural elements category are: cleaning activities in h_1 , replacing bolts / rivets in h_2 , and reparation actions of beams in h_3 . These intervention actions are triggered based on either a certain deterioration state being reached or a recommendation from an inspector [7].

5.2.2 Simulating Interventions and Synthetic Data

A synthetic dataset is generated in order to verify the proposed framework performance, provided that the true effect of interventions is known. This dataset is, by design, similar to the real data, both quantitatively and qualitatively as described in §3.5.1 and §4.4.1. Simulating synthetic interventions is done based on two factors: the structure priority, and the deterioration state. The priority factor is randomly assigned to structures using a uniform distribution $\Omega \sim \mathcal{U}(1, 3)$. This factor emulates the inspector's recommendation for performing an intervention in the real case. The type of intervention is determined using a synthetic decision making system defined by if-then rules, which are detailed in Appendix D. In total, four synthetic intervention actions are defined, h_0 : do nothing, h_1 : preventive maintenance, h_2 : repairs and h_3 : major repairs. Whenever one of the actions $h_{1:3}$ is applied, the timing of the synthetic intervention τ is recorded. The true improvement, represented by the network-scale change in the condition δ , the speed $\dot{\delta}$ and the acceleration $\ddot{\delta}$, is defined for each type of intervention by a Normal distribution with parameters shown in Table 5.1.

Table 5.1 Types of synthetic interventions with their corresponding expected improvement represented by an expected value and a standard deviation.

Type	μ_δ	σ_δ	$\mu_{\dot{\delta}}$	$\sigma_{\dot{\delta}}$	$\mu_{\ddot{\delta}}$	$\sigma_{\ddot{\delta}}$
h_1	0	10^{-4}	0.2	0.05	0	10^{-4}
h_2	7.5	2	0.3	0.1	0	10^{-4}
h_3	18.75	4	0.4	0.15	0	10^{-4}

In order for a structural element to be included in the intervention quantification framework, it has to have at least 3 observations in total, with one of the observations before or after the intervention. As for the synthetic structural attributes, a single attribute is considered

and is defined by the relation,

$$z_j = 10 \times |\dot{x}_0^j| + 4 + w_0 : W_0 \sim \mathcal{N}(w_0; 0, 0.5^2). \quad (5.1)$$

Other characteristics and thresholds that are required in order to simulate realistic inspection data are inherited from the measures defined in §3.5.1.

5.3 Quantifying the Effects of Interventions on Structural Elements

Analyzing the effect of interventions coincides with the deterioration analyses of structural elements. This is because the type of an intervention h_r is determined by a large extent based on the deterioration state of the structural element. In this section, the relationship between interventions and deterioration analyses is explained, followed by the formulation of the proposed framework for quantifying the effect of interventions.

5.3.1 Integrating Interventions within SSM-KR

In this chapter, the deterioration analysis are performed using the SSM-KR deterioration model detailed in §4.3. In order to accommodate the effect of interventions in the SSM-KR model, the state vector is augmented to include the following components,

$$\mathbf{x}_{p,t}^j = [x_{p,t}^j \ \dot{x}_{p,t}^j \ \ddot{x}_{p,t}^j \ \delta_t \ \dot{\delta}_t \ \ddot{\delta}_t]^T, \quad (5.2)$$

where $\mathbf{x}_{p,t}^j$ is the state vector at time t : $\mathbf{X}_t \sim \mathcal{N}(\boldsymbol{\mu}_t, \boldsymbol{\Sigma}_t)$, composed of the vector $[x_{p,t}^j \ \dot{x}_{p,t}^j \ \ddot{x}_{p,t}^j]$ which describes the condition, speed, and acceleration components, and the vector $[\delta_t \ \dot{\delta}_t \ \ddot{\delta}_t]$ which represents the changes in the condition, speed, and acceleration following an intervention h_r . The effect of an intervention on a structural element is quantified within SSM-KR by modifying the transition model, such that it becomes dependent on the intervention time τ as in,

$$\mathbf{x}_t = \mathbf{A}_t \mathbf{x}_{t-1} + \mathbf{w}_t, \quad \mathbf{w}_t : \begin{cases} \mathbf{W}^{ki} \sim \mathcal{N}(\mathbf{0}, \mathbf{Q}_t^{ki}) \\ \mathbf{W}^r \sim \mathcal{N}(\mathbf{0}, \mathbf{Q}_t^r) \end{cases} \quad (5.3)$$

The transition matrix \mathbf{A}_t is defined by,

$$\mathbf{A}_{t=\tau} = \begin{bmatrix} \mathbf{A}^{ki} & \mathbf{I}_{3 \times 3} \\ \mathbf{0}_{3 \times 3} & \mathbf{I}_{3 \times 3} \end{bmatrix}, \quad \mathbf{A}_{t \neq \tau} = \begin{bmatrix} \mathbf{A}^{ki} & \mathbf{0}_{3 \times 3} \\ \mathbf{0}_{3 \times 3} & \mathbf{I}_{3 \times 3} \end{bmatrix}, \quad (5.4)$$

with \mathbf{I} representing the identity matrix and \mathbf{A}^{ki} defined by,

$$\mathbf{A}^{\text{ki}} = \begin{bmatrix} 1 & \Delta t & \frac{\Delta t^2}{2} \\ 0 & 1 & \Delta t \\ 0 & 0 & 1 \end{bmatrix}. \quad (5.5)$$

The full covariance for the transition model errors is described by the matrix \mathbf{Q}_t defined as,

$$\mathbf{Q}_{t=\tau} = \begin{bmatrix} \mathbf{Q}^{\text{ki}} + \mathbf{Q}^r & \mathbf{0}_{3 \times 3} \\ \mathbf{0}_{3 \times 3} & \mathbf{Q}^r \end{bmatrix}, \quad \mathbf{Q}_{t \neq \tau} = \begin{bmatrix} \mathbf{Q}^{\text{ki}} & \mathbf{0}_{3 \times 3} \\ \mathbf{0}_{3 \times 3} & \mathbf{0}_{3 \times 3} \end{bmatrix}, \quad (5.6)$$

with \mathbf{Q}^r and \mathbf{Q}^{ki} defined as,

$$\mathbf{Q}^r = \text{diag} \left(\begin{bmatrix} \sigma_{w_r}^2 & \dot{\sigma}_{w_r}^2 & \ddot{\sigma}_{w_r}^2 \end{bmatrix} \right), \quad \mathbf{Q}^{\text{ki}} = \sigma_w^2 \begin{bmatrix} \frac{\Delta t^5}{20} & \frac{\Delta t^4}{8} & \frac{\Delta t^3}{6} \\ \frac{\Delta t^4}{8} & \frac{\Delta t^3}{3} & \frac{\Delta t^2}{2} \\ \frac{\Delta t^3}{6} & \frac{\Delta t^2}{2} & \Delta t \end{bmatrix}. \quad (5.7)$$

The standard deviation σ_w characterizes the kinematic model process noise, while $\boldsymbol{\sigma}_{w_r}$ is a vector containing the standard deviations describing the element-level intervention errors.

Because of the large variability and limited data in each time-series, it is assumed that the deterioration state of a structural element after an intervention is either staying the same as it was prior to the intervention or is improving by a positive quantity. Consequently, the expected deterioration speed at time $t = \tau$ is bounded with $\dot{\mu}_\tau \in [\dot{\mu}_{\tau-1}, 0]$ and similarly for the acceleration, $\ddot{\mu}_\tau \in [\ddot{\mu}_{\tau-1}, 0]$. In order to accommodate the aforementioned bounds, the following state constraints are applied in the KF,

$$\begin{aligned} \dot{\mu}_{\tau-1} &\leq \dot{\mu}_\tau \leq 0, \\ \ddot{\mu}_{\tau-1} - \ddot{\sigma}_{\tau-1} &\leq \ddot{\mu}_\tau \leq \ddot{\sigma}_{\tau-1}. \end{aligned} \quad (5.8)$$

The acceleration is allowed to be positive to accommodate cases where the acceleration is slightly positive or near zero at the time step before the intervention $t = \tau - 1$. This implies that the deterioration speed was declining at that point in time. In order to ensure the consistency in the model, the state constraints are also applied in the KS after changing the bounds as,

$$\begin{aligned} \dot{\mu}_\tau &\leq \dot{\mu}_{\tau+1}, \\ \ddot{\mu}_\tau &\leq \ddot{\mu}_{\tau+1} + \ddot{\sigma}_{\tau+1}. \end{aligned} \quad (5.9)$$

The state constraints are only examined at the transition from time $t = \tau - 1$ to time $t = \tau$ or reversely; if one of the constraints is violated, the PDF truncation method is applied.

5.3.2 State Estimation and Model Parameters

The hidden state δ_t , $\dot{\delta}_t$ and $\ddot{\delta}_t$ representing the network-scale effects of interventions are estimated based on sequential updating from the inspection data. For a given type of intervention $h_r \in \mathcal{R}$, the expected value for each component is initially set to zero $\mu_t^\delta = \mu_t^{\dot{\delta}} = 0$, except for the speed $\mu^{\dot{\delta}_t}$. This is because assigning $\mu^{\dot{\delta}_t} \approx 0$ can trigger the state constraints defined in Equation 5.8, resulting in truncating the PDF of the state at an early stage.

After the initialization step, the intervention quantification framework presented in §5.3.1 is applied, through which the states δ_t , $\dot{\delta}_t$ and $\ddot{\delta}_t$ are updated based on the inspection data before and after intervention h_r on the element e_p^j . The updated state is then utilized in the analyses of structural element e_{p+1}^j which allows the states δ_t , $\dot{\delta}_t$ and $\ddot{\delta}_t$ to be updated with another set of inspections before and after intervention h_r . The sequential updates are carried out up to the last structural element with the intervention h_r . Therefore, the estimation quality for quantifying the effect of an intervention type depends on the number of structural elements that underwent the same type of intervention. Following the update from the data of the last structural element, the updated states δ_t , $\dot{\delta}_t$ and $\ddot{\delta}_t$ can be utilized in modelling the element-level interventions within the SSM-KR framework.

The parameters associated with the intervention quantification framework are defined in the set $\boldsymbol{\theta}_r = \{\sigma_{w_r}, \dot{\sigma}_{w_r}, \ddot{\sigma}_{w_r}, \sigma_{h_r}, \dot{\sigma}_{h_r}, \ddot{\sigma}_{h_r}\}$, where $\sigma_{h_r}, \dot{\sigma}_{h_r}, \ddot{\sigma}_{h_r}$ are the standard deviations associated with the prior knowledge for the states δ_t , $\dot{\delta}_t$ and $\ddot{\delta}_t$, at the beginning of the sequential estimation process. The subscript in $\boldsymbol{\theta}_r$ is a reference to the intervention category h_r , as each intervention category has its own set of parameters. The estimation for the aforementioned parameters is done using the *Maximum Likelihood Estimate* (MLE). The network-scale log-likelihood is,

$$\mathcal{L}(\boldsymbol{\theta}_r) = \sum_{j=1}^{B_r} \sum_{p=1}^{E_r^j} \sum_{t=1}^{T_p} \ln f(y_{t,p}^j | y_{1:t-1,p}^j, \boldsymbol{\theta}_r), \quad (5.10)$$

where B_r , E_r^j are respectively the total number of bridges and structural elements that underwent intervention h_r , and T_p is the number of observation per time series. The parameters estimation problem is defined as,

$$\begin{aligned} \boldsymbol{\theta}_r^* &= \arg \max_{\boldsymbol{\theta}_r} \mathcal{L}(\boldsymbol{\theta}_r), \\ \text{subject to: } &\sigma_{w_r}, \dot{\sigma}_{w_r}, \ddot{\sigma}_{w_r} > 0, \\ &\sigma_{h_r}, \dot{\sigma}_{h_r}, \ddot{\sigma}_{h_r} > 0. \end{aligned} \quad (5.11)$$

Solving the optimization problem defined above is done using the *Newton-Raphson* method, similar to Appendix B.

5.4 Case Studies

In this section, the performance of the proposed framework is verified using synthetic data and thereafter validated with real data.

5.4.1 Model Verification Using Synthetic Data

The synthetic dataset is composed of $E = 17000$ structural elements with a total of $E_r = 414$ structural elements that underwent interventions belonging to categories $h_{1:3}$. The observations in the synthetic dataset are obtained from $I = 223$ inspectors. The structural elements without interventions are utilized for training the SSM-KR deterioration model. Thereafter, the pre-trained deterioration model is utilized for modelling interventions as described in §5.3.1. The optimized model parameters $\theta_{1:3}$ for each intervention category are shown in Table 5.2. The state estimation for the network-scale change in the condition δ and the speed

Table 5.2 Estimated model parameters for synthetic interventions.

Intervention	σ_{w_r}	$\dot{\sigma}_{w_r}$	$\ddot{\sigma}_{w_r}$	σ_{h_r}	$\dot{\sigma}_{h_r}$	$\ddot{\sigma}_{h_r}$
h_1	1.42	0.03	0.01	0.26	0.79	0.09
h_2	3.10	0.79	0.05	6.77	0.63	0.03
h_3	3.82	0.75	0.04	9.82	0.78	0.002

$\dot{\delta}$ are shown in Figure 5.1. In this figure, the expected change in the condition μ^δ converges to the true change δ for each intervention category $h_{1:3}$. Moreover, the state estimations shows that the proposed framework provides reliable estimates with as little as 20 structural elements with interventions. On the other hand, the estimates for the network-scale change in the deterioration speed $\dot{\delta}$ is not as accurate as the condition estimates δ . The limited performance in estimating $\dot{\delta}$ is noticeable in the case of intervention category h_3 . The main reasons for the limited predictive capacity of $\dot{\delta}$ are: the fact that the deterioration speed is not directly observable, and there are few observations before and/or after the intervention. As for interventions of type h_3 , this category of interventions is mainly applied on structures having an average health condition, which is associated with a higher uncertainty in the estimates of the deterioration state (see §3.2). Nonetheless, if the number of observations before and/or after the intervention is sufficient, the state estimation of $\dot{\delta}$ converges to the true value. An example that demonstrates the effect of the number of observations on μ^δ is shown in Figure 5.2. In this example, the expected value μ^δ for the intervention h_3 approaches the true change, as the number of observations per time series increases. Although estimating $\dot{\delta}$ is limited for interventions of type h_3 , the resulting state $\dot{\delta}$ can be considered as a good initial

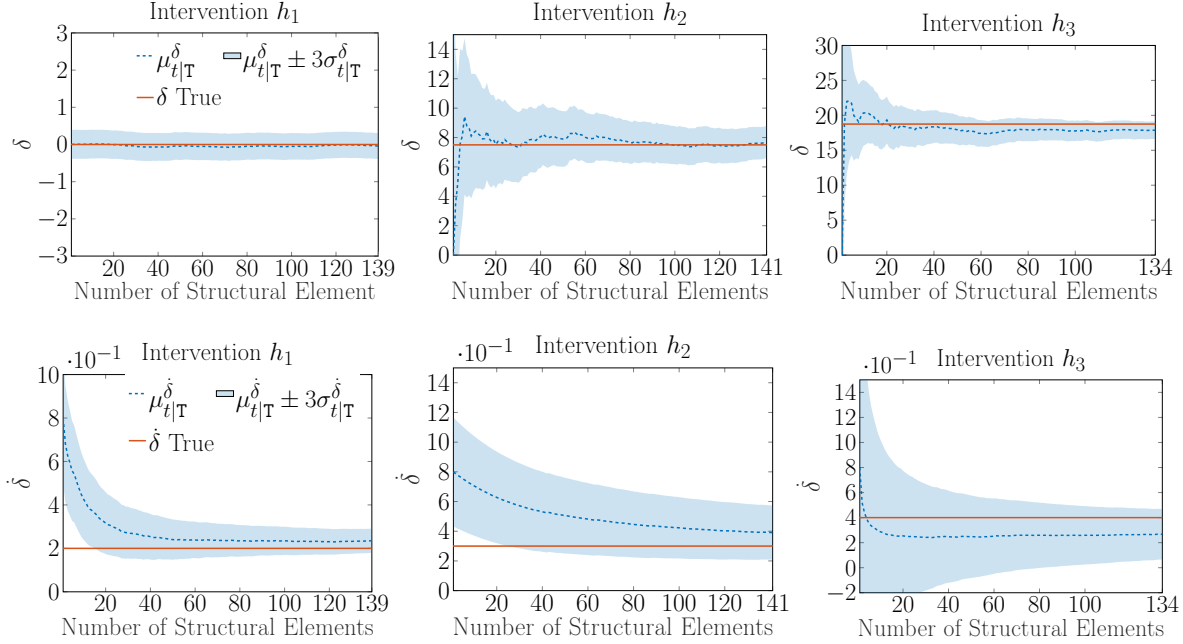


Figure 5.1 Recursive estimation for the network-scale change in the deterioration condition δ and speed $\dot{\delta}$ based on data from $E_1 = 139$ structural elements underwent intervention h_1 , $E_2 = 141$ elements underwent intervention h_2 , and $E_3 = 134$ elements underwent intervention h_3 .

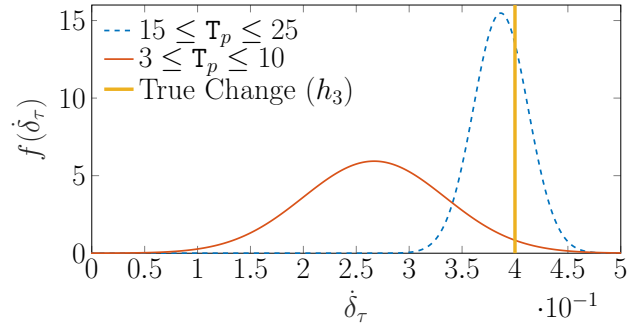


Figure 5.2 The effect of the number of observations per time series T_p on the state estimate of $\dot{\delta}_\tau$ under the same intervention h_3 at time $\tau \approx \frac{T_p}{2}$.

estimate for the effect of interventions at the structural element level. This initial estimate is subsequently updated according to the data of each structural element using the KS. This is demonstrated in Figures 5.3-5.5, with examples of time series for synthetic structural elements. Figure 5.3 illustrates an example of a deterioration behaviour with an intervention h_1 . In this example, the true deterioration state before and after the intervention is within the confidence interval of the model, despite having a single observation before the intervention.

Another example shown in Figure 5.4, illustrates the model performance in the case of a

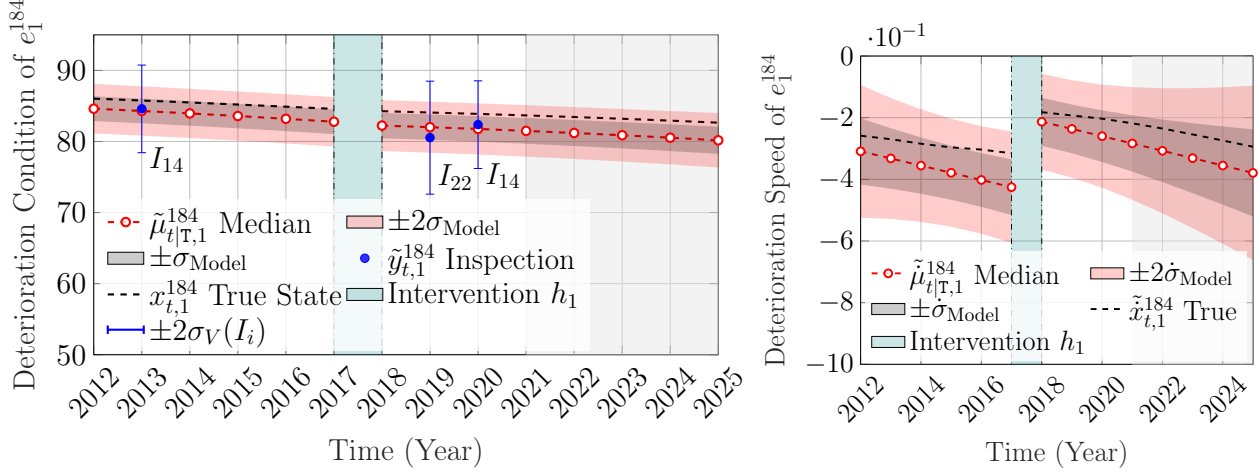


Figure 5.3 Deterioration state analysis for the condition and the speed based on the observations $\tilde{y}_{t,1}^{184} \in [25, 100]$ of the synthetic structural element e_1^{184} with an intervention h_1 at time $\tau = 2018$, error bars representing the inspectors' uncertainty estimates, and the shaded area representing the forecast period.

synthetic structural element with an intervention of category h_2 . In this case, the estimate of the deterioration state is consistent with the true speed and condition, even though a single observation exist after the intervention.

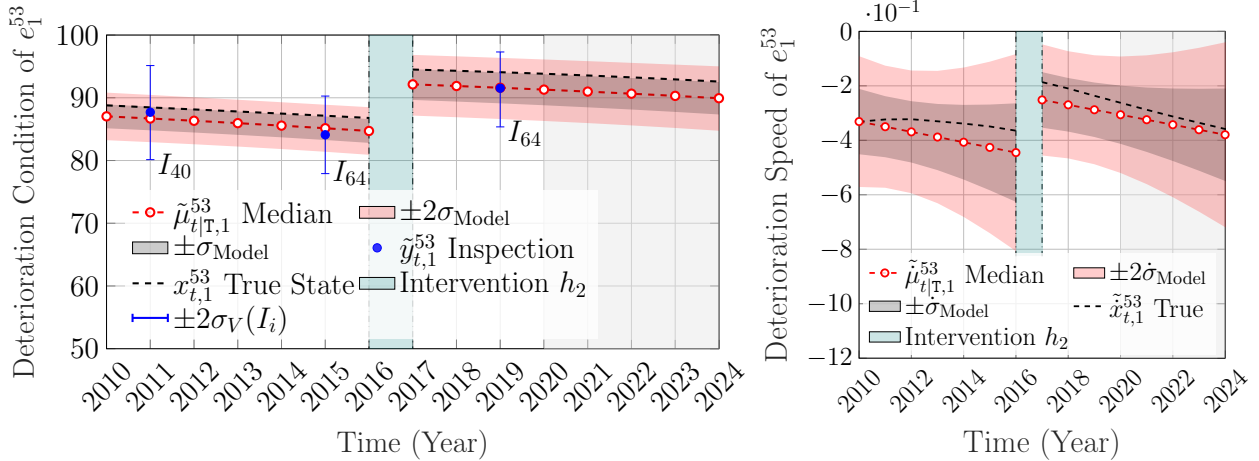


Figure 5.4 Deterioration state analysis for the condition and the speed based on the observations $\tilde{y}_{t,1}^{53} \in [25, 100]$ of the synthetic structural element e_1^{53} with an intervention h_2 at time $\tau = 2017$, error bars representing the inspectors' uncertainty estimates, and the shaded area representing the forecast period.

The last example of time series analyses is shown in Figure 5.5, where the model performance

is examined for a structural element with an intervention of category h_3 . This example shows that although the capacity for estimating $\dot{\delta}$ is limited for this intervention category, the proposed framework has yielded an acceptable performance in estimating the deterioration state as verified by the true state being within the confidence interval of the model estimates.

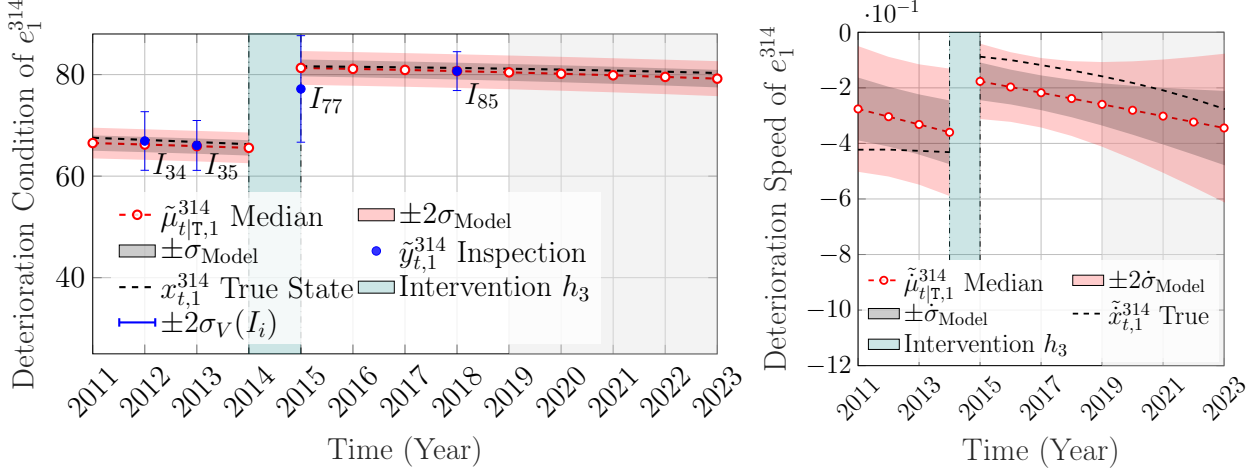


Figure 5.5 Deterioration state analysis for the condition and the speed based on the observations $\tilde{y}_{t,1}^{314} \in [25, 100]$ of the synthetic structural element e_1^{314} with an intervention h_3 at time $\tau = 2015$, error bars representing the inspectors' uncertainty estimates, and the shaded area representing the forecast period.

In order to examine the capacity of modelling the effects of interventions for the entire population of synthetic structural elements, the errors in the state estimates after an intervention are examined. Table 5.3 shows the expected errors in the deterioration condition $\mathbb{E}[\epsilon] = \mu_{\tau|\tau} - x_\tau$, and the deterioration speed $\mathbb{E}[\dot{\epsilon}] = \dot{\mu}_{\tau|\tau} - \dot{x}_\tau$, alongside the standard deviations σ_ϵ , $\dot{\sigma}_\epsilon$ and the skewness γ and $\dot{\gamma}$ for the condition and the speed, respectively.

Table 5.3 The error in the state estimate following an intervention represented by the expected error \pm standard deviation and skewness γ for a sample of 414 synthetic structural elements.

Intervention	$\mathbb{E}[\epsilon] \pm \sigma_\epsilon$	γ	$\mathbb{E}[\dot{\epsilon}] \pm \dot{\sigma}_\epsilon$	$\dot{\gamma}$
h_1	-0.22 ± 1.62	-0.09	0.04 ± 0.12	0.38
h_2	$+0.09 \pm 1.75$	-0.34	0.09 ± 0.13	0.01
h_3	-0.54 ± 2.29	0.05	0.10 ± 0.15	0.38

The error estimates reported in Table 5.3 show that for a sample of $E_r = 414$ synthetic structural elements, the distribution of errors is approximately symmetric (i.e. $-0.5 < \gamma < 0.5$), and that the bias in the estimates is insignificant compared to the range of values of which the

speed and the condition can take. Moreover, it is noticed that the estimated error increases with major interventions (i.e. h_3 vs. h_1); this is attributed to the fact that major interventions are applied to structures having an average health condition, which is associated with an increase in the uncertainty of the deterioration state estimates.

5.4.2 Model Validation Using Real Data

Analyses with real data involves two types of structural element; the *front walls* and the *beams* of different bridges. The first dataset consists in the interventions and inspections for front walls which is classified as an abutment element [7]. This dataset includes a total of $E = 16360$ structural elements taken from $B = 8278$ bridges. The subset of bridges that underwent interventions is composed of $B_r = 193$ bridges with $E_r = 319$ front wall structural elements. The type of interventions involved in the analyses on front walls are categorized according to the structures' inspection manual [7]. The first intervention category h_2 is composed of activities that relate to strengthening and consolidation. The second intervention category h_3 includes a variety of repair activities, such as the repair of concrete elements and masonry wall elements. Quantifying the effect of the aforementioned intervention categories is done using the proposed framework. The estimated model parameters for each category of interventions are shown in Table 5.4. The recursive state estimation for the ex-

Table 5.4 Estimated model parameters for interventions on the front wall structural elements.

Intervention	σ_{w_r}	$\dot{\sigma}_{w_r}$	$\ddot{\sigma}_{w_r}$	σ_{h_r}	$\dot{\sigma}_{h_r}$	$\ddot{\sigma}_{h_r}$
h_2	6.03	0.05	0.02	5.00	0.27	0.03
h_3	9.34	0.05	0.01	9.99	0.31	0.02

pected network-scale improvement in the condition δ and speed $\dot{\delta}$ are shown in Figure 5.6. In this figure, the network-scale improvement in the condition from applying h_2 interventions is $\mu_2^\delta = 13.57$ with $\sigma_2^\delta = 1.38$, compared to $\mu_3^\delta = 17.56$ with $\sigma_3^\delta = 1.28$ gained from applying h_3 interventions. Similarly, the deterioration speed improvement for h_3 interventions is $\mu_3^{\dot{\delta}} = 0.16$ with $\sigma_3^{\dot{\delta}} = 0.05$, which is better than h_2 interventions with $\mu_2^{\dot{\delta}} = 0.13$ and $\sigma_2^{\dot{\delta}} = 0.06$. Moreover, it can be noticed that the uncertainty of the network-scale estimate for δ and $\dot{\delta}$ is decreasing as the number of structural elements that underwent interventions h_2 and h_3 increases.

Examples of time series analyses for structural elements that underwent an intervention from each category are shown in Figures 5.7-5.8. Figure 5.7 shows an example of a front wall structural element that underwent an intervention of type h_2 . In this figure, the estimate of the deterioration condition before the intervention has a lower uncertainty due to the ob-

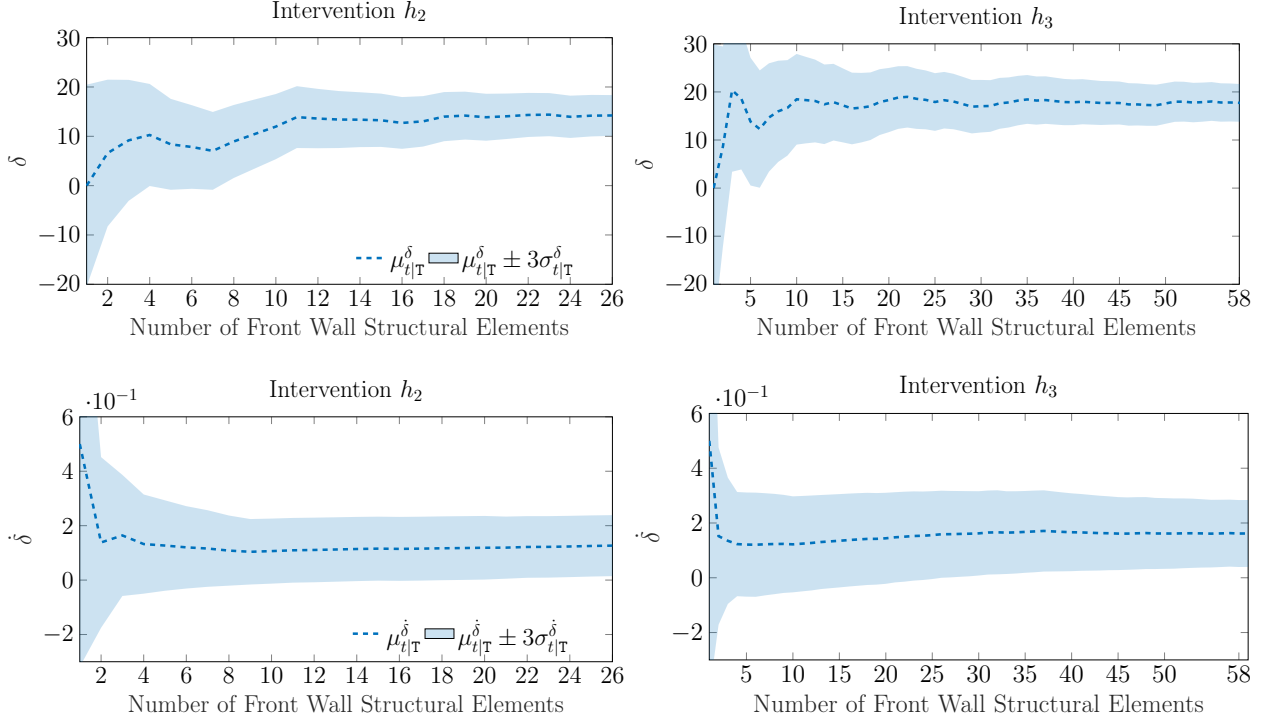


Figure 5.6 Recursive estimation for the network-scale change in the deterioration condition and speed of the front wall structural elements, using data from $E_2 = 26$ elements that underwent intervention h_2 , and $E_3 = 58$ elements that underwent intervention h_3 .

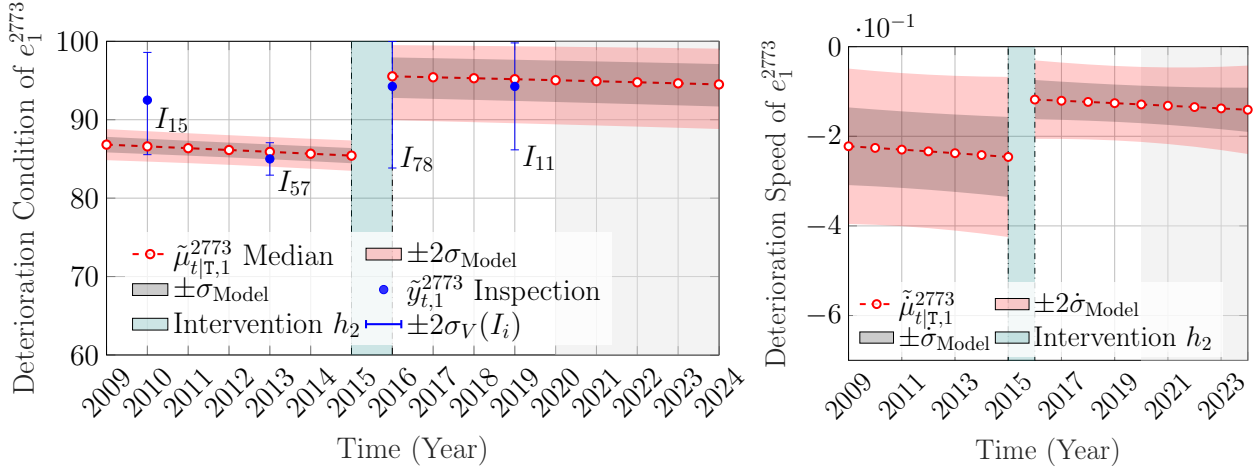


Figure 5.7 Deterioration state analysis for the condition and the speed based on the observations $\tilde{y}_{t,1}^{2773} \in [25, 100]$ of the front wall structural element e_1^{2773} with an intervention h_2 at time $\tau = 2016$, error bars representing the inspectors' uncertainty estimates, and the shaded area representing the forecast period.

servation from an inspector with a low uncertainty. The second time series example, shown in Figure 5.8, is for a concrete front wall element that underwent repairs activities from the intervention category h_3 . In Figure 5.8 it is noticed that the deterioration speed estimate has

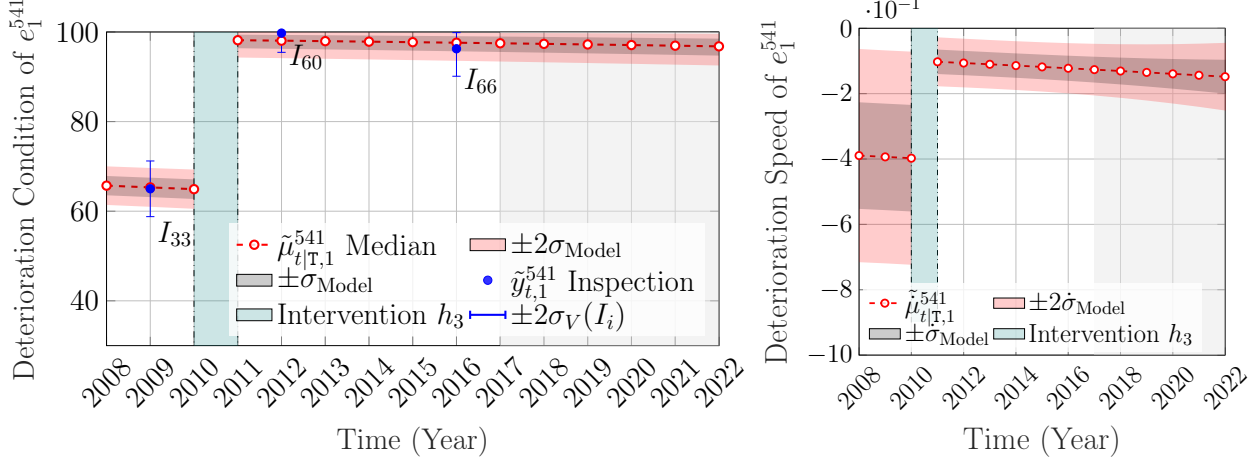


Figure 5.8 Deterioration state analysis for the condition and the speed based on the observations $\hat{y}_{t,1}^{541} \in [25, 100]$ of the front wall structural element e_1^{541} with an intervention h_3 at time $\tau = 2011$, error bars representing the inspectors' uncertainty estimates, and the shaded area representing the forecast period.

a high uncertainty before the intervention compared to the estimate after the intervention. This is justified by the fact that a single observation is available before the intervention compared to two observations after; in addition, if the state estimate of the deterioration speed is near zero (upper bound), this estimate is ensured to be nonpositive using the monotonicity constraint $\dot{\mu}_{t,p}^j + 2\dot{\sigma}_{t,p}^j \leq 0$, if this constraint is violated, the PDF of the speed is truncated using the PDF truncation method described in §2.3.3.

The second database consists in the inspections and interventions of beam structural elements. This dataset includes a total of $E = 24824$ structural elements from $B = 2881$ bridges. The number of bridges that underwent interventions on beams is $B_r = 95$, with $E_r = 485$ beam structural elements. A single intervention category h_3 is examined with activities that includes repair works for concrete and steel beam elements [7]. The estimated model parameters associated with h_3 are reported in Table 5.5. The hidden state estimation for the

Table 5.5 Estimated model parameters for interventions on the beam structural elements.

Intervention	σ_{w_r}	$\dot{\sigma}_{w_r}$	$\ddot{\sigma}_{w_r}$	σ_{h_r}	$\dot{\sigma}_{h_r}$	$\ddot{\sigma}_{h_r}$
h_3	5.68	0.06	0.01	6.75	0.12	0.02

expected improvement in the condition and the speed are shown in Figure 5.9.

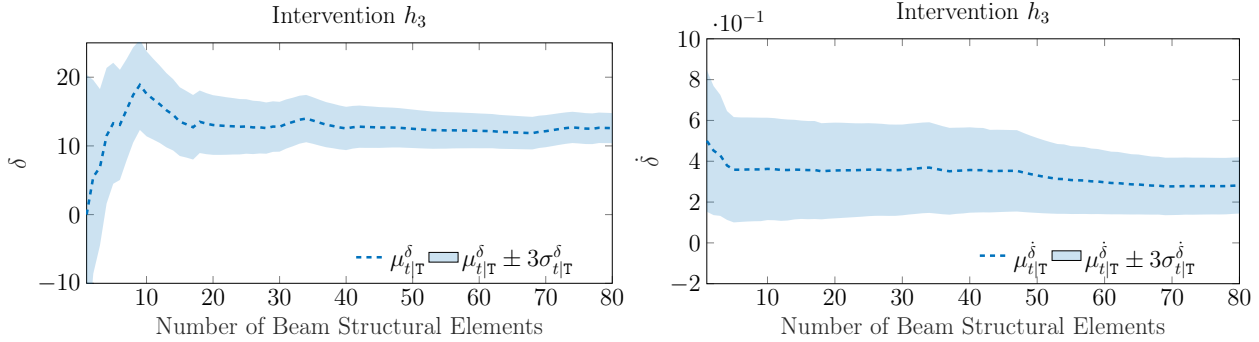


Figure 5.9 Recursive estimation for the network-scale change in the deterioration condition and speed based on $E_3 = 80$ beam structural elements that underwent intervention h_3 .

From this figure, it is noticed that the network-scale expected improvement in the condition is $\mu_3^\delta = 12.61$ with $\sigma_3^\delta = 0.77$, while the improvement in the speed is $\mu_3^{\dot{\delta}} = 0.28$ with $\sigma_3^{\dot{\delta}} = 0.06$. An example of beam structural element that underwent repairs of type h_3 is shown in Figure 5.10. In this example, the condition and speed state estimates show improvements in the health state of structural element e_1^{520} , following the intervention at year $\tau = 2011$.

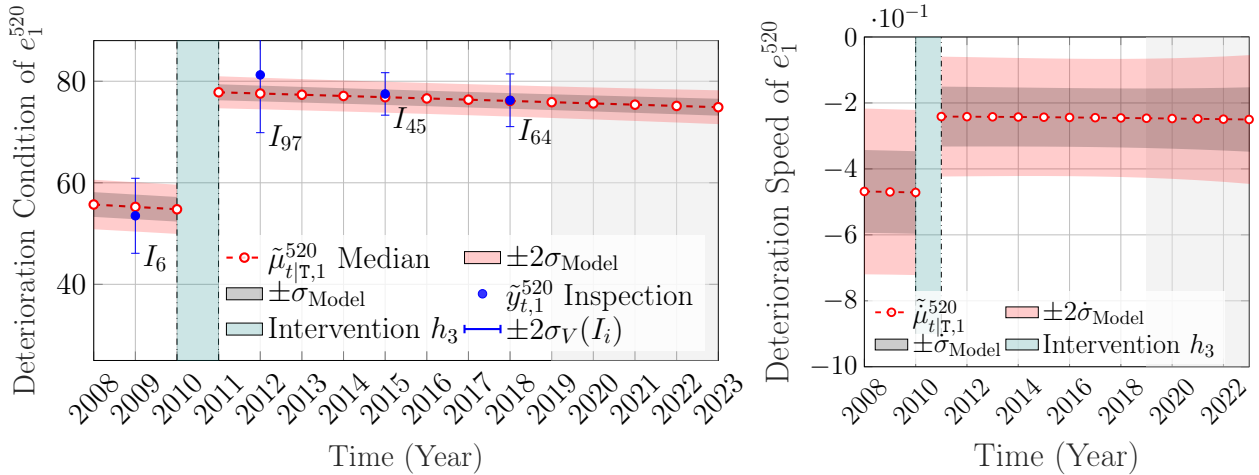


Figure 5.10 Deterioration state analysis for the condition and the speed based on the observations $\tilde{y}_{t,1}^{520} \in [25, 100]$ of the beam structural element e_1^{520} with an intervention h_3 at time $\tau = 2011$, error bars representing the inspectors' uncertainty estimates, and the shaded area representing the forecast period.

5.5 Conclusion

In this chapter, the effect of interventions is quantified as random variable based on visual inspections. The proposed recursive quantification framework is integrated within the SSM-KR deterioration model. The performance of the proposed method is verified with synthetic data that emulates real data with interventions. The verification results demonstrated the predictive capacity with the true expected improvements being within the confidence interval of the model estimates, for each intervention category. Furthermore, the errors in the deterioration state estimates following an intervention are reported for a sample of synthetic structural elements. The error estimates have shown that major repairs have a larger error after an intervention. This is justified by the fact that the deterioration state estimates have a larger uncertainty in structures with an average health condition. This limitation can be mitigated if more observations become available. Furthermore, the proposed framework is validated with real data that includes two types of structural elements, namely front walls and beams structural elements. The validation involved estimating the expected improvement following different intervention categories as well as time series analyses for individual structural elements. The analyses with real data have shown a similar performance in comparison with the synthetic data. In summary, the proposed framework enables estimating the effect of interventions, locally and on network-scale, as random variables. This lays the ground work for performing probabilistic service-life deterioration analyses, risk analyses, and interventions planning.

CHAPTER 6 Network-Scale Deterioration Analyses

6.1 Introduction

In the previous chapters, a framework has been proposed to model the deterioration behaviour at the element-level, in addition to an intervention model that accommodates the effect of interventions on structural elements. These models are sufficient when examining the elements of a single bridge. However, for a network-scale analysis, decision makers are interested in identifying the overall deterioration state of bridges and of the network collectively [50, 57–60], so that they can examine the effectiveness of previous interventions on bridges, as well as the long term trend for the network’s condition. This also lays the foundations for solving problems such as prioritizing interventions on bridges under budgetary constraints [50, 57]. This chapter focuses on the estimation of the overall deterioration states of bridges as well as for an entire network. In §6.2, the network-scale data is presented, which includes information about the different types of structural systems as well as intervention costs and traffic data. The framework proposed for estimating the deterioration states of individual bridges and of the entire network is presented in §6.3. This is followed by deterioration analyses on a selection of bridges, with and without interventions, along with analyses on the entire network in §6.4. Finally, §6.5 presents a summary for the analyses and results obtained in this chapter. The main contributions in this chapter are:

- A method for estimating the overall deterioration states and the effect of interventions for bridges as well as the entire network.
- An assessment for the effects of interventions performed on the network.

6.2 Network-Scale Data

In this section, structural element groups are presented along with other information relevant to assessing the overall deterioration state of bridges as well as for the entire network.

6.2.1 Structural Element Groups

In this study, structural elements are divided into two main groups: primary \mathcal{G}_1 and secondary \mathcal{G}_2 . The primary group represents structural elements that support or transfer the vertical loads to other elements or to the ground [7]. This group is represented by

$\mathcal{G}_1 = \{\mathcal{S}_{1,1}, \dots, \mathcal{S}_{1,\mathsf{G}_1}\}$, and consists in $\mathsf{G}_1 = 45$ structural element categories, of which 40 categories are evaluated through visual inspections. On the other hand, the secondary structural element group $\mathcal{G}_2 = \{\mathcal{S}_{2,1}, \dots, \mathcal{S}_{2,\mathsf{G}_2}\}$ consists in $\mathsf{G}_2 = 44$ structural element categories with 29 categories evaluated using visual inspections. Figure 6.1 shows two bar charts for each structural group with the number of structural elements that are inspected in each category. The reported numbers correspond to the inspections and interventions data collected from late 2007 up to the end of 2019.

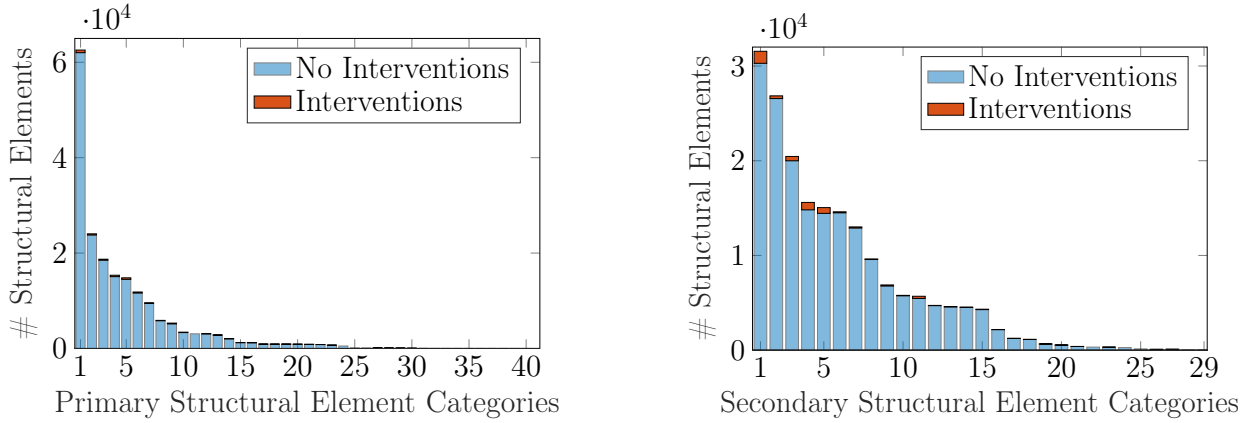


Figure 6.1 Primary \mathcal{G}_1 and secondary \mathcal{G}_2 structural elements categories without interventions represented by the light blue colour and with interventions represented by the red colour, with the categories sorted in a descending order based on the number of elements.

The top three categories in each group are reported in Table 6.1, while the full list of categories are reported in Appendix F. From the bar chart, it is noticed that there is a variability in the number of structural elements across the different categories, implying that a normalization is required when evaluating the aggregated deterioration of a bridge. This is to avoid biasing the aggregated deterioration state towards a single or few structural categories.

Table 6.1 Structural element groups sorted using descending order based on the number of elements in each category.

Primary \mathcal{G}_1	Secondary \mathcal{G}_2
$\mathcal{S}_{1,1}$: Beams	$\mathcal{S}_{2,1}$: Safety Barriers (left or right)
$\mathcal{S}_{1,2}$: External Side	$\mathcal{S}_{2,2}$: Wing/return walls
$\mathcal{S}_{1,3}$: Bearing Seat	$\mathcal{S}_{2,3}$: Wheel Guard

6.2.2 Bridge-level Data

The data at the bridge-level represent information about the structural attributes associated with the set of bridges \mathcal{B} that contains $B \approx 7000$ bridges. The structural attributes include the annual average of daily traffic (AADT), the annual average of daily truck-traffic (AADTT), and the length of the bridge. Bridge-level data also include information about the annual intervention costs associated with each bridge. These information are available only for a subset $\mathcal{B}_c \subset \mathcal{B}$, with $B_c = 2999$ bridges. Figure 6.2 shows the aggregated relative annual costs associated with interventions on bridges. The relative costs, with respect to the year 2012, are considered in order to avoid unnecessary disclosure of information.

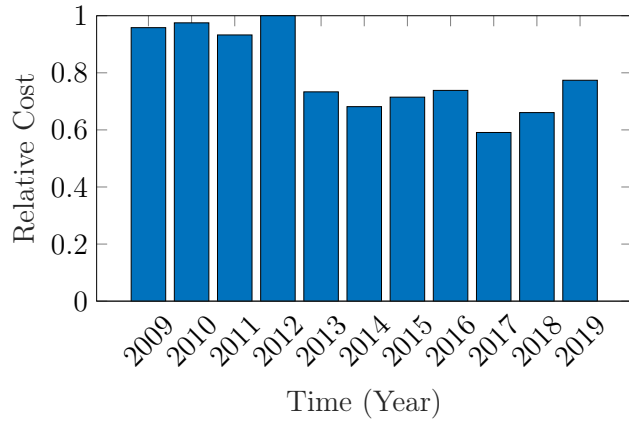


Figure 6.2 Relative annual aggregated costs of interventions for the set $\mathcal{B}_c \subset \mathcal{B}$, with $B_c = 2999$ bridges, which represent all bridges with reported costs.

From Figure 6.2, intervention costs show variations over time; these variations can be cross-checked with improvements in the condition, as well as the number of reported interventions. It must be noted that the reported costs also cover repair works on structural elements that were not inspected visually, therefore, the conclusions derived with regards to the costs are limited by the incompleteness of the available data.

6.3 Network-Scale Deterioration Analyses

Estimating the overall deterioration state of a bridge starts from the deterioration estimates of the structural components e_p^j that makes up a bridge b_j . These analyses are performed using both the SSM model presented in Chapter 3, and the SSM-KR deterioration model presented in Chapter 4. Generally, the SSM model is utilized only when the number of structural elements, or the number of bridges that share the same element category is less than 100. Otherwise, if a structural category \mathcal{S}^* exist within more than 100 bridges, the

deterioration states for element $e \in \mathcal{S}^*$ are estimated using the SSM-KR model. The next subsections describe the estimation process of the deterioration states for each bridge as well as the network, followed by techniques utilized in handling missing data and outliers.

6.3.1 Estimating the Deterioration State of a Bridge

After estimating the deterioration states for each structural element, the deterioration states of the elements categories \mathcal{S}_m^j are estimated. This is done to reduce biases resulting from having more structural elements in a single structural category compared to other categories. Furthermore, the contribution of a structural element to the deterioration state estimate of a structural category is assumed to be associated with the quantity of the structural element. Thus, the deterioration state $\mathbf{o}_{m,t}^j$ of the structural category \mathcal{S}_m^j in bridge b_j is expressed by,

$$\mathbf{o}_{m,t}^j = \sum_{p=1}^{P_m^j} \left(\mathbf{x}_{p,t}^j \times \frac{d_p^j}{\sum_p d_p^j} \right), \quad (6.1)$$

where P_m^j is the number of structural elements in category \mathcal{S}_m^j and bridge b_j , and d_p^j refers to the quantity associated with the structural element e_p^j . The quantity is determined based on either the dimensions of the structural element or the number of units that make up an element [7]. Thereafter, estimating the bridge deterioration state \mathbf{s}_t^j is done using a weighted sum of the structural categories,

$$\mathbf{s}_t^j = \sum_{m=1}^{S_j} \left(\mathbf{o}_{m,t}^j \times \frac{1}{G^j} \right), \quad (6.2)$$

where G^j is the number of structural element categories in bridge b_j . Since there are two groups of structural elements \mathcal{G}_1 & \mathcal{G}_2 in each bridge, the deterioration state of each bridge will be represented by $\mathbf{s}_{t,1}^j$ for the primary group \mathcal{G}_1 , and $\mathbf{s}_{t,2}^j$ for the secondary group \mathcal{G}_2 . Figure 6.3 illustrates a breakdown for the structural components of a bridge $b_j \in \mathcal{B}$, along with the corresponding deterioration states associated with each component, which has the same colour code. From Figure 6.3, the deterioration state for each bridge b_j is represented by $\tilde{\mathbf{s}}_{t,1}^j$ for the primary group \mathcal{G}_1 , and $\tilde{\mathbf{s}}_{t,2}^j$ for the secondary group \mathcal{G}_2 . The deterioration state estimates for each group $\mathcal{G}_{1:2}$, are obtained by aggregating the deterioration state estimates $\tilde{\mathbf{o}}_{m,t}^j$ of each structural category \mathcal{S}_m^j . Similarly, the deterioration state estimates for a structural category \mathcal{S}_m^j are based on the aggregation of the deterioration states $\tilde{\mathbf{x}}_{t,p}^j$ of structural elements $e_p^j \in \mathcal{S}_m^j$.

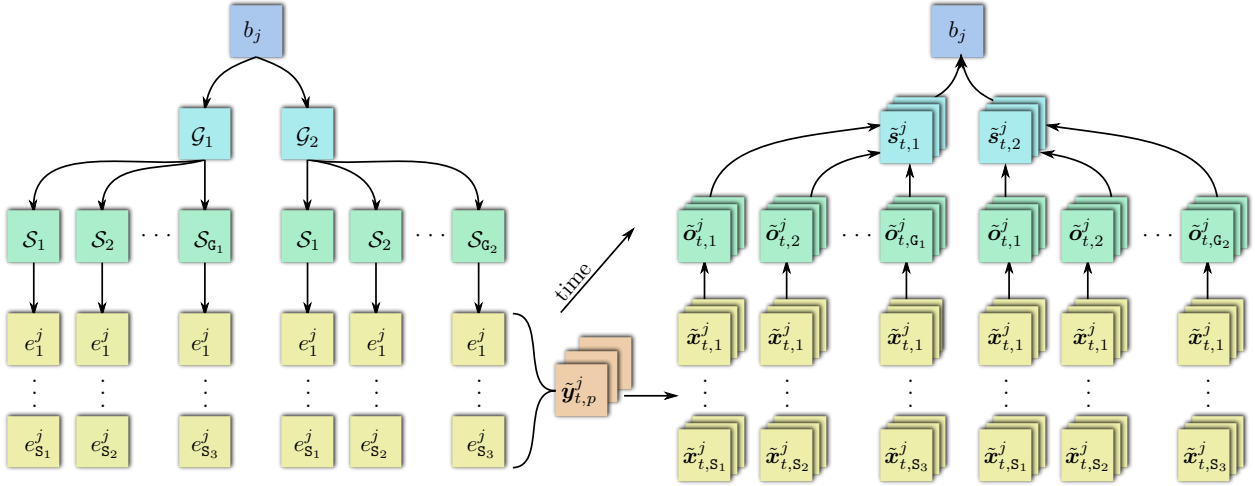


Figure 6.3 Hierarchy of the structural components in bridge b_j , with their corresponding deterioration states, with each level in the hierarchy differentiated using a unique colour.

6.3.2 Estimating the Deterioration State of the Network

Following the estimation of the deterioration state for each bridge, the deterioration state of the network \mathbf{q}_t is quantified using a weighted sum of the deterioration states of each bridge. The weights in this case can be either equal for all bridges (i.e., $\frac{1}{B}$), or based on one of the attributes z_j associated with each bridge. For example, determining the weights based on AADT or AADTT, highlights the overall traffic resilience in the network, such that if the overall health state of the network is high, then the anticipated disruption in traffic is low, due to little maintenance being required. Additionally, estimating the weights based on the length/size of the bridge, can reveal potential costs and disruptions in the connectivity of the network [50, 57]. From the analysis performed on bridges, it is concluded that there is no significant differences among the overall estimates of the network's condition, when using weights based on each of the aforementioned factors (see Appendix E). Therefore, the network-scale deterioration analysis in this thesis considers equal weights for all bridges,

$$\mathbf{q}_t = \sum_{j=1}^B \left(s_{j,t} \times \frac{1}{B} \right). \quad (6.3)$$

In this thesis, the network's overall deterioration state is represented by $\tilde{\mathbf{q}}_{t,1}$ for the primary structural elements group \mathcal{G}_1 , and $\tilde{\mathbf{q}}_{t,2}$ for the secondary structural elements group \mathcal{G}_2 .

6.3.3 Deterioration States Aggregation Method

The aggregation of the deterioration states in Equations 6.1-6.3 is done using the Gaussian mixture. The Gaussian mixture is an approach utilized to estimate the probability density (PDF) for a weighted sum of J Normally distributed random variables [81], such that,

$$p(\hat{\mathbf{x}}_t) = \sum_{j=1}^J \lambda^j \mathcal{N}(\mathbf{x}_t^j; \boldsymbol{\mu}_{t|t}^j, \boldsymbol{\Sigma}_{t|t}^j), \quad (6.4)$$

where J is the total number of components and λ^j is the mixture weight which pertain to $\sum_{j=1}^J \lambda^j = 1$. In the context of analyzing the deterioration of a system composed of multiple components, the overall deterioration state of the system can be approximated by a single Normal PDF, provided that the PDFs of the components are within close proximity of each other [82, 83]. Therefore, the expected value $\hat{\boldsymbol{\mu}}_{t|t}$ and covariance $\hat{\boldsymbol{\Sigma}}_{t|t}$ of the system are,

$$\begin{aligned} \hat{\boldsymbol{\mu}}_{t|t} &= \sum_{j=1}^J \lambda^j \boldsymbol{\mu}_{t|t}^j, \\ \hat{\boldsymbol{\Sigma}}_{t|t} &= \sum_{j=1}^J \lambda^j \boldsymbol{\Sigma}_{t|t}^j + \sum_{j=1}^J \lambda^j (\boldsymbol{\mu}_{t|t}^j - \hat{\boldsymbol{\mu}}_{t|t})(\boldsymbol{\mu}_{t|t}^j - \hat{\boldsymbol{\mu}}_{t|t})^\top. \end{aligned} \quad (6.5)$$

The covariance $\hat{\boldsymbol{\Sigma}}_{t|t}$ here is composed of the summation of two terms. The first term represents the "within components" contribution to the total variance, while the second term represents the "between components" contribution to the total variance [82].

6.3.4 Missing Data and Outliers

Performing deterioration analysis on a large dataset of elements and structures requires handling missing data and outliers. This is done using different methods and criteria which are discussed in details in this subsection.

Missing Attributes Data

In the context of this study, missing attributes data can be either 1) missing traffic data or 2) missing elements quantities. In the case of traffic data, missing information are imputed using the k -nearest neighbour algorithm (k -NN) [84], where the missing traffic data are estimated based on the data of $k = 5$ nearest bridges. On the other hand, if an element's quantity d_p^j is missing, the average quantity of elements within the same category is considered for replacing the missing value.

Missing Interventions Data

There are three cases for missing interventions data, which are either, 1) the type of intervention h_r is missing, 2) the prior estimate for the effect of an intervention h_r on structural category \mathcal{S} is unavailable, or 3) the intervention is not reported in the database.

In the first case where the year of intervention τ is known, but the type of intervention h_r is missing, the type of h_r is determined using the maximum likelihood estimate (MLE), with the log-likelihood described by,

$$\mathcal{L}_{h_r}(h_r) = \sum_{t=1}^{T_p} \ln f(y_{t,p}^j | y_{1:t-1,p}^j, h_r, \boldsymbol{\theta}), \quad (6.6)$$

where \mathcal{L}_{h_r} is the log-likelihood estimate for applying the effect of intervention $\boldsymbol{\delta}_r$ associated with intervention type h_r .

For the second case when the year of intervention τ and the type of intervention h_r are known, but the effect of this intervention $\boldsymbol{\delta}_r$ is not available, then the average estimate of the same intervention type h_r in other structural categories \mathcal{S} is utilized in approximating the missing values. The Appendix G contains the full list for the estimated network-scale effect of interventions for different structural categories.

The third case where interventions on bridges are not reported in the database is common among small bridges, those with low traffic loads, and for specific types of structural elements. Figure 6.4 shows an example of structural element e_1^{2905} , which has an improvement in the condition with no records of interventions. From Figure 6.4, the condition has improved according to the observations between years $t = 2011$ and $t = 2014$. This improvement is reported by the same inspector I_{12} who has reported the condition prior to the jump at the year $t = 2011$.

The presence of such cases can be handled using one of two options: The first option is to assume there was no intervention, which ultimately can result into a bias in the model estimates towards underestimating the condition, as shown in Figure 6.4. The second option is to assume that an intervention has taken place at the time of a positive jump in the condition, with a type of intervention determined using Equation 6.6. In order to apply the second option, it is required to detect patterns of improvement in the inspection data of

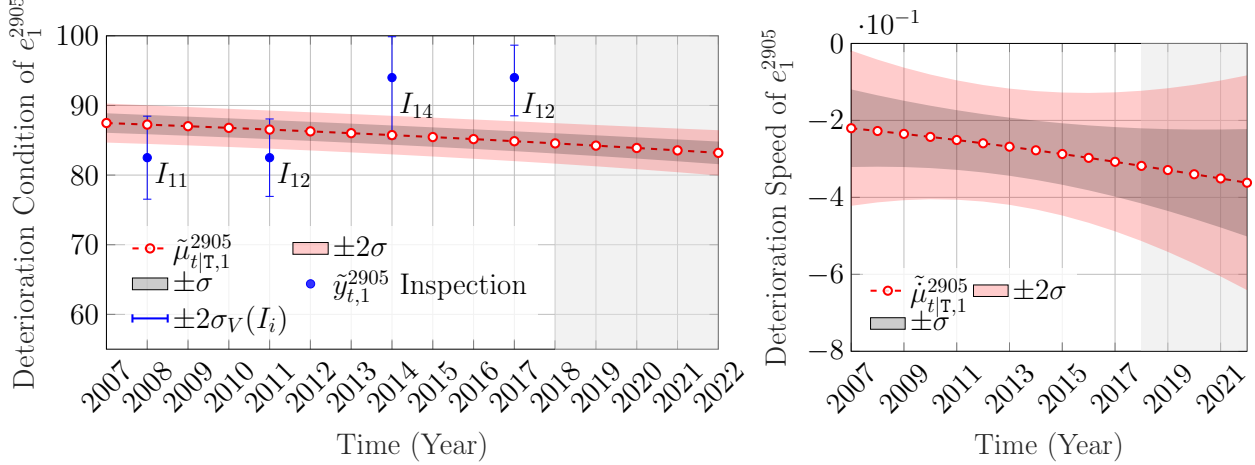


Figure 6.4 Deterioration state analysis for the condition and the speed based on the $\tilde{y}_{t,1}^{2905} \in [25, 100]$ of *front-wall* element, error bars representing the inspectors' uncertainty estimates, and the shaded area representing the forecast period.

structural elements, which is done using the metric,

$$\Delta_p = \frac{\sum_t \Delta_{t,p}^+}{\sum_t |\Delta_{t,p}^\pm|}, \quad \Delta_{t,p}^\pm = y_{t+\Delta t,p} - y_{t,p},$$

$$\Delta_{t,p}^+ = \begin{cases} \Delta_{t,p}^\pm, & \Delta_{t,p}^\pm > 0, \\ 0, & \Delta_{t,p}^\pm \leq 0, \end{cases} \quad (6.7)$$

where Δ_p is the ratio between the total positive changes in the condition Δ_p^+ , to all changes in the condition Δ_p^\pm for structural element e_p^j , with Δt being a reference to the time span between two consecutive observations. The ratio Δ_p is always positive and defined only for structural elements with three or more observations, and at least one observation showing improvement in the condition. Using the metric defined in Equation 6.7 on the same example in Figure 6.4, would yield $\Delta_1 = 1$. If an intervention is triggered for this case, the changes in the structural element e_1^{2905} condition and speed correspond to those shown in Figure 6.5. From Figure 6.5, the condition estimates of the model appears to be consistent with the reported observations after triggering the intervention automatically at year $\tau = 2012$. The network-scale analysis in this thesis are performed for both cases, i.e., using only the available intervention data, and accounting for the potentially unreported interventions through triggering interventions automatically.

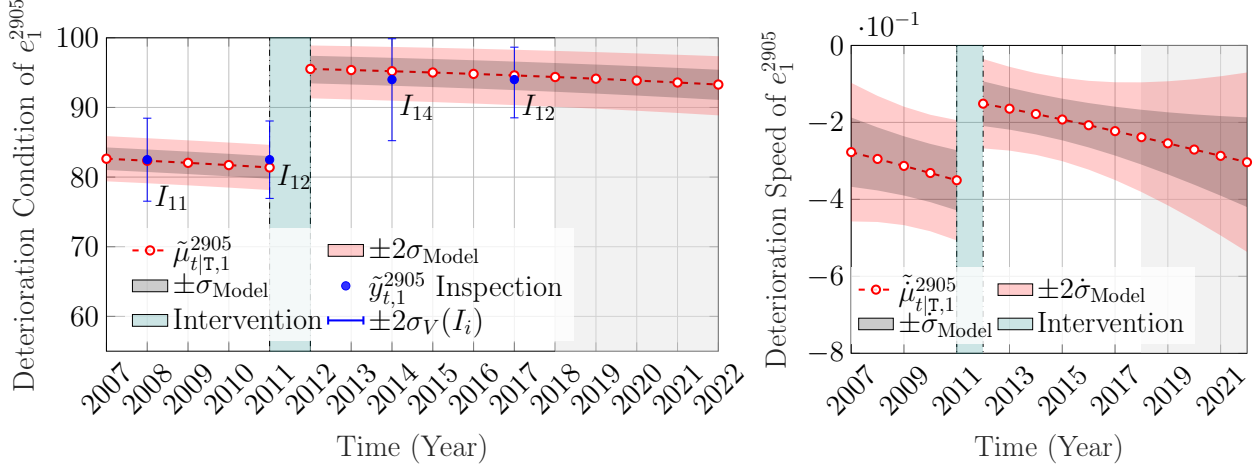


Figure 6.5 Deterioration state analysis for the condition and the speed based on the $\tilde{y}_{t,1}^{2905} \in [25, 100]$ of *front-wall* element, with an intervention automatically triggered at $\tau = 2012$, error bars representing the inspectors' uncertainty estimates, and the shaded area representing the forecast period.

Handling Outliers

An outlier is a data point significantly different from other observations, which can have a negative effect on the model performance or can cause numerical instability in the update step (see §2.3.3). The causes of an outlier are attributed either to 1) an incomplete interventions database or 2) an erratic entry in the inspections database. In the context of visual inspections, an outlier is assumed to exist in the time-series if:

1. There is a significant difference between consecutive observations $\|y_{t+\Delta t,p} - y_{t,p}\| > 15$.
 2. There is a significant condition improvement in a short period of time $T < 8$ years, with observations, $\max(\mathbf{y}_{t,p}) - \min(\mathbf{y}_{t,p}) > 15$, and $\sum_{t=1}^T (y_{t+\Delta t,p} - y_{t,p}) > 0$.
 3. The number of observations that indicate significant improvement, $y_{t+\Delta t} - y_t > 5$ in the structural element is greater than the number of observations indicating otherwise.
- Note that Δt refers to the time span between two consecutive observations.

If an outlier is detected based on the thresholds above, there are two possible lines of actions. If the outlier happened at a time t that matches the time τ of other interventions on the same bridge, then the outlier is classified as an intervention with the type h_r determined according to Equation 6.6. Otherwise, the outlier is considered as an erratic input and is removed from the time-series. Removing an outlier is done by relying on the standard deviations $\sigma_V(I_i)$ associated with each inspection $y_{t,p}^j$. The timestamp associated with the outlier t_ϕ^j is

determined based on the maximum difference between each inspection $y_{t,p}^j$, and the weighted average of all inspections \hat{y} , such that,

$$\begin{aligned} t_\phi^j &= \arg \max_t \|\mathbf{y}_{t,p}^j - \hat{y}\|, \\ \hat{y} &= \sum_t^{T_p} y_{t,p}^j \frac{\phi_t}{\sum \phi_t}, \end{aligned} \quad (6.8)$$

where t_ϕ^j is the timestamp that corresponds to the outlier observation $y_{t_\phi,p}^j$, and \hat{y} is a weighted average with the weights $\phi_t = \frac{1}{\sigma_V(I_i)}$. This approach allocates higher weights to more informative observations, which make inspections with a small $\sigma_V(I_i)$ unlikely to be selected for removal.

6.4 Case Studies

In this section, the capacity to aggregate the deterioration states is first demonstrated for individual bridges, followed by analyses on the entire network of bridges. It should be noted that for all examples presented in this chapter, the model forecasts for future deterioration states are done while assuming that no interventions are performed after the year 2020.

6.4.1 Deterioration Analyses for a Bridge Without Interventions

The first case study is about the bridge b_{990} , which is located in the Greater Montreal area. The length of the bridge is: $z_5 = 480.5$ m, which serves a traffic load AADT: $z_6 = 23700$, and AADTT: $z_7 = 1185$. The components that are visually inspected in the bridge are: $G_1 = 8$ elements categories from the primary elements group \mathcal{G}_1 and $G_2 = 14$ elements categories from the secondary elements group \mathcal{G}_2 . Figure 6.6 shows a bar graph for the number of elements in each structural category. The top three categories with most structural elements in each structural group in bridge b_{990} are shown in Table 6.2, while the full list of components is available in Appendix F.

Table 6.2 Structural element categories sorted using descending order based on the number of elements in bridge b_{990} .

Primary \mathcal{G}_1	Secondary \mathcal{G}_2
$\mathcal{S}_{1,1}$: Beams	$\mathcal{S}_{2,1}$: Bracing
$\mathcal{S}_{1,2}$: External Sides	$\mathcal{S}_{2,2}$: Wheel Guard
$\mathcal{S}_{1,3}$: Bearing pad	$\mathcal{S}_{2,3}$: Safety Barriers (left or right)

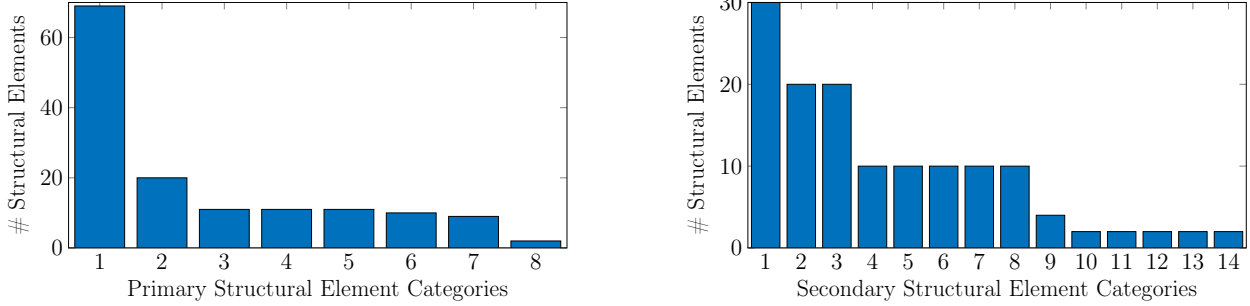


Figure 6.6 Primary and secondary structural elements categories in bridge b_{990} .

The primary elements categories has a total of $E_{990}^1 = 143$ elements, most of which are *beam* elements. Analyzing the deterioration of a structural category \mathcal{S}^j for the bridge b_j requires modelling the deterioration for each element $e_p^j \in \mathcal{S}^j$. Thereafter, the overall deterioration state $\mathbf{o}_{m,t}^j$ of the structural category \mathcal{S}_m^j can be obtained using the Gaussian mixture approach described in §6.3.3, where the mixture weights are based on the element quantity d_p^j such that, $\lambda_p^j = \frac{d_p^j}{\sum_p d_p^j}$. An example that illustrates the deterioration behaviour of a primary structural category is shown in Figure 6.7. In this figure, the overall deterioration condition $\tilde{o}_{m,t}^j$ and speed $\tilde{\dot{o}}_{m,t}^j$ are estimated for the *external-sides* element category $\mathcal{S}_{1,2}^{990}$, with $\tilde{y}_{op,t}^{990}$ representing the aggregated observations using the Gaussian mixture for all $e_p^{990} \in \mathcal{S}_{1,2}^{990}$.

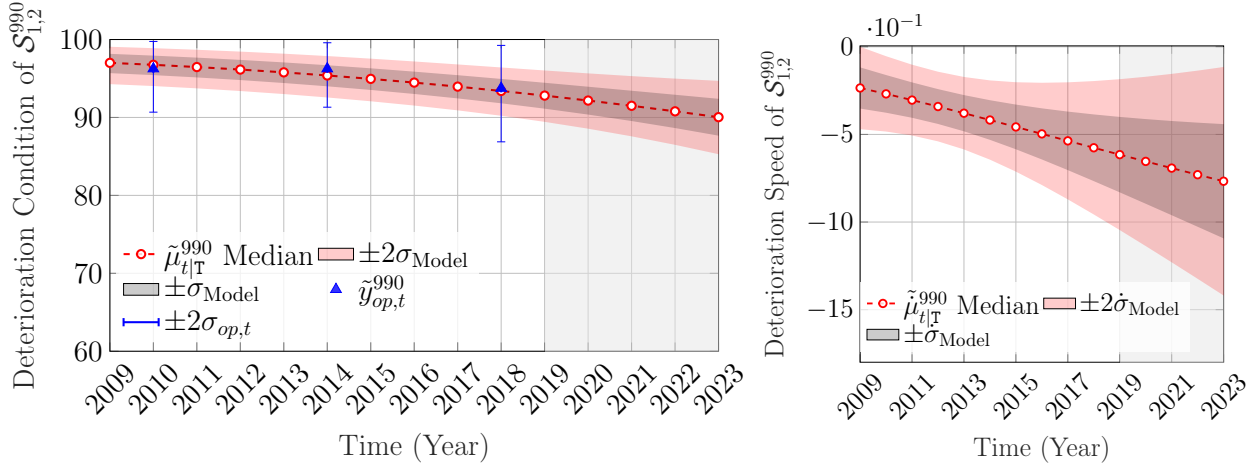


Figure 6.7 Deterioration state analysis for the condition and the speed based on the deterioration state estimates of *external-sides* elements $e_{1:20}^{990}$, with the aggregated observations $\tilde{y}_{op,t}^{990} \in [25, 100]$, and their corresponding uncertainty estimates represented by the error bars, with the shaded area representing the forecast period.

The overall deterioration state estimates $\tilde{s}_{1,t}^j$ for the primary structural group \mathcal{G}_1^{990} is shown in Figure 6.8, which summarizes the deterioration state estimates for all primary structural

elements in b_{990} . These estimates are again obtained using the Gaussian mixture reduction approach, with mixture weights $\lambda^j = \frac{1}{G_1}$. Furthermore, $\tilde{y}_{gp,t}^{990}$ in Figure 6.8, represents the aggregation of all observations on the primary structural elements.

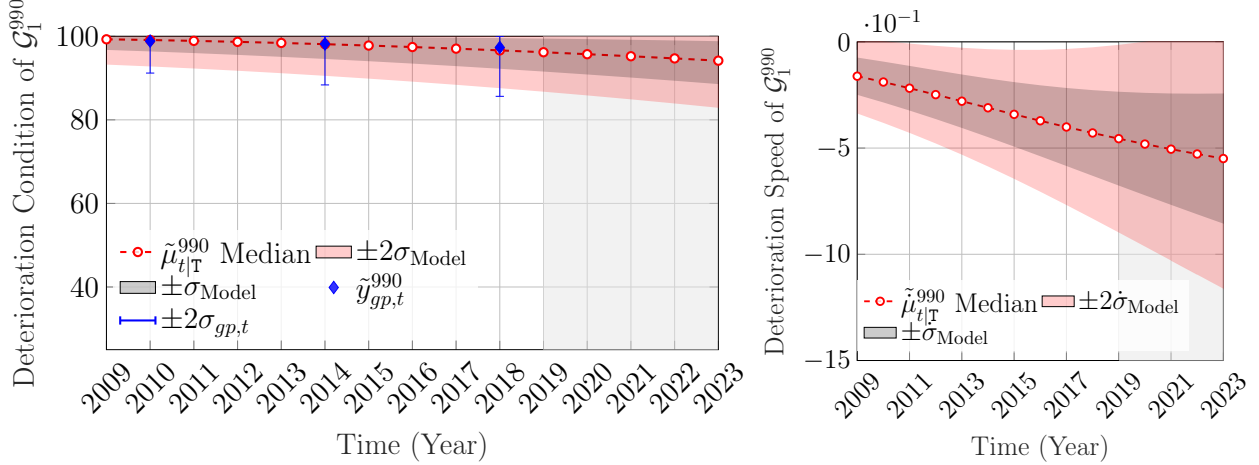


Figure 6.8 Deterioration state analysis for the condition and the speed of group \mathcal{G}_1^{990} , based on the deterioration state estimates of primary categories $\mathcal{S}_{1,1:8}^{990}$, with the aggregated observations $\tilde{y}_{gp,t}^{990} \in [25, 100]$, and their corresponding uncertainty estimates represented by the error bars, with the shaded area representing the forecast period.

The deterioration analyses for a secondary structural category are demonstrated with an example case in Figure 6.9. This example illustrates the deterioration condition $\tilde{o}_{m,t}^j$ and speed $\tilde{o}_{m,t}^j$ estimates for the *wheel guard* element category $\mathcal{S}_{2,2}^{990}$, with $\tilde{y}_{os,t}^{990}$ representing the aggregated observations in the secondary category $\mathcal{S}_{2,2}^{990}$. In Figure 6.9, the discrepancy between the model estimates and the aggregated observations is attributed to the initial deterioration speed, which is estimated based on the data from this bridge, as well as similar bridges that have *wheel guard* elements (see Chapter 4).

The overall deterioration state estimates $\tilde{s}_{t,2}^j$ for the secondary structural group $\mathcal{G}_2^{990} = \{\mathcal{S}_{2,1}^{990}, \dots, \mathcal{S}_{2,14}^{990}\}$ is shown in Figure 6.10. These estimates are obtained based on the deterioration condition $\tilde{o}_{m,t}^j$ and speed $\tilde{o}_{m,t}^j$ estimates for each secondary category, and mixture weights $\lambda^j = \frac{1}{G_2}$. From this figure, $\tilde{y}_{gs,t}^{990}$ is the aggregated observation for the secondary structural group \mathcal{G}_2^{990} .

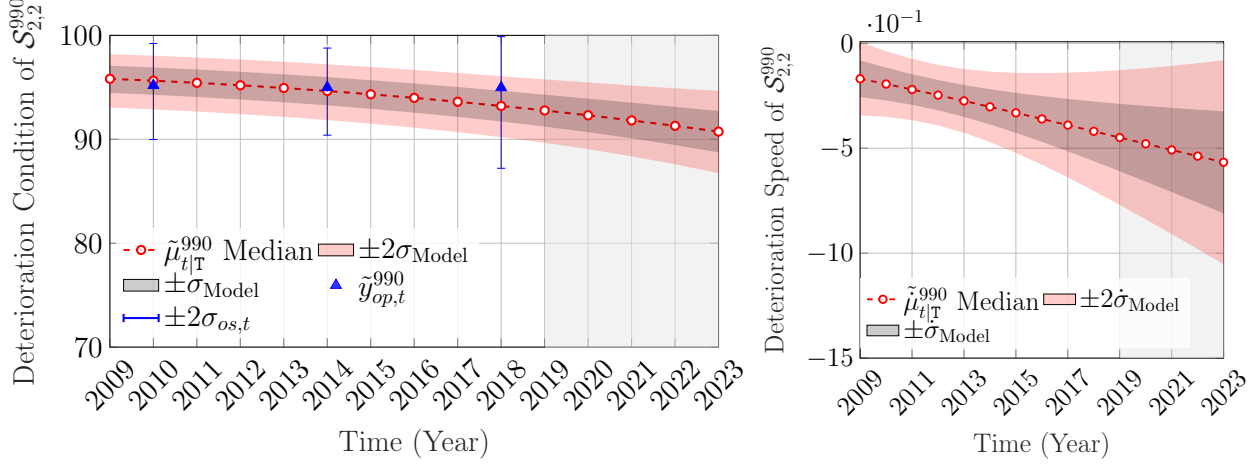


Figure 6.9 Deterioration state analysis for the condition and the speed based on the deterioration state estimates of *wheel guard* elements $e_{1:20}^{990}$, with the aggregated observations $\tilde{y}_{os,t}^{990} \in [25, 100]$, and their corresponding uncertainty estimates represented by the error bars, with the shaded area representing the forecast period.

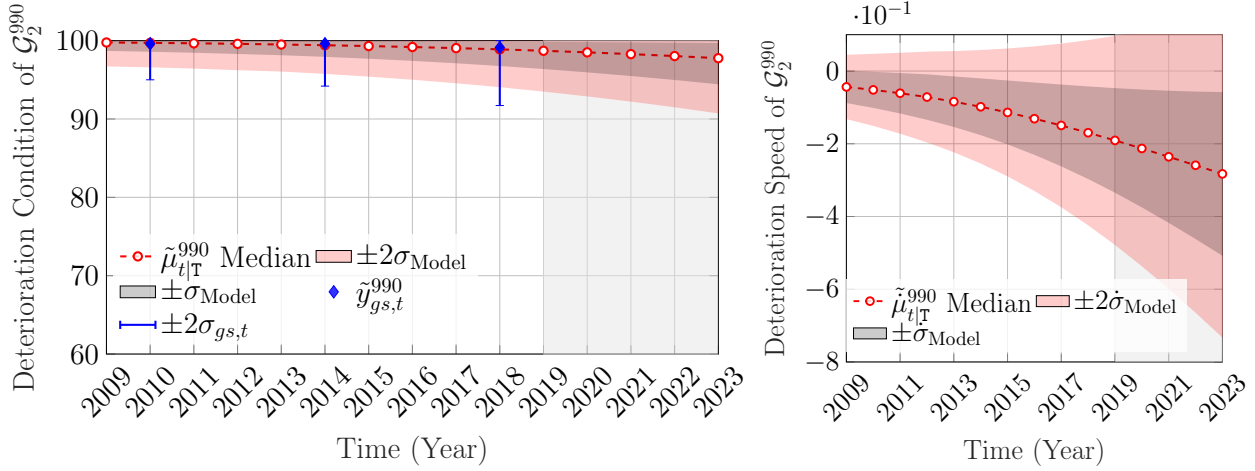


Figure 6.10 Deterioration state analysis for the condition and the speed of group G_2^{990} , based on the deterioration state estimates of secondary categories $S_{2,1:16}^{990}$, with the aggregated observations $\tilde{y}_{gs,t}^{990} \in [25, 100]$, and their corresponding uncertainty estimates represented by the error bars, with the shaded area representing the forecast period.

The results shown in this section demonstrate the capacity to aggregate the deterioration states of structural elements in order to obtain the overall deterioration state of the bridge, which is expressed by the deterioration state estimates for the primary G_1 , and the secondary G_2 structural elements.

6.4.2 Deterioration Analyses of Bridge With Interventions

In this case study, the deterioration analyses are performed for the visual inspection data for the bridge b_{3348} , which is located in the Greater Montreal area, with a length: $z_5 = 64.5$ m, traffic load AADT: $z_6 = 53000$, and AADTT: $z_7 = 3710$. The interventions database indicates that the bridge has undergone repair works in year $\tau = 2015$, however, the annual costs database shows that the bridge have had also other interventions with unknown type earlier in the year $\tau = 2012$. The structural components that are visually inspected include $G_1 = 8$ element categories from \mathcal{G}_1^{3348} , with $E^1 = 74$ elements and $G_2 = 15$ element categories from \mathcal{G}_2^{3348} with $E^2 = 54$. The bar graphs for \mathcal{G}_1^{3348} and \mathcal{G}_2^{3348} components are shown in Figure 6.11. In each graph, there are elements without interventions represented by the blue colour, elements with interventions represented by the red colour, and elements with uncategorized interventions represented by the orange colour. An uncategorized intervention is determined when the outlier criteria are met (see §6.3.4), and the outlier has occurred at a time t where interventions are reported in the database for the bridge.

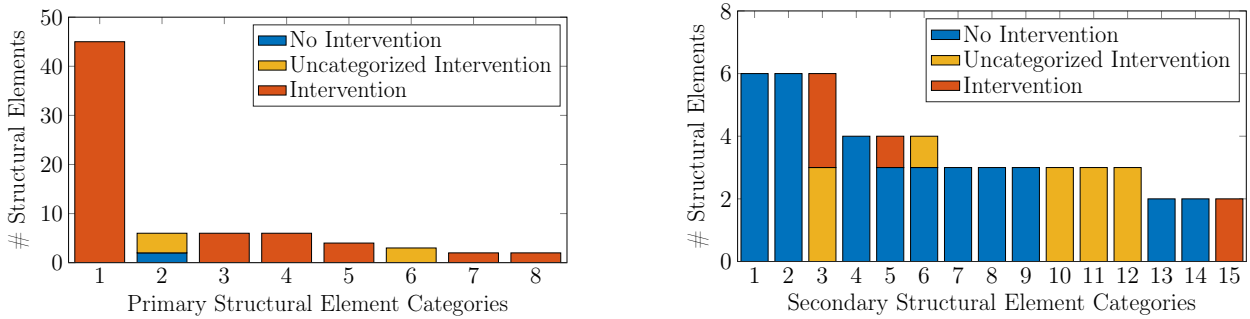


Figure 6.11 Primary and secondary structural elements categories of bridge b_{3348} without interventions represented by the blue colour, with interventions represented by the red colour, and with uncategorized interventions in the orange.

The top three categories in each group are reported in Table 6.3, while the full list of categories is available in Appendix F.

Table 6.3 Structural element categories sorted using descending order based on the number of elements in bridge b_{3348} .

Primary \mathcal{G}_1	Secondary \mathcal{G}_2
$\mathcal{S}_{1,1}$: Beams	$\mathcal{S}_{2,1}$: Diaphragms
$\mathcal{S}_{1,2}$: External Sides	$\mathcal{S}_{2,2}$: Safety Barriers (left or right)
$\mathcal{S}_{1,3}$: Bearing Pad	$\mathcal{S}_{2,3}$: Bracing

The deterioration analysis are performed on all the structural elements with visual inspection data using the SSM-KR deterioration model. An example for the deterioration analysis on a structural category $\mathcal{S}_1^{3348} \in \mathcal{G}_1^{3348}$ is shown in Figure 6.12. This example is for the deterioration analysis of the *slab* elements category $\mathcal{S}_{1,6}^{3348}$ based on inspection data from three *concrete slabs*. The state estimates for the deterioration condition $\tilde{o}_{m,t}^j$ and speed $\tilde{o}_{m,t}^j$ are shown in Figure 6.12. From this example, the aggregated observations $\tilde{\mathbf{y}}_{op,t}^{3348}$, and the model estimates $\tilde{\mathbf{o}}_{6,t}^{3348}$ after the intervention appears to be consistent with each other due to the small variability in the recorded data.

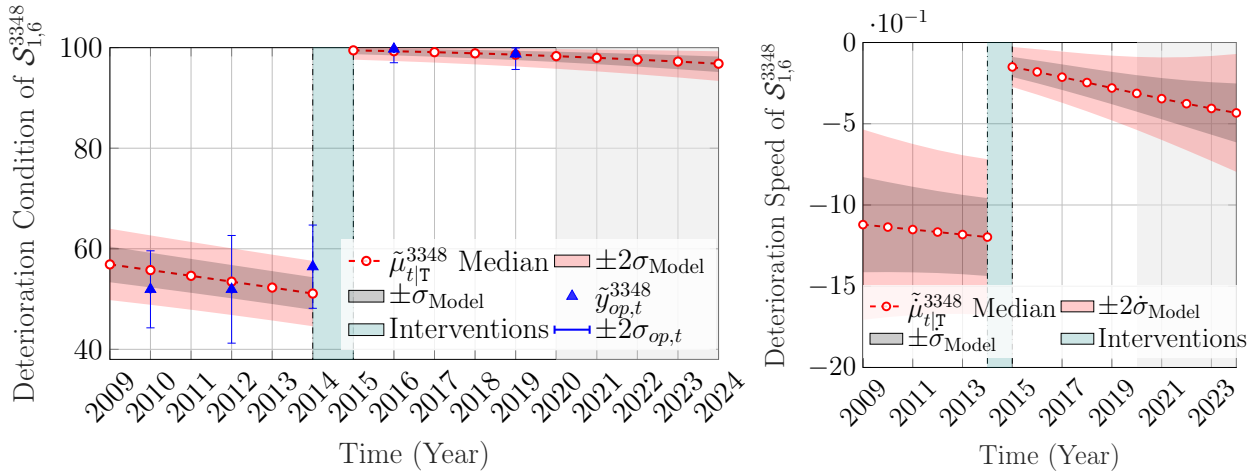


Figure 6.12 Deterioration state analysis for the condition and the speed based on the deterioration state estimates of *concrete slab* elements $e_{1:3}^{3348}$, with the interventions at time $\tau = 2015$, the aggregated observations $\tilde{\mathbf{y}}_{op,t}^{3348} \in [25, 100]$, with their corresponding uncertainty estimates represented by the error bars, and the shaded area representing the forecast period.

The overall state estimates for the primary structural group \mathcal{G}_1^{3348} is shown in Figure 6.13. In Figure 6.13, the overall improvement due to interventions in the year $\tau = 2015$ is noticeable in the condition $\tilde{s}_{t,1}^j$ and the speed $\tilde{s}_{t,1}^j$ state estimates. Moreover, the uncertainty of the state estimate prior to the intervention is significantly larger than the uncertainty after the intervention, which implies a large variability between the elements' deterioration states before the interventions.

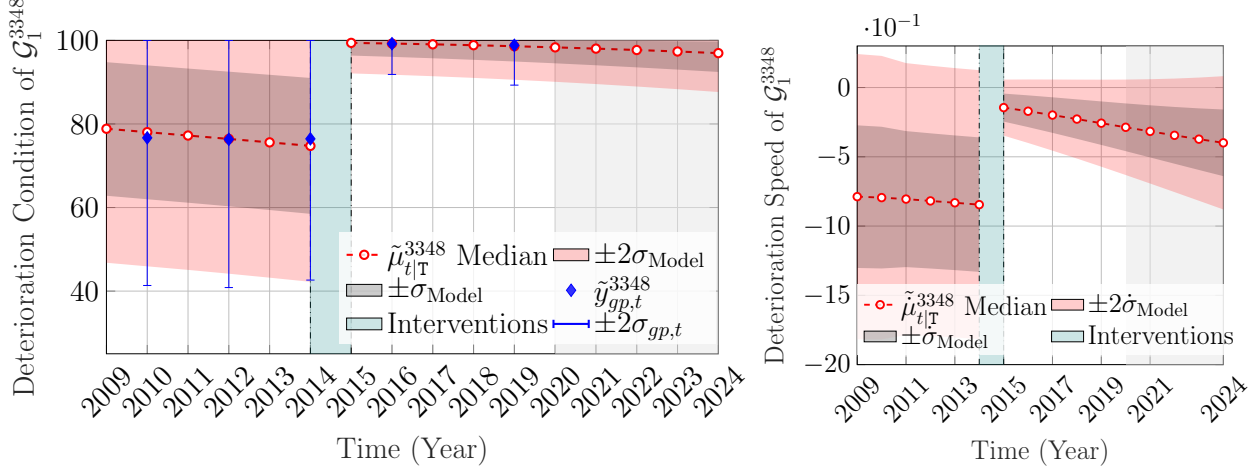


Figure 6.13 Deterioration state analysis for the condition and the speed based on the deterioration state estimates of the primary categories $\mathcal{S}_{1,1:8}^{3348}$, with the interventions at time $\tau = 2015$, the aggregated observations $\tilde{y}_{gp,t}^{3348} \in [25, 100]$, with their corresponding uncertainty estimates represented by the error bars, and the shaded area representing the forecast period.

On the other hand, an example for the deterioration state estimates of $\mathcal{S}_2^{3348} \in \mathcal{G}_2^{3348}$, is shown in Figure 6.14. This example is for the *pavement* elements category $\mathcal{S}_{2,12}^{3348}$ which had an uncategorized interventions in the year $\tau = 2015$. The type of intervention in this case is determined based on the MLE criterion described in §6.3.4.

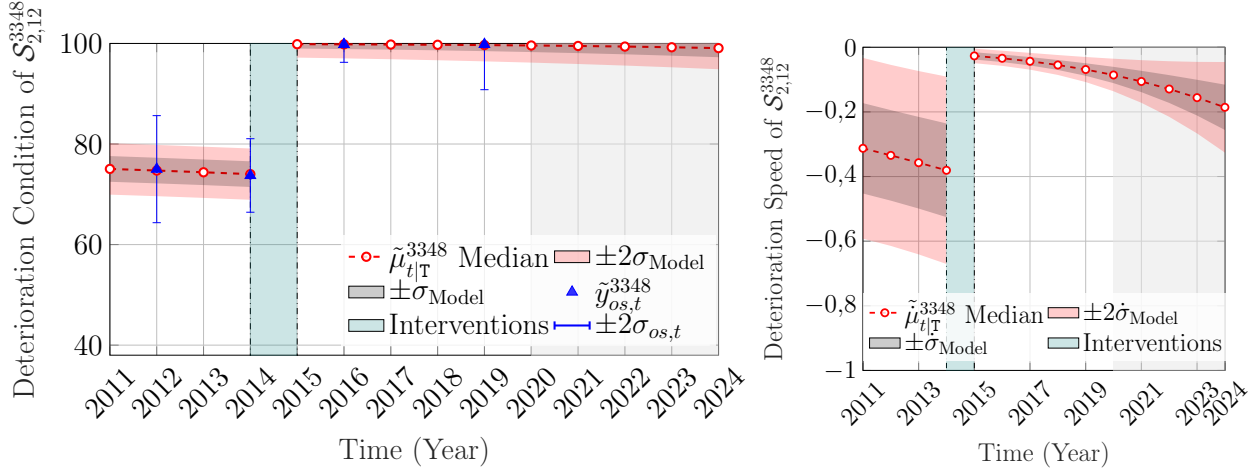


Figure 6.14 Deterioration state analysis for the condition and the speed based on the deterioration state estimates of *pavement* elements $e_{1:3}^{3348}$, with the interventions at time $\tau = 2015$, the aggregated observations $\tilde{y}_{os,t}^{3348} \in [25, 100]$, with their corresponding uncertainty estimates represented by the error bars, and the shaded area representing the forecast period.

The overall deterioration state estimates $\tilde{s}_{t,2}^j$ for the secondary group \mathcal{G}_2^{3348} is illustrated in Figure 6.15, which shows two major interventions at years $\tau_1 = 2012$ and $\tau_2 = 2015$. The first set of interventions is for the *sidewalk* elements category $\mathcal{S}_{2,11}^{3348}$, while the second

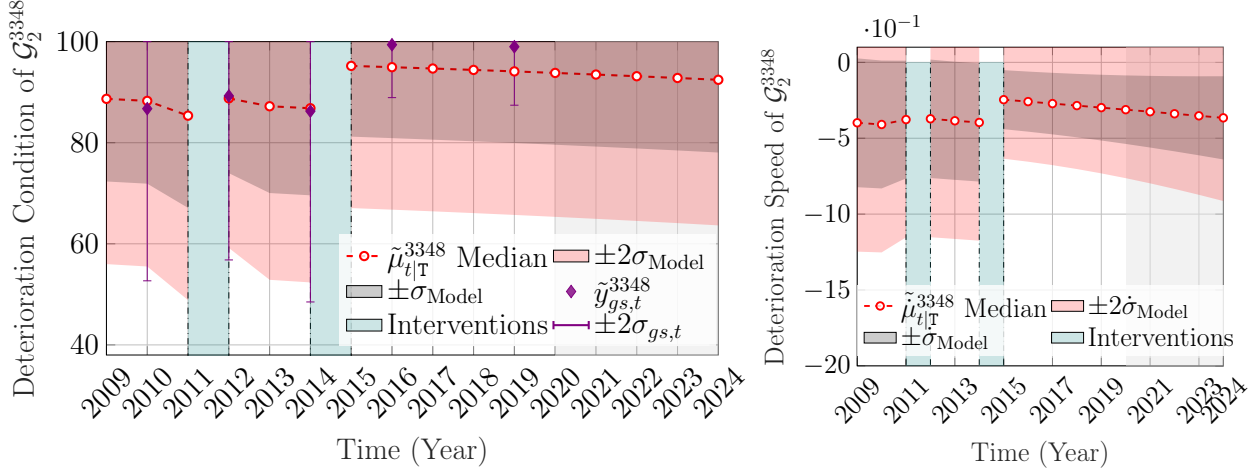


Figure 6.15 Deterioration state analysis for the condition and the speed based on the deterioration state estimates of the secondary categories $\mathcal{S}_{2,1:15}^{3348}$, with $\tilde{y}_{gs,t}^{3348} \in [25, 100]$ representing the aggregation for a subset of observations, with their corresponding uncertainty estimates represented by the error bars, and the shaded area representing the forecast period.

set of interventions involved more elements categories, which overall resulted in significant improvement in \mathcal{G}_2^{3348} . Nonetheless, the uncertainty for \mathcal{G}_2^{3348} is noticeably larger than the primary group \mathcal{G}_1^{3348} in Figure 6.13. This is because there are two structural elements categories in \mathcal{G}_2^{3348} that were not inspected in year $t = 2015$ or afterwards, in addition to one element category not inspected prior to year $t = 2015$, which led to $\tilde{y}_{gs,t}^{3348}$ (distinguished with the violet colour) representing the aggregation for a subset of observations in \mathcal{G}_2^{3348} .

The results in this section demonstrate the capacity to aggregate the deterioration states of elements with interventions, in order to obtain the overall deterioration states for the bridge b_{3348} . It is noticeable in this case that the overall deterioration states for \mathcal{G}_1 and \mathcal{G}_2 have a higher uncertainty relative to the previous case in §6.4.1. This is attributed to the uncertainty associated with the effect of interventions, in addition to not performing post-intervention inspections for some of the structural elements.

6.4.3 Deterioration State of the Network

After estimating the deterioration state for each bridge $b_j \in \mathcal{B}$, it becomes feasible to estimate the overall deterioration state of the network for the primary structural elements group $\tilde{\mathbf{q}}_{t,1}$, and the secondary structural elements group $\tilde{\mathbf{q}}_{t,2}$. The main goals in this case study are,

1. Examine the overall network-scale deterioration state estimates over time.
2. Quantify the effect of interventions performed on the network throughout the time-window of inspections.

For that end, a set of bridges \mathcal{B} is considered in the deterioration analysis. The set \mathcal{B} contains $B \approx 7000$ bridges, which collectively represent all bridges in the inspections database. The inspections time-window for this set is from year $t = 2009$ to year $t = 2019$, during which multiple interventions are performed, which are detailed in §6.4.4.

Estimating the deterioration state for the network is done based on the aggregation of the deterioration state estimates for all bridge using the Gaussian mixture approach defined in Equation 6.5, and by using equal weights $\lambda^j = \frac{1}{B}$. Such an approach considers an equal contribution for all bridges to the overall state of the network $\tilde{\mathbf{q}}_{t,1}$ and $\tilde{\mathbf{q}}_{t,2}$. Figures 6.16 and 6.17 show the network's condition and speed estimates for the primary and secondary structural elements.

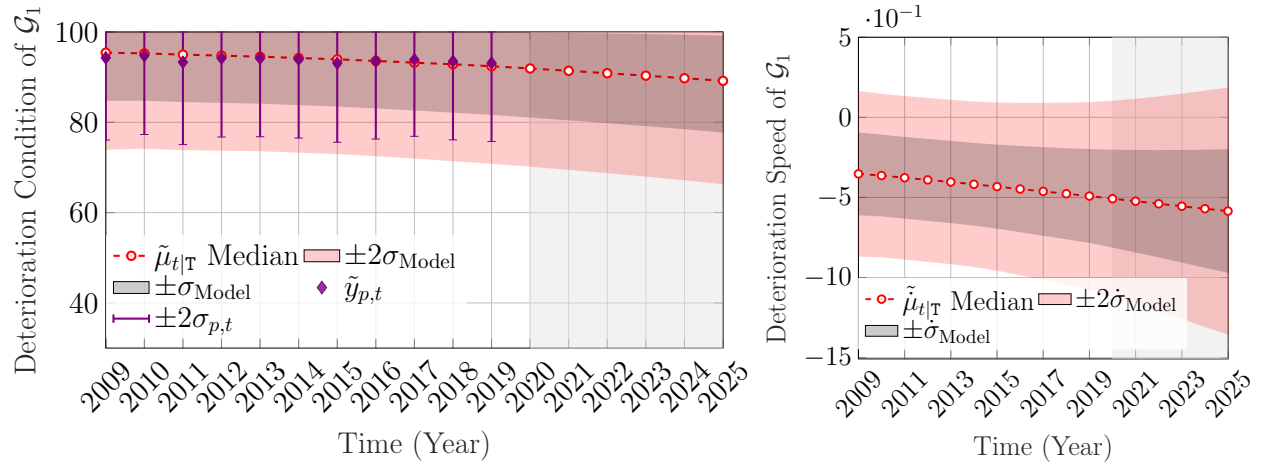


Figure 6.16 Deterioration state analysis for the network's condition and speed based on the average state of the primary structural elements from $B \approx 7000$ bridges, with the shaded area representing the forecast period.

From Figures 6.16 and 6.17, approximately 95% of bridges have a condition $\tilde{\mu}_{t|\mathbb{T}} \in [74, 100]$ for the primary structural elements, and $\tilde{\mu}_{t|\mathbb{T}} \in [71, 100]$ for the secondary structural elements, and overall, the health state for the secondary structural elements is higher than the primary structural elements. This is attributed to the frequency of interventions for the secondary structural elements being higher, relative to the primary structural elements (see Figure 6.20 in §6.4.4).

The network's condition estimates in Figures 6.16 and 6.17, do not fully match the inspection

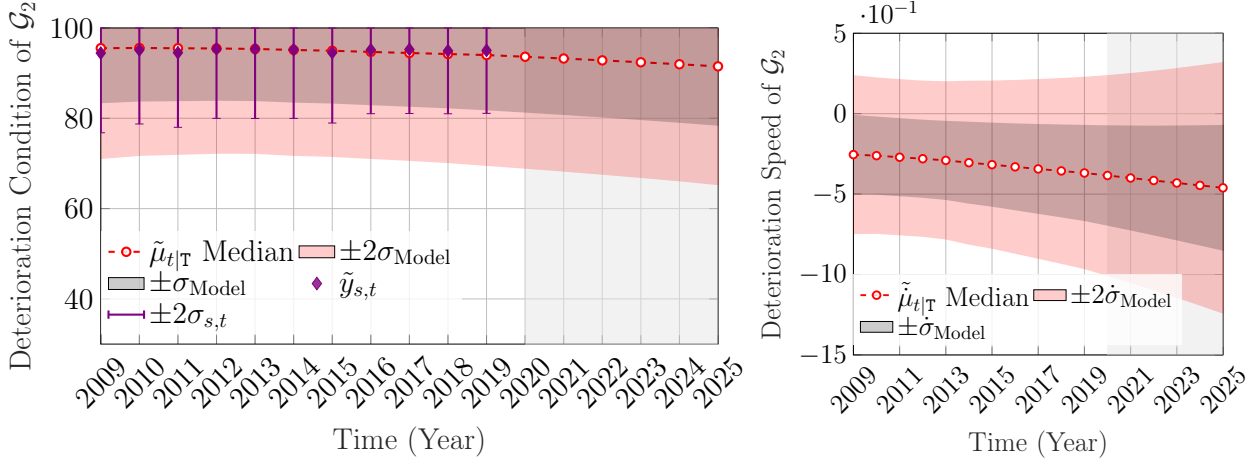


Figure 6.17 Deterioration state analysis for the network’s condition and speed based on the average state of the secondary structural elements from $B \approx 7000$ bridges, with the shaded area representing the forecast period.

data, especially in the case of the secondary group \mathcal{G}_2 . This is attributed to the incompleteness of the database, and having unreported interventions as discussed in §6.3.4. In order to assess the effect of unreported interventions, the criterion defined in Equation 6.7 is applied to identify structural elements with improving patterns and automatically trigger an intervention event. In this case, an intervention is triggered automatically if more than 90% of the changes among the observations indicate improvement in the condition (i.e., $\Delta_p > 0.9$) for any structural element e_p^j . The deterioration state estimates of the modified framework are shown in Figures 6.18 and 6.19.

The modified framework shows an overall better association with the trend of the inspection data, compared to the original framework (Figures 6.16 and 6.17). Therefore, in the case of relying only on the available interventions database, the network’s condition and speed estimates presented in Figures 6.16 and 6.17, can be interpreted as a lower bound estimates.

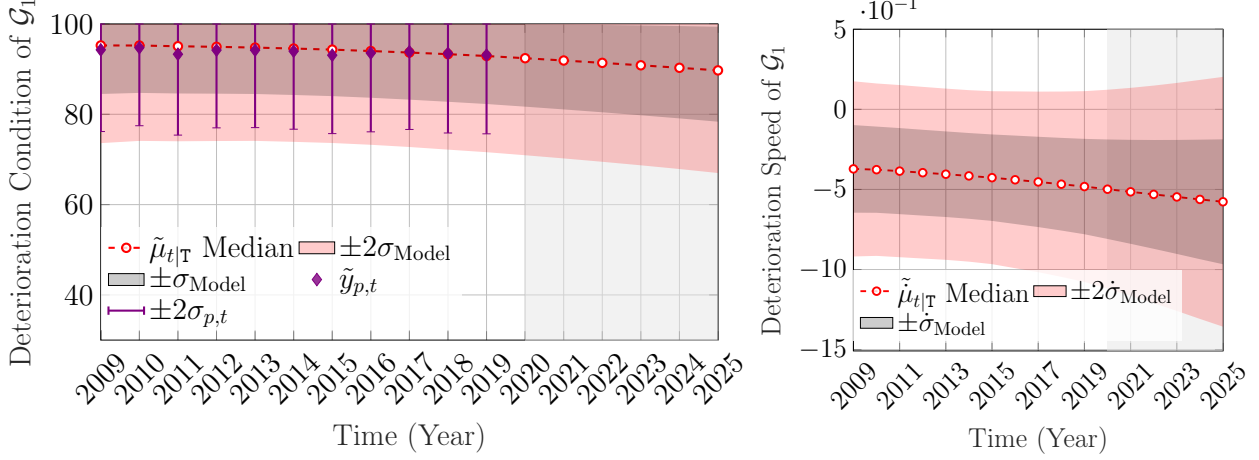


Figure 6.18 Deterioration state analysis for the network's condition and speed based on the average state of the primary structural elements from $B \approx 7000$ bridges, with automatically triggered interventions, and the shaded area representing the forecast period.

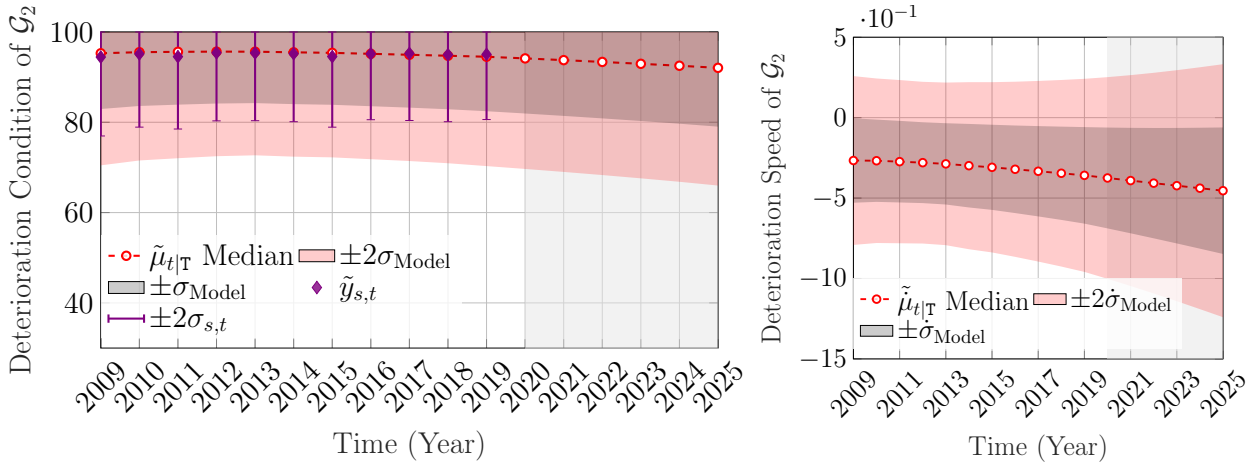


Figure 6.19 Deterioration state analysis for the network's condition and speed based on the average state of the secondary structural elements from $B \approx 7000$ bridges, with automatically triggered interventions, and the shaded area representing the forecast period.

Furthermore, it should be taken into consideration that the estimates presented in this section are only based on the visually inspected elements, whereas it is possible to have some structural elements that are not being inspected.

6.4.4 Network-Scale Effect of Interventions and Investments

The effects of interventions are quantified for each structural category \mathcal{S} as part of the network-scale deterioration analysis. Figure 6.20 illustrates the cumulative ratio for the total number of elements with interventions E_r over the total number of inspected elements E .

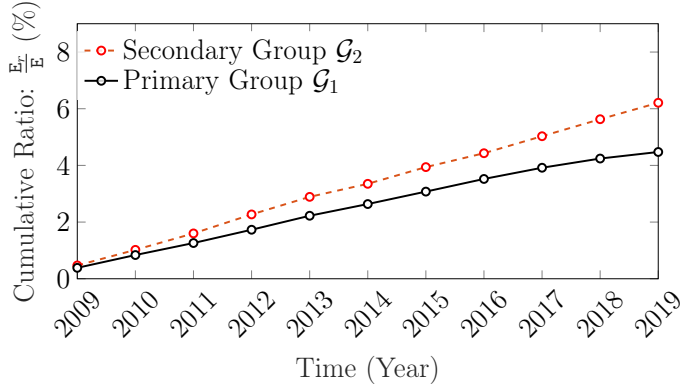


Figure 6.20 Cumulative ratio for the total number of elements with intervention E_r to the total number of visually inspected elements E , in each structural group \mathcal{G}_1 and \mathcal{G}_2 .

From Figure 6.20, it is noticed that since the year 2009 approximately 6% of the total number of inspected secondary elements have undergone interventions, compared to 4% of the primary elements.

The network-scale expected improvement in the condition for each structural category is reported in Appendix G. These estimates are based on the framework presented in Chapter 5, and the intervention/inspection data available for each structural category \mathcal{S} . Based on the estimates in Appendix G, the overall aggregated expected improvement in the condition for the primary structural elements \mathcal{G}_1 and the secondary structural elements \mathcal{G}_2 are reported in Table 6.4.

Table 6.4 Aggregated expected improvement in the condition for the primary structural elements \mathcal{G}_1 and the secondary structural elements \mathcal{G}_2 .

Structural Group	$\hat{\mu}_1^\delta \pm \hat{\sigma}_1^\delta$	$\hat{\mu}_2^\delta \pm \hat{\sigma}_2^\delta$	$\hat{\mu}_3^\delta \pm \hat{\sigma}_3^\delta$
Primary \mathcal{G}_1	0.8±5.5	10.7±8.3	14.3 ± 9.4
Secondary \mathcal{G}_2	17.5±3.8	9.5±6.5	17.9 ± 5.4

From Table 6.4, the aggregated improvements in the condition associated with the primary structural elements \mathcal{G}_1 coincides with the initial assumption that h_1 type of interventions have a minor effect relative to h_2 and h_3 . However, this is not the case for the secondary structural

elements \mathcal{G}_2 , as h_1 interventions show a significant effect on the condition. The reason behind this discrepancy is that minor interventions for the secondary structural elements are under reported in the database (see Table G.2), and thus the estimated effect of h_1 is based only on two structural categories, of which in both of them, h_1 have a significant effect on the condition. An example for a reported h_1 intervention in the secondary elements \mathcal{G}_2 , is the *asphalt resurfacing* for the *pavement* elements [7]. It should be noted that Table 6.4 is provided to offer an insight about the overall effect of interventions, but is not necessarily fully representative, as many types of interventions are under reported (see Appendix G). In order to assess the relation between interventions and costs, the subset of bridges $\mathcal{B}_c \subset \mathcal{B}$ with $B_c = 2999$ bridges, is considered in this assessment. Figure 6.21 shows a comparisons between the costs, number of interventions and the network-scale expected improvement in the condition following an intervention. All values in this figure are aggregated for each year, and the relative values are considered in order to perform the comparisons. From Figure 6.21, it is noticed that the highest costs are associated with years 2009-2012, which also correspond to the highest network-scale expected improvement in the condition, and some of the highest number of interventions performed. Nonetheless, intervention costs can vary among the structural categories, as well as the type of interventions performed, therefore, it is not a necessity for the number of interventions to be perfectly correlated with the costs.

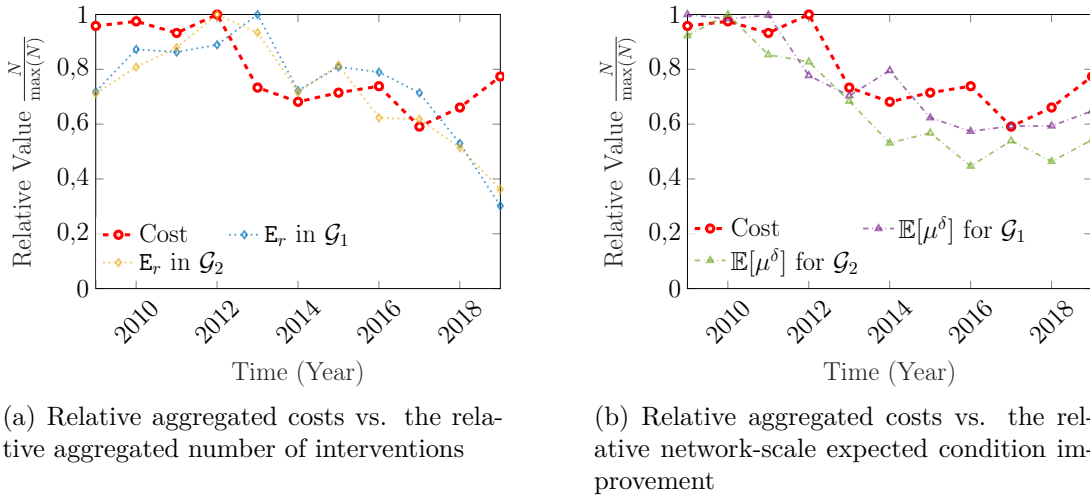


Figure 6.21 Comparison between the costs, number of interventions E_r , and the network-scale expected condition improvement $\mathbb{E}[\mu^\delta]$ for interventions performed on the primary and secondary structural elements from $B = 2999$ bridges.

6.5 Conclusion

In this chapter, the application of SSM/SSM-KR deterioration model is extended beyond structural elements to include estimates for the deterioration state of structural systems, bridges, as well as the entire network of bridges. The hierarchy of systems in each bridge b_j starts with two groups, primary \mathcal{G}_1^j , and secondary \mathcal{G}_2^j at the top, with each group encompassing multiple structural categories \mathcal{S}^j , and each structural category containing multiple structural elements e^j . Estimating the deterioration state for a structural category \mathcal{S}^j is done based on the deterioration state estimates of the structural elements within it, and by using a Gaussian mixture with the weights determined based on the quantity associated with each element $e^j \in \mathcal{S}^j$. After estimating the deterioration states $\tilde{\sigma}_t^j$ for all categories within a bridge, the deterioration states \tilde{s}_t^j for the structural group \mathcal{G} are estimated using equal mixture weights, based on the number of categories in the group. These analysis are followed by assessing the network's deterioration state \tilde{q}_t based on $B \approx 7000$ bridges, and by using equal mixture weights for all bridges. From the analysis, it is found that approximately 95% of bridges have a condition $\tilde{\mu}_{t|\mathbb{T}} \in [74, 100]$ for \mathcal{G}_1 , and $\tilde{\mu}_{t|\mathbb{T}} \in [71, 100]$ for \mathcal{G}_2 , and overall the health state is sustained at a high level. Finally, the spending costs associated with interventions are analyzed for a subset of bridges. The analysis involved a comparison between the costs, the improvement in the health state, and the number of interventions. The comparison results have shown that the highest investments were associated with the highest expected improvements in the network's condition but not necessarily the highest number of interventions at a given year. Such a discrepancy is justifiable because intervention costs can vary among the structural categories, as well as the type of interventions performed.

CHAPTER 7 Conclusion

7.1 Thesis Conclusions

The research work presented in this thesis has proposed new methods that improve the interpretability and utility of network-scale visual inspection data. The following are the conclusions derived from the analyses in this thesis.

In the context of visual inspections where the data is often sparse and the evaluations are subjective, the inspectors' uncertainty have a key role within the deterioration modelling process. This has been asserted in theoretical studies, however, empirical studies have neglected it. In order to account for such limitation and other limitations identified in the literature, this thesis proposed the use of SSM as a deterioration model. The SSM model relies on kinematic model to quantify the deterioration condition and the deterioration speed of structural elements. The formulation of the SSM accounts for the subjective nature of visual inspections by estimating the observations error associated with each inspector, and considering the inspection uncertainty dependent on the deterioration state. The performance of the proposed model is verified using synthetic data and validated using real inspection data taken from the network of bridges in Quebec province. The analyses have shown that the SSM deterioration model is unbiased towards underestimating or overestimating the structural elements condition. However, estimating the deterioration speed is found to be challenging, because of the limited number of observations on the condition, and the fact that the deterioration speed is not directly observed. In order to improve the capacity of estimating the deterioration speed, a hybrid framework SSM-KR is proposed. The SSM-KR combines the SSM model with a kernel regression (KR) approach. The role of KR in this context is exploit the similarities among bridges in order to improve the deterioration speed estimates. Comparisons between SSM-KR and SSM using synthetic data have shown that the SSM-KR deterioration speed estimates have a better consistency throughout the analyses time-window. Moreover, comparisons using real data are performed based on the log-likelihood of an independent test set. The results have shown that SSM-KR has an overall better log-likelihood than SSM in the independent test set. Using SSM-KR comes at the cost of additional computational complexity which is discussed in the limitations section.

Another key aspect when modelling the deterioration of structural elements is to quantify and model the effect of interventions. Quantifying the effect of interventions is commonly based on either the expert judgement or ad hoc estimation from visual inspection data. In this thesis, the effect of interventions is modelled using a stochastic framework which quantifies the

changes at the structural element-level and on a network-scale. The capacity for quantifying the effect of interventions is verified using synthetic data. The results have shown that the true state, before and after an intervention, is within the confidence interval of the model estimate. In addition, the network-scale estimate for the effect of an intervention is shown to converge to the true network-scale effect, provided that a sufficient number of structural elements with the same intervention exist. Furthermore, validation analysis are performed using real data, of which the results in the real cases have resembled the results obtained in the synthetic case.

Following the deterioration analysis on structural elements, the methods developed in this thesis are applied on a network-scale, in order to estimate the deterioration states for each bridge and the entire network. The analysis involved two groups of structural elements, the primary group which includes all elements that support or transfer vertical loads to other elements (e.g., beams), and the secondary group which includes elements involved in the serviceability of the bridge (e.g., pavement). From the analysis, approximately 95% of bridges have a condition $\tilde{\mu}_{t|\mathcal{T}} \in [74, 100]$ for the primary structural elements, and $\tilde{\mu}_{t|\mathcal{T}} \in [71, 100]$ for the secondary structural elements, and overall the health state of the secondary structural elements is higher than the primary structural elements. Moreover, unreported interventions are shown to affect the network's deterioration state estimates which are detailed in the chapter.

In conclusion, the methods proposed in this thesis have shown the capacity to effectively quantify the inspectors uncertainties along with robust estimation for the deterioration condition and speed based on limited number of observations per structural element. In addition, these methods have also shown a good performance in quantifying the effect of interventions locally for each structural element, and on a network-scale. Overall, the proposed methods improve the capacity to interpret the network-scale visual inspection data, which provide the foundations for decision making and maintenance planning.

7.2 Limitations

This section examines the limitations that exist in the proposed deterioration model and other methods proposed in this thesis. Resolving these limitations can further improve the scalability and robustness of the proposed approaches.

7.2.1 State Constraints

In this work, state constraints are utilized in order to reinforce knowledge about the physics of the problem when no direct observations are available. Hence, the constraints are applied on the hidden states of the deterioration speed and acceleration only. The method utilized in applying the state constraints is the PDF truncation method described in §2.3.3. In this method, when a state violates the constraints, the PDF of this state is truncated and approximated into a new PDF that satisfies the boundaries of the constraints. This approximation can cause biases in the constrained state estimate, especially in cases when the prior knowledge of the state is poorly defined. One potential solution to overcome this limitation is by performing a space transformation on the deterioration speed, such that the kinematic model used in modelling the deterioration is always monotonic. Nonetheless, such a solution also implies compromising the linearity in the system of equations describing the kinematic model, therefore, further investigation is required to assess the feasibility of such approach.

7.2.2 Kernel Regression & Structural Attributes

The kernel regression approach is utilized within the SSM-KR deterioration model in order to exploit information about structural attributes in the deterioration analysis. In this framework, the number of covariates Q and the number of reference points for each covariate M can affect the computational cost associated with the recursive estimation framework presented in §4.3.2. This is because increasing Q and/or M will result in increasing the size of the state vector $\dot{\mathbf{x}}_z$ represented by $\dot{\boldsymbol{\mu}}_{z|T} \in \mathbb{R}^{M^Q \times 1}$ and $\dot{\boldsymbol{\Sigma}}_{z|T} \in \mathbb{R}^{M^Q \times M^Q}$, which consequently increases the computational demand for computing the KR equations. Nonetheless, resolving the computational complexity in cases with large M^Q is possible by either utilizing dimensionality reduction approaches, such as principal components analyses (PCA) [72], or other low rank approximation methods [73, 74], or by using parametric regression methods instead of a non-parametric approach.

7.2.3 Deterioration Speed Estimate Following an Intervention

In the context of deterioration modelling, estimating the deterioration speed is challenging due to not having direct observations on the speed, and having a limited number of observations for the deterioration condition. The estimation challenge further increases when an event, such as an intervention, inflicts uncertain changes on the deterioration state, resulting in increasing the uncertainty of the speed state estimate following an intervention. Since this limitation is mainly attributed to the lack of observations, making use of deterioration pat-

terns associated with structural attributes have the potential of overcoming such limitation and enhancing the state estimates of the post-intervention speed.

7.2.4 Observations Error Estimate for the Inspectors

In the current framework, there are few hypotheses associated with the observations errors, which can be considered as limitations in the proposed deterioration model. The first hypothesis is to neglect the presence of the inspector bias such that, $\mu_V(I_i) = 0$ for all inspectors. This hypothesis can generally affect the estimation of the inspectors uncertainty $\sigma_V(I_i)$. Accounting for this limitation by parameterizing the expected value $\mu_V(I_i)$, will cause doubling the number of model parameters. The second hypothesis is to consider the inspectors' $\mu_V = 0$ and $\sigma_V(I_i)$ to be fixed over time (stationary), in addition to the parameters $\sigma_V(I_i)$ being estimated using a deterministic point estimate approach, where the uncertainty associated with each parameter is neglected. One solution with the premise to account for the issues above is the use of adaptive filters, where the system states and the model parameters are estimated online together [86, 87].

7.3 Future Work

This section presents future research directions, which include potential improvements on the deterioration framework and other use cases for the tools developed in this thesis.

7.3.1 Supporting the Model with Additional Deterioration Information

The SSM-KR framework mainly relies on information that are common and shared across the network of bridges. Nonetheless, this framework has the capacity to incorporate supplementary information from analytical deterioration models of individual cases. An example of such information is the corrosion caused by carbonation/chloride in reinforced concrete elements [88]. Another example is to incorporate data that relate to climate change in order to improve the long term forecast of the deterioration model. The potential of such an extension can be demonstrated by a generic formulation for the state vector and the model matrices to include new components (i.e., change in temperature) as in,

$$\begin{aligned} \underline{\boldsymbol{x}}_{p,t}^j &= [\boldsymbol{x}_{p,t}^j \ \check{\boldsymbol{x}}_{p,t}^j]^\top, \\ \underline{\boldsymbol{A}}_t &= \text{blockdiag}(\boldsymbol{A}_t, \check{\boldsymbol{A}}_t), \\ \underline{\boldsymbol{R}}_t &= \text{blockdiag}(\boldsymbol{R}_t, \check{\boldsymbol{R}}_t), \\ \underline{\boldsymbol{Q}}_t &= \text{blockdiag}(\boldsymbol{Q}_t, \check{\boldsymbol{Q}}_t), \end{aligned} \tag{7.1}$$

where $\check{\mathbf{x}}_{p,t}^j$ represents the hidden states of the new component, $\check{\mathbf{A}}$ the transition matrix of the new component, $\check{\mathbf{R}}$ and $\check{\mathbf{Q}}$ are the observations and transition error covariance matrices of the new component. The observation matrix $\underline{\mathbf{C}}$ for the modified framework is described by,

$$\underline{\mathbf{C}} = \begin{bmatrix} \mathbf{C} & \mathbf{C}_\theta \\ \mathbf{0} & \check{\mathbf{C}} \end{bmatrix}, \quad (7.2)$$

where $\check{\mathbf{C}}$ is the observation matrix of the new component, and \mathbf{C}_θ is a vector that includes regression coefficients which allow modelling the dependence between the deterioration based on visual inspections and the new component variables. The regression coefficients are additional model parameters that can be estimated using the MLE approach [89]. It should be noted that this formulation is general, and real applications may impose additional modelling challenges and modifications.

7.3.2 Handling Abnormal Observations in Real Time

The methods proposed in this thesis account only for the gradual deterioration in infrastructures, however, abnormal changes can be also accommodated in the deterioration framework. An example of abnormal changes, is the sudden deterioration of a structure due to external effects, such as hazards, extreme events, or a change in the health state due to undocumented interventions. Therefore, it is important to identify abnormal observations in real time to determine the type of the anomaly and include it in the deterioration model [90, 91]. This can help inspectors in knowing that their inspection results are abnormal given previous inspections, which consequently can prevent erratic inputs in the database, and helps explaining/labeling abnormal changes in the condition. Following the identification of an abnormal condition, actions can be taken in the form of further inspections or interventions on the structure.

7.3.3 Planning Network-Scale Interventions

One of the key reasons for analyzing the deterioration behaviour is to determine the type and the timing of interventions to be applied, such that the service life of bridges is maximized at minimal costs. Existing approaches have attempted to formulate the intervention planning problem based on different factors that relates to the deterioration condition, traffic, expected improvement and financial costs [92–94]. However, the proposed deterioration model in this thesis has enabled estimating the deterioration speed, in addition to improving the estimation of the effect of interventions. These additional factors can increase the efficiency of decision

making and prioritizing interventions on the network of bridges.

REFERENCES

- [1] D. Canning and M. Fay, “The effect of transportation networks on economic growth,” *Columbia University*, 1993.
- [2] S. Démurger, “Infrastructure development and economic growth: an explanation for regional disparities in china?” *Journal of Comparative economics*, vol. 29, no. 1, pp. 95–117
- [3] M.-C. Scutaru, N. Tăranu, C.-C. Comisu, and C. Chingălată, “Development of bridge structural helth monitoring,” *Buletinul Institutului Politehnic din Iasi. Sectia Construcții, Arhitectura*, vol. 63, no. 2, 2017.
- [4] D. Agdas, J. A. Rice, J. R. Martinez, and I. R. Lasa, “Comparison of visual inspection and structural-health monitoring as bridge condition assessment methods,” *Journal of Performance of Constructed Facilities*, vol. 30, no. 3, p. 04015049, 2015.
- [5] M. Moore, B. M. Phares, B. Graybeal, D. Rolander, and G. Washer, “Reliability of visual inspection for highway bridges, volume i,” Turner-Fairbank Highway Research Center, 6300 Georgetown Pike, Tech. Rep., 2001.
- [6] J. W. Soetjipto, T. J. W. Adi, and N. Anwar, *Bridge Deterioration Prediction Model Based On Hybrid Markov-System Dynamic*. EDP Sciences, 2017, vol. 138.
- [7] *Manuel d’Inspection des Structures*, Ministère des Transports, de la Mobilité Durable et de l’Électrification des Transports, Jan 2014.
- [8] H. Mackenzie, “Canada’s infrastructure gap,” Canadian Centre for Policy Alternatives, Tech. Rep., 2013.
- [9] D. Sutherland, S. Araujo, B. Égert, and T. J. Kozluk, “Infrastructure investment: links to growth and the role of public policies,” 2009.
- [10] M. Ryall, *Bridge management*. CRC Press, 2007.
- [11] Y. Hu, “Mobile location-based bridge inspection decision-support system,” Master’s thesis, Concordia University, 2006.
- [12] J. Lee, K. Sanmugarasa, M. Blumenstein, and Y.-C. Loo, “Improving the reliability of a bridge management system (bms) using an ann-based backward prediction model (bpm),” *Automation in Construction*, vol. 17, no. 6, pp. 758–772

- [13] S. Madanat, “Optimal infrastructure management decisions under uncertainty,” *Transportation Research Part C: Emerging Technologies*, vol. 1, no. 1, pp. 77–88
- [14] C. Ferreira, L. C. Neves, J. C. Matos, and J. M. S. Soares, “A degradation and maintenance model: Application to portuguese context,” *Proceedings of Bridge Maintenance, Safety, Management and Life Extension*, pp. 483–489, 2014.
- [15] G. Morcous, “Performance prediction of bridge deck systems using markov chains,” *Journal of performance of Constructed Facilities*, vol. 20, no. 2, pp. 146–155
- [16] G. Morcous and Z. Lounis, “Probabilistic and mechanistic deterioration models for bridge management,” *Computing in Civil Engineering (2007)*, pp. 364–373, 2007.
- [17] M. S. Hasan, S. Setunge, D. W. Law, and Y.-C. Koay, “Forecasting deterioration of bridge components from visual inspection data,” *International Journal of Engineering and Technology*, vol. 7, no. 1, pp. 40 2015.
- [18] I. Zambon, A. Vidović, A. Strauss, and J. Matos, “Condition prediction of existing concrete bridges as a combination of visual inspection and analytical models of deterioration,” *Applied Sciences*, vol. 9, no. 1, p. 148, 2019.
- [19] Y.-H. Huang, “Artificial neural network model of bridge deterioration,” *Journal of Performance of Constructed Facilities*, vol. 24, no. 6, pp. 597–602
- [20] M. Hairer, “Ergodic properties of markov processes,” *Open quantum systems II*, 2006.
- [21] G. Fu and D. Devaraj, *Methodology of Homogeneous and Non-homogeneous Markov Chains for Modelling Bridge Element Deterioration*. Michigan Department of Transportation, 2008.
- [22] K. Murphy, *Machine Learning: A Probabilistic Perspective*. MIT Press, 2012.
- [23] J. Kalbfleisch and J. F. Lawless, “The analysis of panel data under a markov assumption,” *Journal of the American Statistical Association*, vol. 80, no. 392, pp. 863–871
- [24] M. Kallen and J. Van Noortwijk, “Statistical inference for markov deterioration models of bridge conditions in the netherlands,” in *Proceedings of the Third International Conference on Bridge Maintenance, Safety and Management*, no. 16-19, 2006.
- [25] C. H. Jackson, “Multi-state models for panel data: the msm package for r,” *Journal of statistical software*, 2011.

- [26] H. N. Van Erp and A. D. Orcesi, “The use of nested sampling for prediction of infrastructure degradation under uncertainty,” *Structure and Infrastructure Engineering*, pp. 1–11
- [27] Y. Zhang, C.-W. Kim, and K. F. Tee, “Maintenance management of offshore structures using markov process model with random transition probabilities,” *Structure and Infrastructure Engineering*, vol. 13, no. 8, pp. 1068–1080, 08 2017.
- [28] L. R. Rabiner, “An introduction to hidden markov models,” *ieee assp magazine*, vol. 3, no. 1, pp. 4–16, 1986.
- [29] P. L. Durango-Cohen, “A time series analysis framework for transportation infrastructure management,” *Transportation Research Part B: Methodological*, vol. 41, no. 5, pp. 493–505
- [30] I. Zambon, A. Vidovic, A. Strauss, J. Matos, and J. Amado, “Comparison of stochastic prediction models based on visual inspections of bridge decks,” *Journal of Civil Engineering and Management*, vol. 23, no. 5, pp. 553–561, 2017.
- [31] S.-K. Ng and F. Moses, “Bridge deterioration modeling using semi-markov theory,” *A. A. Balkema Uitgevers B. V, Structural Safety and Reliability.*, vol. 1, pp. 113–120, 1998.
- [32] G. Puž, J. Radić, and I. Stipanovi Oslaković, “A new model for stochastic analysis of bridge durability,” *Gradevinar*, vol. 62, no. 04., pp. 287–297
- [33] E. K. Winn, “Artificial neural network models for the prediction of bridge deck condition ratings,” Master’s thesis, Michigan State University, 2011.
- [34] C. R. Farrar and K. . Worden, *Structural health monitoring: a machine learning perspective*. John Wiley Sons, 2012.
- [35] R. Matkovskyy and T. Bouraoui, “Application of neural networks to short time series composite indexes: Evidence from the nonlinear autoregressive with exogenous inputs (narx) model,” *Journal of Quantitative Economics*, 2018.
- [36] W. Foster, F. Collopy, and L. Ungar, “Neural network forecasting of short, noisy time series,” *Computers chemical engineering*, vol. 16, no. 4, pp. 293–297
- [37] M. M. M. H. B. D. M. Association., *The DAMA guide to the data management body of knowledge*. Bradley Beach, N.J. : Technics Publications, 2010.

- [38] C.-J. Lu, T.-S. Lee, and C.-C. Chiu, “Financial time series forecasting using independent component analysis and support vector regression,” *Decision Support Systems*, vol. 47, no. 2, pp. 115–125 2009.
- [39] P. Del Moral, “Non-linear filtering: interacting particle resolution,” *Markov processes and related fields*, vol. 2, no. 4, pp. 555–581, 1996.
- [40] R. E. Kalman, “Contributions to the theory of optimal control,” *Bol. Soc. Mat. Mexicana*, vol. 5, no. 2, pp. 102–119, 1960.
- [41] S. J. Julier and J. K. Uhlmann, “Unscented filtering and nonlinear estimation,” *Proceedings of the IEEE*, vol. 92, no. 3, pp. 401–422 0018–9219, 2004.
- [42] N. R. Pal, *Neural information processing [electronic resource]: 11th international conference, ICONIP 2004, Calcutta, India, November 22-25, 2004: proceedings.* Springer Science Business Media, 2004, vol. 11
- [43] H. E. Rauch, C. Striebel, and F. Tung, “Maximum likelihood estimates of linear dynamic systems,” *AIAA journal*, vol. 3, no. 8, pp. 1445–1450 0001–1452, 1965.
- [44] D. Simon, “Kalman filtering with state constraints: a survey of linear and nonlinear algorithms,” *IET Control Theory Applications*, vol. 4, no. 8, pp. 1303–1318
- [45] D. Simon and D. L. Simon, “Constrained kalman filtering via density function truncation for turbofan engine health estimation,” *International Journal of Systems Science*, vol. 41, no. 2, pp. 159–171 2010.
- [46] D. Simon, *Optimal state estimation: Kalman, H infinity, and nonlinear approaches.* John Wiley Sons, 2006.
- [47] *Bridge Preservation Guide Maintaining a Resilient Infrastructure to Preserve Mobility.* U.S. Department of transportation Federal Highway Administration, 2018.
- [48] S.-I. Yang, D. M. Frangopol, Y. Kawakami, and L. C. Neves, “The use of lifetime functions in the optimization of interventions on existing bridges considering maintenance and failure costs,” *Reliability Engineering System Safety*, vol. 91, no. 6, pp. 698–705
- [49] D. Fernando, B. T. Adey, and S. Walbridge, “A methodology for the prediction of structure level costs based on element condition states,” *Structure and Infrastructure Engineering*, vol. 9, no. 8, pp. 735–748 2013.

- [50] W. Zhang and N. Wang, “Bridge network maintenance prioritization under budget constraint,” *Structural safety*, vol. 67, pp. 96–104 2017.
- [51] D. Fernando, B. T. Adey, and N. Lethanh, “A model for the evaluation of intervention strategies for bridges affected by manifest and latent deterioration processes,” *Structure and Infrastructure Engineering*, vol. 11, no. 11, pp. 1466–1483
- [52] M. Sánchez-Silva, D. M. Frangopol, J. Padgett, and M. Soliman, “Maintenance and operation of infrastructure systems,” *Journal of Structural Engineering*, vol. 142, no. 9, pp. F4 016 004 2016.
- [53] T. U. Saeed, Y. Qiao, S. Chen, K. Gkritza, and S. Labi, “Methodology for probabilistic modeling of highway bridge infrastructure condition: Accounting for improvement effectiveness and incorporating random effects,” *Journal of Infrastructure Systems*, vol. 23, no. 4, pp. 04 017 030 1076–0342, 2017.
- [54] A. Petcherdchoo, L. A. Neves, and D. M. Frangopol, “Optimizing lifetime condition and reliability of deteriorating structures with emphasis on bridges,” *Journal of structural engineering*, vol. 134, no. 4, pp. 544–552
- [55] M. Liu and D. M. Frangopol, “Bridge annual maintenance prioritization under uncertainty by multiobjective combinatorial optimization,” *Computer[A+2010]Aided Civil and Infrastructure Engineering*, vol. 20, no. 5, pp. 343–353
- [56] P. Bocchini and D. M. Frangopol, “A probabilistic computational framework for bridge network optimal maintenance scheduling,” *Reliability Engineering System Safety*, vol. 96, no. 2, pp. 332–349 2011.
- [57] S. B. Chase, Y. Adu-Gyamfi, A. Aktan, and E. Minaie, “Synthesis of national and international methodologies used for bridge health indices,” Tech. Rep., 2016.
- [58] I. Srikanth and M. Arockiasamy, “Deterioration models for prediction of remaining useful life of timber and concrete bridges—a review,” *Journal of traffic and transportation engineering (English edition)* 2095-7564, 2020.
- [59] Z. Allah Bukhsh, I. Stipanovic, G. Klanker, A. O’Connor, and A. G. Doree, “Network level bridges maintenance planning using multi-attribute utility theory,” *Structure and infrastructure engineering*, vol. 15, no. 7, pp. 872–885
- [60] F. Ghodoosi, A. Bagchi, and T. Zayed, “System-level deterioration model for reinforced concrete bridge decks,” *Journal of Bridge Engineering*, vol. 20, no. 5, pp. 04 014 081

- [61] B. T. Adey and R. Hajdin, “Methodology for determination of financial needs of gradually deteriorating bridges with only structure level data,” *Structure and Infrastructure Engineering*, vol. 7, no. 7-8, pp. 645–660
- [62] A. Strauss, A. Vidovic, I. Zambon, F. Dengg, N. Tanasic, and J. C. . . Matos, “Performance indicators for roadway bridges,” 2016.
- [63] S. Inkoom, J. O. Sobanjo, P. D. Thompson, R. Kerr, and R. Twumasi-Boakye, “Bridge health index: Study of element condition states and importance weights,” *Transportation Research Record*, vol. 2612, no. 1, pp. 67–75
- [64] J. Bennetts, G. Webb, P. Vardanega, S. Denton, and N. Loudon, “Quantifying uncertainty in visual inspection data,” pp. 2252–2259, 2018.
- [65] Y. An, E. Chatzi, S. Sim, S. Laflamme, B. Blachowski, and J. Ou, “Recent progress and future trends on damage identification methods for bridge structures,” *Structural Control and Health Monitoring*, vol. 26, no. 10, pp. 1545–2255, 2019.
- [66] A. R. DiDonato and A. H. Morris Jr, “Computation of the incomplete gamma function ratios and their inverse,” *ACM Transactions on Mathematical Software (TOMS)*, vol. 12, no. 4, pp. 377–393
- [67] Y. Bar-Shalom, X. R. Li, and T. . . Kirubarajan, *Estimation with applications to tracking and navigation: theory algorithms and software*. John Wiley Sons, 2004.
- [68] A. Galántai, “The theory of newton’s method,” *Journal of Computational and Applied Mathematics*, vol. 124, no. 1-2, pp. 25–44 0377–0427, 2000.
- [69] J. Quiggin, *Generalized expected utility theory: The rank-dependent model*. Springer Science Business Media, 2012.
- [70] C. M. Bishop, *Pattern recognition and machine learning*. Springer, 2006.
- [71] E. A. Nadaraya, “On estimating regression,” *Theory of Probability Its Applications*, vol. 9, no. 1, pp. 141–142
- [72] I. T. Jolliffe, *Principal components in regression analysis*. Springer, 1986, pp. 129–155.
- [73] E. Cosme, J. Verron, P. Brasseur, J. Blum, and D. Auroux, “Smoothing problems in a bayesian framework and their linear gaussian solutions,” *Monthly Weather Review*, vol. 140, no. 2, pp. 683–695

- [74] E. A. Pnevmatikakis, K. R. Rad, J. Huggins, and L. Paninski, “Fast kalman filtering and forward–backward smoothing via a low-rank perturbative approach,” *Journal of Computational and Graphical Statistics*, vol. 23, no. 2, pp. 316–339
- [75] D. Duvenaud, “Automatic model construction with gaussian processes,” 2014.
- [76] K. P. Murphy, *Machine learning: a probabilistic perspective*. MIT press, 2012.
- [77] C. K. Williams and C. E. Rasmussen, *Gaussian processes for machine learning*. MIT press Cambridge, MA, 2006, vol. 2, no. 3.
- [78] J. Aitchison and C. G. Aitken, “Multivariate binary discrimination by the kernel method,” *Biometrika*, vol. 63, no. 3, pp. 413–420 1464–3510, 1976.
- [79] D. Titterington, “A comparative study of kernel-based density estimates for categorical data,” *Technometrics*, vol. 22, no. 2, pp. 259–268 0040–1706, 1980.
- [80] K.-T. . X. Chang, *Introduction to geographic information systems*. McGraw-Hill Higher Education Boston, 2006.
- [81] D. A. Reynolds, “Gaussian mixture models.” *Encyclopedia of biometrics*, vol. 741, 2009.
- [82] A. R. Runnalls, “Kullback-leibler approach to gaussian mixture reduction,” *IEEE Transactions on Aerospace and Electronic Systems*, vol. 43, no. 3, pp. 989–999
- [83] D. J. Salmond, *Mixture reduction algorithms for target tracking in clutter*. International Society for Optics and Photonics, 1990, vol. 1305.
- [84] T. Hastie, R. Tibshirani, G. Sherlock, M. Eisen, P. Brown, and D. Botstein, “Imputing missing data for gene expression arrays,” 1999.
- [85] A. Setyawan, J. Nainggolan, and A. Budiarto, “Predicting the remaining service life of road using pavement condition index,” *Procedia Engineering*, vol. 125, pp. 417–423
- [86] T. S. Jaakkola and M. I. Jordan, “Bayesian parameter estimation via variational methods,” *Statistics and Computing*, vol. 10, no. 1, pp. 25–37
- [87] S. Sarkka and A. Nummenmaa, “Recursive noise adaptive kalman filtering by variational bayesian approximations,” *IEEE Transactions on Automatic control*, vol. 54, no. 3, pp. 596–600

- [88] N. Rakotovao Ravahatra, E. Bastidas-Arteaga, F. Schoefs, T. de Larrard, and F. Duprat, “Probabilistic and sensitivity analysis of analytical models of corrosion onset for reinforced concrete structures,” *European Journal of Environmental and Civil Engineering*, pp. 1–30
- [89] J.-A. Goulet, “Bayesian dynamic linear models for structural health monitoring,” *Structural Control and Health Monitoring*, vol. 24, no. 12, pp. e2035
- [90] X. Xu, Y. Ren, Q. Huang, Z.-Y. Fan, Z.-J. Tong, W.-J. Chang, and B. Liu, “Anomaly detection for large span bridges during operational phase using structural health monitoring data,” *Smart Materials and Structures*, vol. 29, no. 4, pp. 045 029
- [91] G. D. Ghare and R. S. Barga, “Real time anomaly detection for data streams,” 2020.
- [92] M. Liu and D. M. Frangopol, “Optimizing bridge network maintenance management under uncertainty with conflicting criteria: Life-cycle maintenance, failure, and user costs,” *Journal of structural Engineering*, vol. 132, no. 11, pp. 1835–1845
- [93] P. Bocchini and D. M. Frangopol, “A probabilistic computational framework for bridge network optimal maintenance scheduling,” *Reliability Engineering System Safety*, vol. 96, no. 2, pp. 332–349 2011.
- [94] S. Wei, Y. Bao, and H. Li, “Optimal policy for structure maintenance: A deep reinforcement learning framework,” *Structural Safety*, vol. 83, pp. 101 906

APPENDIX A PARAMETER ESTIMATION FRAMEWORK FOR SSM DETERIORATION MODEL

Algorithm 1 Parameter estimation framework (SSM)

Require: : $\boldsymbol{\theta}_0^s$: Initial parameters vector

- 1: $L_1 \leftarrow -10^{10}$ (Initial *log-likelihood*)
- 2: $\epsilon \leftarrow 10^{-3}$ (Convergence tolerance)
- 3: $\rho_1 \leftarrow 10, \rho_2 \leftarrow 10$ (Stall limits)
- 4: $\zeta_1 \leftarrow 1, \zeta_2 \leftarrow 1$ (Initial stall)
- 5: $\nu_1 \leftarrow 300, \nu_2 \leftarrow 1$ (Iteration limit per parameter)
- 6: $\boldsymbol{\theta}_1^s \leftarrow \text{NewtonRaphson}(\mathcal{L}(\boldsymbol{\theta}^s), \boldsymbol{\theta}_0^s, \nu_1)$
- 7: $\sigma_V(I_{1:\mathbb{I}}) = \sigma_V, \sigma_V \in \boldsymbol{\theta}_1^s$
- 8: $L_2 \leftarrow \mathcal{L}(\boldsymbol{\theta}_1^s)$
- 9:
- 10: **for** $n := 1$ to 5 **do**
- 11: **while** $|L_{j+1} - L_j| \leq \epsilon$ or $\zeta_1 \geq \rho_1$ **do**
- 12: **while** $|L_{j+1} - L_j| \leq \epsilon$ or $\zeta_2 \geq \rho_2$ **do**
- 13: $L_j \leftarrow L_{j+1}$
- 14: **for** $i := 1$ to \mathbb{I} **do**
- 15: $\sigma_V(I_i) \leftarrow \text{NewtonRaphson}(\mathcal{L}(\sigma_V(I_i)), \sigma_V(I_{i0}), \nu_2)$
- 16: $L_{j+1} \leftarrow \mathcal{L}(\sigma_V(I_{1:\mathbb{I}}))$
- 17: **if** $|(L_{j+1} - L_j)/L_j| \leq 0.05$ **then**
- 18: $\zeta_2 = \zeta_2 + 1$
- 19: $\boldsymbol{\theta}_{j+1}^m \leftarrow \text{NewtonRaphson}(\mathcal{L}(\boldsymbol{\theta}^m), \boldsymbol{\theta}_j^m, \nu_1)$
- 20: $L_j \leftarrow \mathcal{L}(\boldsymbol{\theta}_{j+1}^m)$
- 21: $\zeta_1 = \zeta_1 + 1$
- 22: **return** $\boldsymbol{\theta}_{j+1}^m$ and $\sigma_V(I_{1:\mathbb{I}})$ (Resulting parameters)

APPENDIX B PARAMETER ESTIMATION FRAMEWORK FOR SSM-KR DETERIORATION MODEL

Algorithm 2 Parameter estimation framework for SSM-KR

Require: $\boldsymbol{\theta}_0^s$: Initial SSM parameters

Require: $\boldsymbol{\theta}_0, \dot{\mathbf{x}}_z$: Initial KR parameters and state respectively

```

1:  $L_1 \leftarrow -10^{10}$  (Initial log-likelihood),  $\epsilon \leftarrow 10^{-3}$  (Convergence tolerance)
2:  $\rho_1 \leftarrow 10, \rho_2 \leftarrow 10$  (Stall limits)
3:  $\zeta_1 \leftarrow 1, \zeta_2 \leftarrow 1$  (Initial stall),
4:  $\nu_1 \leftarrow 300, \nu_2 \leftarrow 1$  (Iteration limit per parameter)
5:  $\boldsymbol{\theta}_1^s \leftarrow \text{NewtonRaphson}(\mathcal{L}(\boldsymbol{\theta}^s), \boldsymbol{\theta}_0^s, \nu_1)$ 
6:  $\sigma_V(I_{1:\mathbb{I}}) = \sigma_V, \sigma_V \in \boldsymbol{\theta}_1^s$ 
7:  $L_2 \leftarrow \mathcal{L}(\boldsymbol{\theta}_1^s)$ 
8:
9: for  $n := 1$  to 5 do
10:   while  $|L_{j+1} - L_j| \leq \epsilon$  or  $\zeta_1 \geq \rho_1$  do
11:     while  $|L_{j+1} - L_j| \leq \epsilon$  or  $\zeta_2 \geq \rho_2$  do
12:        $L_j \leftarrow L_{j+1}$ 
13:       for  $i := 1$  to  $\mathbb{I}$  do
14:         if  $j = 1$  then
15:            $\sigma_V(I_i) \leftarrow \text{NewtonRaphson}(\mathcal{L}(\sigma_V(I_i)), \boldsymbol{\theta}_j, \nu_2)$ 
16:         else  $\sigma_V(I_i) \leftarrow \text{NewtonRaphson}(\mathcal{L}(\sigma_V(I_i), \dot{\mathbf{x}}_z), \boldsymbol{\theta}_j, \nu_2)$ 
17:          $L_{j+1} \leftarrow \mathcal{L}(\sigma_V(I_{1:\mathbb{I}}))$ 
18:         if  $|(L_{j+1} - L_j)/L_j| \leq 0.05$  then
19:            $\zeta_2 = \zeta_2 + 1$ 
20:         if  $j = 1$  then
21:            $\boldsymbol{\theta}_{j+1}^m \leftarrow \text{NewtonRaphson}(\mathcal{L}(\boldsymbol{\theta}_j^m), \boldsymbol{\theta}_j, \nu_1)$ 
22:         else  $\boldsymbol{\theta}_{j+1}^m \leftarrow \text{NewtonRaphson}(\mathcal{L}(\boldsymbol{\theta}_j^m, \dot{\mathbf{x}}_z), \boldsymbol{\theta}_j, \nu_1)$ 
23:          $[\boldsymbol{\theta}_{j+1}, \dot{\mathbf{x}}_z] \leftarrow \text{NewtonRaphson}(\mathcal{L}(\boldsymbol{\theta}_j, \text{RecursiveEstimation}(\dot{\mathbf{x}}_z)), \boldsymbol{\theta}_j, \nu_1)$ 
24:          $L_j \leftarrow \mathcal{L}(\boldsymbol{\theta}_{j+1})$ 
25:          $\zeta_1 = \zeta_1 + 1, j = j + 1$ 
return  $\boldsymbol{\theta}_{j+1}$  and  $\dot{\mathbf{x}}_z$  (Resulting parameters)

```

APPENDIX C KERNEL FUNCTIONS:

- Aitchison and Aitken kernel function:

$$k^{(\text{AAK})}(z_j, z_c) = \begin{cases} 1 - \ell, & z_j = z_c, \\ \frac{\ell}{c-1}, & z_j \neq z_c. \end{cases}$$

- Radial basis kernel function:

$$k^{(\text{RBF})}(z_j, z_c) = \exp\left(-\frac{(z_j - z_c)^2}{2\ell^2}\right).$$

- Matérn 12 kernel function:

$$k^{(\text{M12})}(z_j, z_c) = \exp\left(-\frac{|z_j - z_c|}{\ell}\right).$$

- Matérn 52 kernel function:

$$k^{(\text{M52})}(z_j, z_c) = \left(1 + \frac{\sqrt{5}(z_j - z_c)}{\ell} + \frac{5}{3} \frac{(z_j - z_c)^2}{\ell^2}\right) \exp\left(-\frac{\sqrt{5}(z_j - z_c)}{\ell}\right).$$

APPENDIX D DECISION MAKING FOR SYNTHETIC INTERVENTIONS

The decision making for synthetic interventions is done based on if-then rules defined in Table D.1. These rules have two inputs and one output, the inputs are the health condition and the priority index of the bridge, while the output is the type of the intervention. In order to limit the number of rules, the deterioration condition and the priority index are discretized into categories as shown in Figures D.1. An example that demonstrates the use of this system is for a structural element that has a health condition 80 and priority 2.5, the applied intervention is h_2 . Moreover, the health condition category V.D. refers to a very damaged state of which a replacement action is required. The replacement actions are not considered in this study, provided that this type of interventions results in changing the entire structural element.

Table D.1 Table of synthetic interventions h_r applied for a given health condition and a priority index.

		Health Condition		
		Damaged	Good	Excellent
3*Priority	High	h_3	h_2	h_1
	Medium	h_3	h_2	h_0
	Low	h_2	h_1	h_0

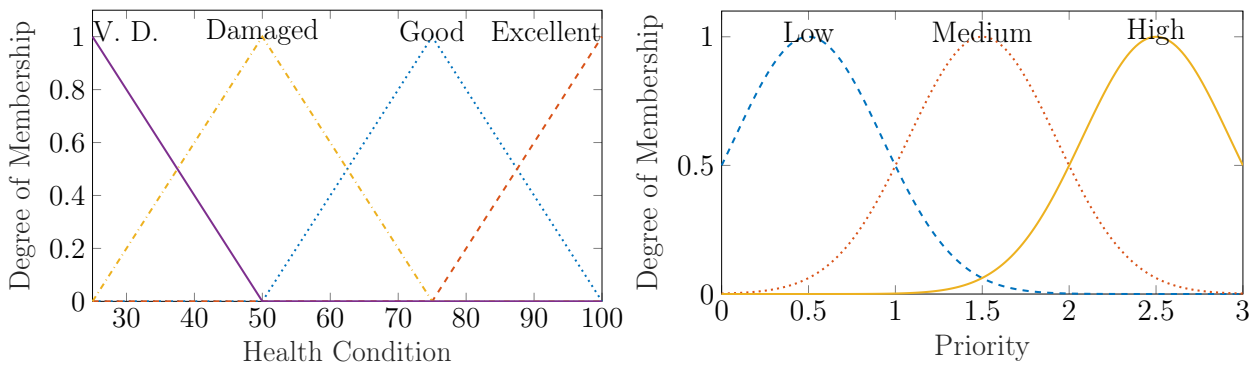


Figure D.1 Categories for the health condition and the priority index.

APPENDIX E NETWORK-SCALE DETERIORATION ANALYSIS BASED ON BRIDGES' ATTRIBUTES

Figure E.1 shows scatter plots for bridges attributes, which are generated from $B \approx 7000$ bridges.

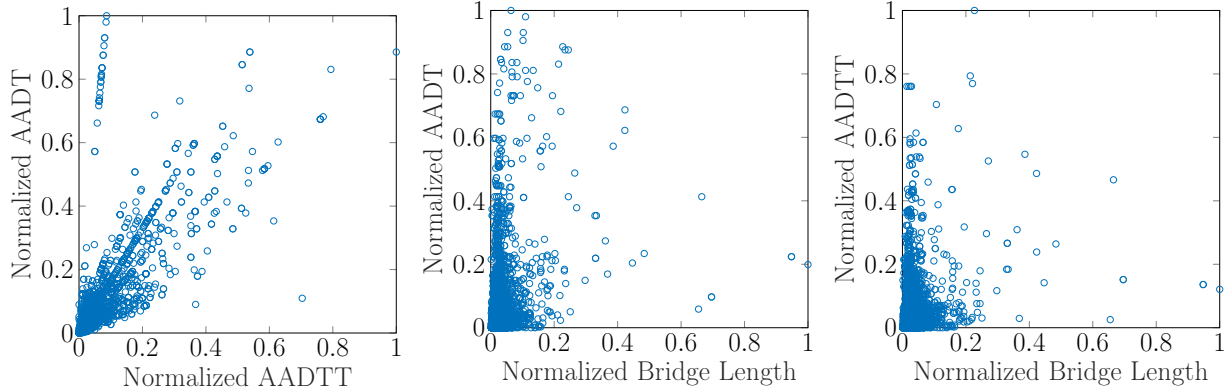


Figure E.1 Scatter plots for the normalized annual average of daily traffic vs. the normalized annual average of daily truck-traffic vs. and the normalized length associated with each bridge in the network.

From Figure E.1, it is noticed that AADTT has some correlation with AADT, demonstrated by similar peaks on the diagonal, while there is a little to no correlation between the traffic load and the bridge length. This assessment implies that the above mentioned factors are different from each other, and therefore each of them can be utilized to draw different conclusions about the overall state of the network.

Estimating the deterioration states for a network of bridges can be done using different approaches, one such approach is by taking the overall average for the deterioration states of all bridges in the network. However, such an approach assumes that the contribution of all bridges is equal across the network, which is not generally true, given the large discrepancies in AADT and other attributes across the network [57]. Therefore, a weighted average, that relies on the available attributes, is considered in examining the overall deterioration condition and speed based on $B \approx 7000$ bridges. The weighted averages for each metric are estimated using the Gaussian mixture approach in Equation 6.5, and in accordance with Equation 6.3. The estimation results are shown in Figure E.2, which outline the network's expected condition and speed in years 2020 and 2025, under the scenario that no maintenance interventions are performed. The letters in the acronyms on each axes are, P: primary, S: secondary, A: AADT, L: bridge length, M: number of bridges, T: AADTT. For example,

in the network condition graph, PL refers to the (P)primary condition of the network based on a weighted average, with the weights determined according to the bridge (L)ength (i.e., $\lambda^j = \frac{z_5^j}{\sum z_5}$).

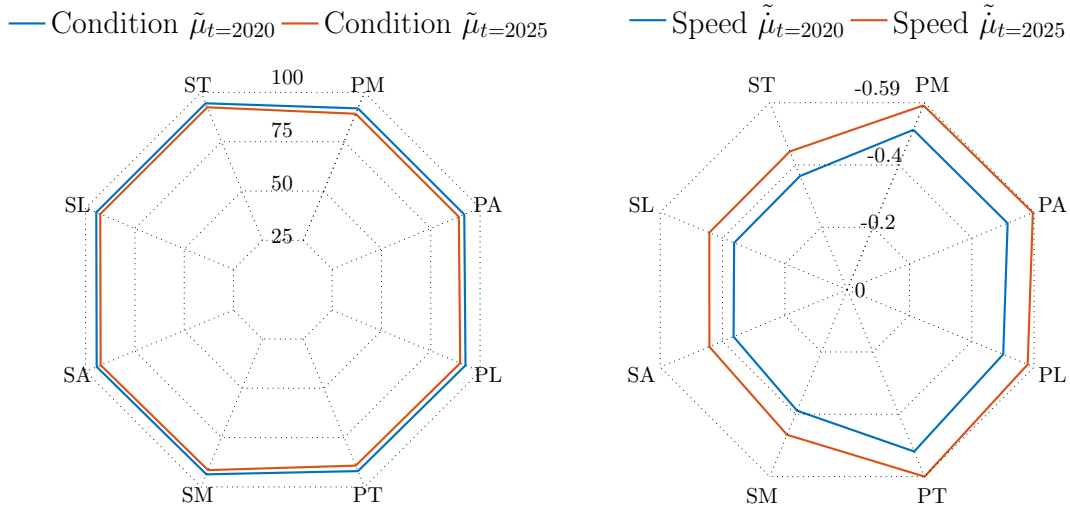


Figure E.2 Expected values for the network's deterioration condition and speed based on a weighted average of $B \approx 7000$ according to: number of bridges, AADT, bridge length and number of trucks for the primary and secondary groups.

Although the condition estimates in Figure E.2 show no apparent difference, the network's condition estimates weighted by the bridge length have the highest scores with, PL: $\tilde{\mu}_{t=2020} = 92.6 \in [25, 100]$, and SL: $\tilde{\mu}_{t=2020} = 94.6 \in [25, 100]$, compared to the weighted average based on the number of bridges, which has the lowest scores, PM: $\tilde{\mu}_{t=2020} = 91.91 \in [25, 100]$. On the other hand, the network's highest deterioration speed is associated with the estimates weighted by AADTT (i.e. $\lambda^j = \frac{z_7}{\sum z_7}$) with, PT: $\tilde{\mu}_{t=2020} = -0.51$, for the primary group, while for the secondary group \mathcal{G}_2 , the network's highest deterioration speed is associated with the estimates weighted by the number of bridges, SM: $\tilde{\mu}_{t=2020} = -0.38$. Moreover, it is noticed that there is a difference in the networks's deterioration speed between the primary and secondary groups. This is explained by the overall health condition of \mathcal{G}_2 being higher than the overall health condition of \mathcal{G}_1 , which is also reflected by the number of interventions performed on the secondary group \mathcal{G}_2 compared to the primary group \mathcal{G}_1 (see Figure 6.20).

APPENDIX F CATEGORIES OF STRUCTURAL ELEMENTS

Table F.1 Categories of inspected structural elements in the network.

Primary \mathcal{G}_1	Secondary \mathcal{G}_2
$\mathcal{S}_{1,1}$: Poutre	$\mathcal{S}_{2,1}$: Glissière (gauche ou droite)
$\mathcal{S}_{1,2}$: Côté extérieur	$\mathcal{S}_{2,2}$: Murs en aile / en retour
$\mathcal{S}_{1,3}$: Assise	$\mathcal{S}_{2,3}$: Chasse-roue
$\mathcal{S}_{1,4}$: Platelage	$\mathcal{S}_{2,4}$: Glissière
$\mathcal{S}_{1,5}$: Mur de front	$\mathcal{S}_{2,5}$: Surface de roulement
$\mathcal{S}_{1,6}$: Appareils d'appui	$\mathcal{S}_{2,6}$: Diaphragmes
$\mathcal{S}_{1,7}$: Blocs d'assise	$\mathcal{S}_{2,7}$: Garde-grève
$\mathcal{S}_{1,8}$: Chevêtre	$\mathcal{S}_{2,8}$: Contreventements
$\mathcal{S}_{1,9}$: Colonnes / bancs	$\mathcal{S}_{2,9}$: Trottoir
$\mathcal{S}_{1,10}$: Fût	$\mathcal{S}_{2,10}$: Mur en aile*
$\mathcal{S}_{1,11}$: Dessous de la dalle/voûte*	$\mathcal{S}_{2,11}$: Autres éléments
$\mathcal{S}_{1,12}$: Murs naiss. voûte coins infér.*	$\mathcal{S}_{2,12}$: Épaulements
$\mathcal{S}_{1,13}$: Radier	$\mathcal{S}_{2,13}$: Élément en élastomère
$\mathcal{S}_{1,14}$: Mur*	$\mathcal{S}_{2,14}$: Acier structural - tablier
$\mathcal{S}_{1,15}$: Entretoises	$\mathcal{S}_{2,15}$: Mur de tête*
$\mathcal{S}_{1,16}$: Colonnes	$\mathcal{S}_{2,16}$: Butoirs
$\mathcal{S}_{1,17}$: Montants / poteaux	$\mathcal{S}_{2,17}$: Glissière médiane
$\mathcal{S}_{1,18}$: Corde supérieure	$\mathcal{S}_{2,18}$: Garde-fou
$\mathcal{S}_{1,19}$: Diagonales	$\mathcal{S}_{2,19}$: Acier structural - unités de fondation
$\mathcal{S}_{1,20}$: Corde inférieure	$\mathcal{S}_{2,20}$: Bande médiane
$\mathcal{S}_{1,21}$: Longerons	$\mathcal{S}_{2,21}$: Portique d'extrémité
$\mathcal{S}_{1,22}$: Assemblages	$\mathcal{S}_{2,22}$: Chasse-roue / trottoir*
$\mathcal{S}_{1,23}$: Diaphrag. extrém. int. ptres caissons	$\mathcal{S}_{2,23}$: Acier structural - ptres triangulées
$\mathcal{S}_{1,24}$: Voûte Dalle*	$\mathcal{S}_{2,24}$: Revêtement de mur*
$\mathcal{S}_{1,25}$: Corbeaux	$\mathcal{S}_{2,25}$: Plafond suspendu - Tuiles*
$\mathcal{S}_{1,26}$: Suspentes/montants	$\mathcal{S}_{2,26}$: Toiture
$\mathcal{S}_{1,27}$: Tympan	$\mathcal{S}_{2,27}$: Lambris
$\mathcal{S}_{1,28}$: Arc	$\mathcal{S}_{2,28}$: Paralumes*
$\mathcal{S}_{1,29}$: Tirants	$\mathcal{S}_{2,29}$: Cadre de support*
$\mathcal{S}_{1,30}$: Voûte	
$\mathcal{S}_{1,31}$: Tirant	
$\mathcal{S}_{1,32}$: Assise / Blocs d'assise*	
$\mathcal{S}_{1,33}$: Bras d'articulation	
$\mathcal{S}_{1,34}$: Haubans et accessoires	
$\mathcal{S}_{1,35}$: Sabots d'attache des torons	
$\mathcal{S}_{1,36}$: Câble porteur et accessoires	
$\mathcal{S}_{1,37}$: Membrure supérieure	
$\mathcal{S}_{1,38}$: Suspentes et accessoires	
$\mathcal{S}_{1,39}$: Chambre d'épanouiss. câbles	
$\mathcal{S}_{1,40}$: Stabilisateurs transversaux	

* Category is not included in the deterioration analysis due to

not being part of the selected set of structures.

Table F.2 Categories of structural elements that are visually inspected in bridge b_{990} .

Primary \mathcal{G}_1	Secondary \mathcal{G}_2
$\mathcal{S}_{1,1}$: Poutre	$\mathcal{S}_{2,1}$: Contreventements
$\mathcal{S}_{1,2}$: Côté extérieur	$\mathcal{S}_{2,2}$: Chasse-roue
$\mathcal{S}_{1,3}$: Blocs d'assise	$\mathcal{S}_{2,3}$: Glissière (gauche ou droite)
$\mathcal{S}_{1,4}$: Assise	$\mathcal{S}_{2,4}$: Acier structural - tablier
$\mathcal{S}_{1,5}$: Appareils d'appui	$\mathcal{S}_{2,5}$: Diaphragmes
$\mathcal{S}_{1,6}$: Platelage	$\mathcal{S}_{2,6}$: Garde-fou
$\mathcal{S}_{1,7}$: Fût	$\mathcal{S}_{2,7}$: Surface de roulement
$\mathcal{S}_{1,8}$: Mur de front	$\mathcal{S}_{2,8}$: Trottoir
	$\mathcal{S}_{2,9}$: Murs en aile / en retour
	$\mathcal{S}_{2,10}$: Garde-grève
	$\mathcal{S}_{2,11}$: Glissière
	$\mathcal{S}_{2,12}$: Épaulements
	$\mathcal{S}_{2,13}$: Élément en élastomère
	$\mathcal{S}_{2,14}$: Autres éléments

Table F.3 Categories of structural elements that are visually inspected in bridge b_{3348} .

Primary \mathcal{G}_1	Secondary \mathcal{G}_2
$\mathcal{S}_{1,1}$: Poutre	$\mathcal{S}_{2,1}$: Diaphragmes
$\mathcal{S}_{1,2}$: Côté extérieur	$\mathcal{S}_{2,2}$: Glissière (gauche ou droite)
$\mathcal{S}_{1,3}$: Blocs d'assise	$\mathcal{S}_{2,3}$: Contreventements
$\mathcal{S}_{1,4}$: Appareils d'appui	$\mathcal{S}_{2,4}$: Épaulements
$\mathcal{S}_{1,5}$: Assise	$\mathcal{S}_{2,5}$: Murs en aile / en retour
$\mathcal{S}_{1,6}$: Platelage	$\mathcal{S}_{2,6}$: Autres éléments
$\mathcal{S}_{1,7}$: Mur de front	$\mathcal{S}_{2,7}$: Chasse-roue
$\mathcal{S}_{1,8}$: Fût	$\mathcal{S}_{2,8}$: Garde-fou
	$\mathcal{S}_{2,9}$: Glissière médiane
	$\mathcal{S}_{2,10}$: Acier structural - tablier
	$\mathcal{S}_{2,11}$: Trottoir
	$\mathcal{S}_{2,12}$: Surface de roulement
	$\mathcal{S}_{2,13}$: Glissière
	$\mathcal{S}_{2,14}$: Élément en élastomère
	$\mathcal{S}_{2,15}$: Garde-grève

APPENDIX G NETWORK-SCALE EFFECT OF INTERVENTIONS ON STRUCTURAL CATEGORIES

Table G.1 Effect of interventions on the primary categories of structural elements.

Structural Category \mathcal{S}_1	$\mu_1^\delta \pm \sigma_1^\delta$	$\mu_2^\delta \pm \sigma_2^\delta$	$\mu_3^\delta \pm \sigma_3^\delta$
$\mathcal{S}_{1,1}$: Poutre	NA	NA	12.6 ± 0.8
$\mathcal{S}_{1,2}$: Côté extérieur	0.02 ± 1.2	NA	15.9 ± 1.2
$\mathcal{S}_{1,3}$: Assise	NA	NA	21.3 ± 1.8
$\mathcal{S}_{1,4}$: Platelage	1.9 ± 3.3	11.4 ± 2.2	20.6 ± 1.3
$\mathcal{S}_{1,5}$: Mur de front	NA	13.6 ± 1.4	17.6 ± 1.3
$\mathcal{S}_{1,6}$: Appareils d'appui	NA	NA	32.1 ± 1.6
$\mathcal{S}_{1,7}$: Blocs d'assise	NA	NA	27.5 ± 2.8
$\mathcal{S}_{1,8}$: Chevêtre	NA	NA	16.2 ± 2.1
$\mathcal{S}_{1,9}$: Colonnes / bancs	NA	NA	0.4 ± 1.8
$\mathcal{S}_{1,10}$: Fût	0.4 ± 1.1	7.1 ± 7.2	20.5 ± 2.1
$\mathcal{S}_{1,13}$: Radier	NA	NA	18.3 ± 2.8
$\mathcal{S}_{1,15}$: Entretoises	NA	NA	7.3 ± 7
$\mathcal{S}_{1,16}$: Colonnes	NA	NA	8.3 ± 0.8
$\mathcal{S}_{1,17}$: Montants / poteaux	NA	NA	NA
$\mathcal{S}_{1,18}$: Corde supérieure	NA	NA	NA
$\mathcal{S}_{1,19}$: Diagonales	NA	NA	2.3 ± 4.4
$\mathcal{S}_{1,20}$: Corde inférieure	NA	NA	7.9 ± 7.3
$\mathcal{S}_{1,21}$: Longerons	NA	NA	8.4 ± 7.1
$\mathcal{S}_{1,22}$: Assemblages	NA	NA	NA
$\mathcal{S}_{1,23}$: Diaphragm. extrém. int. ptres caissons	NA	NA	NA
$\mathcal{S}_{1,25}$: Corbeaux	NA	NA	NA
$\mathcal{S}_{1,26}$: Suspentes/montants	NA	NA	NA
$\mathcal{S}_{1,27}$: Tympan	NA	NA	NA
$\mathcal{S}_{1,28}$: Arc	NA	NA	13.6 ± 1.7
$\mathcal{S}_{1,29}$: Tirants	NA	NA	NA
$\mathcal{S}_{1,30}$: Voûte	NA	NA	2.8 ± 3.9
$\mathcal{S}_{1,31}$: Tirant	NA	NA	NA
$\mathcal{S}_{1,33}$: Bras d'articulation	NA	NA	NA
$\mathcal{S}_{1,34}$: Haubans et accessoires	NA	NA	NA
$\mathcal{S}_{1,35}$: Sabots d'attache des torons	NA	NA	NA
$\mathcal{S}_{1,36}$: Câble porteur et accessoires	NA	NA	NA
$\mathcal{S}_{1,37}$: Membrure supérieure	NA	NA	NA
$\mathcal{S}_{1,38}$: Suspentes et accessoires	NA	NA	NA
$\mathcal{S}_{1,39}$: Chambre d'épanouiss. câbles	NA	NA	NA
$\mathcal{S}_{1,40}$: Stabilisateurs transversaux	NA	NA	NA

Table G.2 Effect of interventions on the secondary categories of structural elements.

Structural Category \mathcal{S}_2	$\mu_1^\delta \pm \sigma_1^\delta$	$\mu_2^\delta \pm \sigma_2^\delta$	$\mu_3^\delta \pm \sigma_3^\delta$
$\mathcal{S}_{2,1}$: Glissière (gauche ou droite)	NA	NA	20.6 ± 1.4
$\mathcal{S}_{2,2}$: Murs en aile / en retour	NA	NA	18 ± 1.3
$\mathcal{S}_{2,3}$: Chasse-roue	NA	NA	18.3 ± 1.4
$\mathcal{S}_{2,4}$: Glissière	NA	9.3 ± 3	15.4 ± 0.8
$\mathcal{S}_{2,5}$: Surface de roulement	20.9 ± 2	NA	27.7 ± 1.2
$\mathcal{S}_{2,6}$: Diaphragmes	NA	NA	16.9 ± 3.1
$\mathcal{S}_{2,7}$: Garde-grève	NA	7.8 ± 7.3	21.8 ± 2.8
$\mathcal{S}_{2,8}$: Contreventements	NA	NA	13.4 ± 2.1
$\mathcal{S}_{2,9}$: Trottoir	NA	NA	11.6 ± 0.9
$\mathcal{S}_{2,11}$: Autres éléments	NA	NA	18.9 ± 2.6
$\mathcal{S}_{2,12}$: Épaulements	NA	11.2 ± 7.6	NA
$\mathcal{S}_{2,13}$: Élément en élastomère	14.2 ± 1.3	NA	NA
$\mathcal{S}_{2,14}$: Acier structural - tablier	NA	NA	24.3 ± 1.6
$\mathcal{S}_{2,16}$: Butoirs	NA	NA	NA
$\mathcal{S}_{2,17}$: Glissière médiane	NA	NA	NA
$\mathcal{S}_{2,18}$: Garde-fou	NA	NA	NA
$\mathcal{S}_{2,19}$: Acier structural - unités de fondation	NA	NA	NA
$\mathcal{S}_{2,20}$: Bande médiane	NA	NA	14.7 ± 4.9
$\mathcal{S}_{2,21}$: Portique d'extrémité	NA	NA	NA
$\mathcal{S}_{2,23}$: Acier structural - ptres triangulées	NA	NA	15.7 ± 5.8
$\mathcal{S}_{2,26}$: Toiture	NA	NA	13.7 ± 6.8
$\mathcal{S}_{2,27}$: Lambris	NA	NA	NA

APPENDIX H NETWORK-SCALE CHARACTERISTICS OF STRUCTURAL CATEGORIES

Table H.1 Number of structures B and elements E with visual inspection data, in addition to the total number of elements with reported interventions E_r , elements with missing data E_Φ , and the total number of outlier observations N_ϕ , for each primary structural category \mathcal{S}_1 .

Structural Category \mathcal{S}_1	B	E	E_r	E_Φ	N_ϕ
$\mathcal{S}_{1,1}$: Poutre	5877	62018	548	1898	3234
$\mathcal{S}_{1,2}$: Côté extérieur	5374	23785	248	1485	1087
$\mathcal{S}_{1,3}$: Assise	6435	18498	213	566	853
$\mathcal{S}_{1,4}$: Platelage	7670	15060	295	609	1586
$\mathcal{S}_{1,5}$: Mur de front	7269	14489	319	528	887
$\mathcal{S}_{1,6}$: Appareils d'appui	3546	11618	221	1624	2173
$\mathcal{S}_{1,7}$: Blocs d'assise	2750	9488	48	326	167
$\mathcal{S}_{1,8}$: Chevêtre	1667	5812	77	372	418
$\mathcal{S}_{1,9}$: Colonnes / bancs	1575	5152	165	413	322
$\mathcal{S}_{1,10}$: Fût	1352	3332	86	181	220
$\mathcal{S}_{1,13}$: Radier	2282	2809	11	0	0
$\mathcal{S}_{1,15}$: Entretoises	276	1221	9	109	26
$\mathcal{S}_{1,16}$: Colonnes	438	1203	5	29	78
$\mathcal{S}_{1,17}$: Montants / poteaux	219	911	6	30	39
$\mathcal{S}_{1,18}$: Corde supérieure	222	908	2	24	41
$\mathcal{S}_{1,19}$: Diagonales	217	907	9	21	37
$\mathcal{S}_{1,20}$: Corde inférieure	213	883	20	48	35
$\mathcal{S}_{1,21}$: Longerons	253	854	9	55	17
$\mathcal{S}_{1,22}$: Assemblages	171	820	5	64	26
$\mathcal{S}_{1,23}$: Diaphragm. extrém. int. ptres caissons	80	694	1	24	14
$\mathcal{S}_{1,25}$: Corbeaux	54	128	0	0	6
$\mathcal{S}_{1,26}$: Suspentes/montants	22	119	0	10	3
$\mathcal{S}_{1,27}$: Tympan	37	99	4	4	17
$\mathcal{S}_{1,28}$: Arc	22	87	2	3	2
$\mathcal{S}_{1,29}$: Tirants	49	78	5	12	9
$\mathcal{S}_{1,30}$: Voûte	36	49	2	4	9
$\mathcal{S}_{1,31}$: Tirant	17	46	0	2	0
$\mathcal{S}_{1,33}$: Bras d'articulation	8	23	0	3	0
$\mathcal{S}_{1,34}$: Haubans et accessoires	4	22	0	0	0
$\mathcal{S}_{1,35}$: Sabots d'attache des torons	4	22	0	0	0
$\mathcal{S}_{1,36}$: Câble porteur et accessoires	4	20	0	5	0
$\mathcal{S}_{1,37}$: Membrure supérieure	1	16	0	0	0
$\mathcal{S}_{1,38}$: Suspentes et accessoires	4	16	0	3	0
$\mathcal{S}_{1,39}$: Chambre d'épanouiss. câbles	2	12	0	0	1
$\mathcal{S}_{1,40}$: Stabilisateurs transversaux	1	2	0	0	0

Table H.2 Number of structures B and elements E with visual inspection data, in addition to the total number of elements with reported interventions E_r , elements with missing data E_Φ , and the total number of outlier observations N_ϕ , for each secondary structural category \mathcal{S}_2 .

Structural Category \mathcal{S}_2	B	E	E_r	E_Φ	N_ϕ
$\mathcal{S}_{2,1}$: Glissière (gauche ou droite)	7755	30285	1269	2066	2212
$\mathcal{S}_{2,2}$: Murs en aile / en retour	6771	26564	285	959	2186
$\mathcal{S}_{2,3}$: Chasse-roue	6017	19997	455	1106	1932
$\mathcal{S}_{2,4}$: Glissière	7590	14817	782	816	1545
$\mathcal{S}_{2,5}$: Surface de roulement	7068	14441	610	1335	1421
$\mathcal{S}_{2,6}$: Diaphragmes	4189	14502	107	473	716
$\mathcal{S}_{2,7}$: Garde-grève	6458	12895	117	377	726
$\mathcal{S}_{2,8}$: Contreventements	2552	9571	61	247	417
$\mathcal{S}_{2,9}$: Trottoir	1603	6774	112	287	424
$\mathcal{S}_{2,11}$: Autres éléments	2569	5460	230	247	372
$\mathcal{S}_{2,12}$: Épaulements	2306	4701	25	249	168
$\mathcal{S}_{2,13}$: Élément en élastomère	2268	4562	42	288	277
$\mathcal{S}_{2,14}$: Acier structural - tablier	2952	4516	25	282	371
$\mathcal{S}_{2,16}$: Butoirs	839	2170	4	39	45
$\mathcal{S}_{2,17}$: Glissière médiane	256	1239	11	71	72
$\mathcal{S}_{2,18}$: Garde-fou	236	1130	11	29	27
$\mathcal{S}_{2,19}$: Acier structural - unités de fondation	261	653	2	58	75
$\mathcal{S}_{2,20}$: Bande médiane	196	538	6	26	59
$\mathcal{S}_{2,21}$: Portique d'extrémité	150	388	6	17	17
$\mathcal{S}_{2,23}$: Acier structural - ptres triangulées	162	314	8	53	14
$\mathcal{S}_{2,26}$: Toiture	59	87	4	2	5
$\mathcal{S}_{2,27}$: Lambris	55	83	11	3	4

Table H.4 Model type and parameters representing the process error and the initial state for the deterioration condition, speed and acceleration, in each secondary structural category \mathcal{S}_2 .

Structural Category	Model	σ_w	σ_0^x	σ_V	$\sigma_0^{\ddot{x}}$	p_1	p_2
$\mathcal{S}_{2,1}$	SSM-KR	0.0010	1.0042	3.0000	0.0015	0.0010	0.0001
$\mathcal{S}_{2,2}$	SSM-KR	0.0049	1.0005	3.0000	0.0500	0.0500	0.1500
$\mathcal{S}_{2,3}$	SSM-KR	0.0054	1.0302	3.0000	0.0500	0.0380	0.0729
$\mathcal{S}_{2,4}$	SSM-KR	0.0010	1.0042	3.0000	0.0020	0.0010	0.0001
$\mathcal{S}_{2,5}$	SSM-KR	0.0050	1.0017	3.0000	0.0252	0.0255	0.0712
$\mathcal{S}_{2,6}$	SSM-KR	0.0054	1.0004	2.3800	0.0500	0.0255	0.0793
$\mathcal{S}_{2,7}$	SSM-KR	0.0051	1.0038	2.7226	0.0500	0.0250	0.0733
$\mathcal{S}_{2,8}$	SSM-KR	0.0047	1.0002	2.0780	0.0500	0.0014	0.0064
$\mathcal{S}_{2,9}$	SSM-KR	0.0054	1.0054	2.7284	0.0500	0.0500	0.1500
$\mathcal{S}_{2,11}$	SSM-KR	0.0024	1.0002	1.7389	0.0195	0.0050	0.0004
$\mathcal{S}_{2,12}$	SSM-KR	0.0053	1.0000	2.5750	0.0246	0.0228	0.1500
$\mathcal{S}_{2,13}$	SSM-KR	0.0011	1.0001	2.4492	0.0499	0.0010	0.0048
$\mathcal{S}_{2,14}$	SSM-KR	0.0036	1.0065	2.8634	0.0500	0.0160	0.0591
$\mathcal{S}_{2,16}$	SSM-KR	0.0010	1.0013	1.5122	0.0500	0.0255	0.0010
$\mathcal{S}_{2,17}$	SSM-KR	0.0056	1.0191	3.0000	0.0500	0.0500	0.1500
$\mathcal{S}_{2,18}$	SSM-KR	0.0010	1.0013	2.0905	0.0010	0.0010	0.0001
$\mathcal{S}_{2,19}$	SSM-KR	0.0041	1.0006	3.0000	0.0420	0.0048	0.0625
$\mathcal{S}_{2,20}$	SSM-KR	0.0100	1.0002	3.0000	0.0500	0.0500	0.1500
$\mathcal{S}_{2,21}$	SSM-KR	0.0010	1.0002	2.1913	0.0001	0.0010	0.0001
$\mathcal{S}_{2,23}$	SSM-KR	0.0049	1.4101	3.0000	0.0236	0.0020	0.1494
$\mathcal{S}_{2,26}$	SSM-KR	0.0010	1.0000	1.4661	0.0243	0.0010	0.0026
$\mathcal{S}_{2,27}$	SSM	0.0014	1.0000	2.9293	0.0161	0.0105	0.0002